

**STRATEGIES TO IMPROVE PREDICTIONS OF OUTCOME IN GLIOBLASTOMA  
MULTIFORME AND MUSCLE-INVASIVE BLADDER CANCER**

By

Cheryl J. Claunch

A DISSERTATION

Presented to the Department of Biomedical Engineering  
Oregon Health & Science University  
School of Medicine

In partial fulfilment of  
the requirements for the degree of

Doctor of Philosophy

July 2018

School of Medicine  
Oregon Health & Science University

---

CERTIFICATE OF APPROVAL

---

This is to certify that the PhD dissertation of  
Cheryl J. Claunch  
has been approved

---

Mentor/Advisor: Joe W. Gray, Ph.D.

---

Co-mentor/Co-Advisor: James E. Korkola, Ph.D.

---

Member/Chair: Rosalie Sears, Ph.D.

---

Member: Shih-Wen Luch, M.D., Ph.D.

---

Member: Leslie L. Muldoon, Ph.D.

## TABLE OF CONTENTS

<b>Tables and Figures .....</b>	<b>vii</b>
<b>Abbreviations .....</b>	<b>xii</b>
<b>Acknowledgements .....</b>	<b>xii</b>
<b>Abstract .....</b>	<b>xiv</b>
<b>Chapter 1. Introduction to Cancer and advancement into the age of precision medicine .....</b>	<b>16</b>
<b>1.1 Defining cancer.....</b>	<b>16</b>
<b>1.2 Cancer in Ancient Times .....</b>	<b>16</b>
<b>1.3 Origin of the term cancer .....</b>	<b>17</b>
<b>1.4 The Advent of Cancer Biology.....</b>	<b>17</b>
<b>1.5 Seed and soil hypothesis.....</b>	<b>18</b>
<b>1.6 Cancer is a Genetic Disease .....</b>	<b>18</b>
<b>1.7 Rous sarcoma virus.....</b>	<b>19</b>
<b>1.8 Two-hit hypothesis .....</b>	<b>19</b>
<b>1.9 The Discovery of Viral Oncogenes .....</b>	<b>20</b>
<b>1.10 The Discovery of Proto-Oncogenes.....</b>	<b>20</b>
<b>1.11 The Discovery of Human Oncogenes .....</b>	<b>21</b>
<b>1.12 Tumor suppressor genes .....</b>	<b>22</b>
1.12.1 Rb gene .....	22
1.12.2 p53 gene.....	23
<b>1.13 The tumor microenvironment (TME).....</b>	<b>25</b>
<b>1.14 Cancer Treatments.....</b>	<b>26</b>
1.14.1 Surgery .....	26

1.14.2	Hormone Therapy .....	28
1.14.3	Radiation Therapy.....	29
1.14.4	Chemotherapy .....	31
1.14.5	Immunotherapy .....	34
1.14.6	Targeted Therapy.....	39
1.14.6.1	Growth signal inhibitors .....	39
1.14.6.2	Angiogenesis inhibitors.....	40
1.14.6.3	Apoptosis-inducing drugs .....	41
<b>1.15</b>	<b>The Omics Era .....</b>	<b>43</b>
<b>1.16</b>	<b>The Promise of Precision Medicine .....</b>	<b>43</b>
<b>1.17</b>	<b>Molecular Classification of Cancers .....</b>	<b>44</b>
<b>1.18</b>	<b>Towards advancing precision medicine – two tales.....</b>	<b>44</b>
<b>1.19</b>	<b>Glioblastoma multiforme (GBM).....</b>	<b>45</b>
1.19.1	Gliomas.....	45
1.19.2	Site .....	46
1.19.3	Epidemiology .....	46
1.19.4	Prognosis.....	46
1.19.5	Prognostic Factors .....	47
1.19.6	Risk factors .....	47
1.19.7	Symptoms.....	48
1.19.8	WHO classification of CNS tumors.....	49
1.19.9	Primary and secondary GBM .....	49
1.19.10	Glioma - CpG island methylator phenotype (G-CIMP) .....	50
1.19.11	Macroscopic and Histologic Features of GBM .....	50
1.19.12	Histological GBM variants .....	52
1.19.13	Treatment.....	52

1.19.14	GBM Molecular Subtypes.....	56
1.19.15	Resistance to standard treatment.....	59
1.19.16	Heterogeneity.....	60
1.19.17	Recent Advancements in Treatment.....	60
1.19.18	Remaining impediments in advancing precision medicine in GBM .....	63
<b>1.20</b>	<b>Bladder Cancer.....</b>	<b>64</b>
1.20.1	Natural History of Bladder Cancer.....	64
1.20.2	Standard of Care in Urothelial Carcinoma.....	64
1.20.3	The tumor microenvironment as a pro-proliferative cue.....	65
1.20.4	Bladder cancer differentiation states.....	66
1.20.5	Molecular subtypes.....	67
1.20.6	Recent Advancements in Treatment.....	71
1.20.7	Remaining impediments in advancing precision medicine in MIBC	75
<b>Chapter 2. Patient stratification in glioblastoma is improved by</b>		
<b>accounting for variations in gene expression caused by different</b>		
<b>histological structures. ....</b>		
		<b>77</b>
<b>2.1</b>	<b>Abstract.....</b>	<b>77</b>
<b>2.2</b>	<b>Introduction.....</b>	<b>77</b>
<b>2.3</b>	<b>Results.....</b>	<b>79</b>
2.3.1	Histologic structures in GBM tumors are molecularly distinct, explaining in part intra-tumoral heterogeneity. ....	79
2.3.2	Distinct biological processes are enriched in tumor structures. ....	81
2.3.3	Molecular subtype classification depends on structure, with CT best able to distinguish subtypes. ....	82

2.3.4	Molecular subtype classification using CT distinguishes tumors with unique biology.....	83
2.3.5	Survival prediction using an established prognostic gene signature is driven by tumor structure. ....	84
2.3.6	A novel prognostic gene signature, created utilizing CT transcriptomics, identifies highest-risk GBM patients. ....	85
<b>2.4</b>	<b>Discussion .....</b>	<b>102</b>
<b>2.5</b>	<b>Online Methods.....</b>	<b>106</b>
2.5.1	Data sets. ....	106
2.5.1.4	IvyGAP.....	106
2.5.1.5	TCGA.....	106
2.5.1.6	Data pre-processing. ....	107
2.5.2	Variation in gene expression is primarily explained by histologic structure. ....	107
2.5.2.7	PCA. ....	107
2.5.2.8	Correlation network analysis. ....	108
2.5.2.9	Gap statistic analysis. ....	108
2.5.2.10	K-means clustering. ....	108
2.5.2.11	Dendrogram.....	108
2.5.3	Structure-based lasso logistic regression classifier. ....	109
2.5.4	Gene Set Enrichment Analysis (GSEA) to assess for enriched biological processes and perform GBM subtype analysis. ....	109
2.5.5	Survival prediction using an established prognostic gene signature and metagene score. ....	110
2.5.6	Cox proportional hazards model for survival analysis.....	111
2.5.6.12	Univariate Analysis. ....	111

2.5.6.13	Multivariate Analysis. ....	111
2.5.6.14	Stepwise selection. ....	112
2.5.6.15	Internal validation. ....	112
2.5.6.16	Finalized survival model. ....	113
2.5.6.17	External validation. ....	113
2.5.6.18	Survival analysis. ....	113
2.5.7	Heatmaps. ....	114
2.5.8	Data availability. ....	114

**Chapter 3. Microenvironment factors influence cell count and differentiation state changes in human bladder cancer cell lines... 115**

<b>3.1</b>	<b>Abstract</b> .....	<b>115</b>
<b>3.2</b>	<b>Introduction</b> .....	<b>116</b>
<b>3.3</b>	<b>Results</b> .....	<b>118</b>
3.3.1	Molecular subtyping of bladder cancer cell lines revealed 5 subtypes. .....	118
3.3.2	Expression of differentiation state markers showed phenotypic heterogeneity in bladder cancer patient tissue and cell lines.....	119
3.3.3	MEMAs identified factors that promote EdU incorporation and induce differentiation state changes. ....	120
3.3.4	LYVE1 promotes EdU incorporation in the presence of cisplatin....	122
3.3.5	Effect of ligand treatment on cell count, proliferation, and differentiation in bladder cancer cell lines. ....	126
<b>3.4</b>	<b>Discussion</b> .....	<b>147</b>
<b>3.5</b>	<b>Materials and Methods</b> .....	<b>151</b>
3.5.1	Cell Lines and Cell Culture.....	151
3.5.2	Heatmap.....	151

3.5.3	MicroEnvironment MicroArrays .....	151
3.5.4	Cell Line Assays and Image Cytometry.....	152
3.5.5	Statistics .....	153
<b>Chapter 4. Conclusions and Future Directions .....</b>		<b>155</b>
4.1	<b>Conclusions .....</b>	<b>155</b>
4.2	<b>Future Directions Validation .....</b>	<b>157</b>
<b>Bibliography .....</b>		<b>160</b>



## Figures and Tables

<b>Figure 1. Macroscopic and histologic view of glioblastoma. ....</b>	<b>51</b>
<b>Figure 2. Kaplan-Meier estimates of overall survival by treatment group.....</b>	<b>55</b>
<b>Figure 3. GBM molecular subtypes as defined by TCGA. ....</b>	<b>57</b>
<b>Figure 4. MIBC molecular subtypes as defined by TCGA.....</b>	<b>68</b>
<b>Figure 5. Variation in GBM sample gene expression is primarily explained by histologic structure. ....</b>	<b>87</b>
<b>Figure 6. Biological processes enriched in tumor structures.....</b>	<b>88</b>
<b>Figure 7. Molecular subtype classification depends on the structure sampled, with Cellular Tumor (CT) able to distinguish biologically distinct subtypes...89</b>	<b>89</b>
<b>Figure 8. Established prognostic gene signature expression is driven by tumor structure.....</b>	<b>90</b>
<b>Figure 9. Novel prognostic gene signature created utilizing solely Cellular Tumor (CT) sample gene expression data.....</b>	<b>91</b>
<b>Figure 10. Heatmap of bladder cancer cell lines hierarchically clustered to identify molecular subtypes.....</b>	<b>129</b>
<b>Figure 11. Expression of differentiation state markers reveals phenotypic heterogeneity in bladder cancer cell lines.....</b>	<b>129</b>
<b>Figure 12. The MicroEnvironment MicroArray (MEMA) platform. ....</b>	<b>130</b>
<b>Figure 13. Microenvironment factors influence EdU incorporation and differentiation state. ....</b>	<b>131</b>
<b>Figure 14. Microenvironment factors influence EdU incorporation and differentiation state after cisplatin treatment. ....</b>	<b>133</b>
<b>Figure 15. LYVE-1 increases bladder cancer cell number in a dose response manner and does so in the presence of cisplatin in tissue-culture treated plates.....</b>	<b>133</b>

<b>Figure 16. LYVE-1 increases bladder cancer cell number in plates pre-coated with collagen I or CD44 and collagen I.....</b>	<b>134</b>
<b>Figure 17. LYVE-1 increases bladder cancer cell number and percentage of cells in S phase in plates pre-coated with CD44 and collagen I.....</b>	<b>136</b>
<b>Figure 18. Effect of soluble ligand treatment on cell count, proliferation, and differentiation in bladder cancer cell lines. ....</b>	<b>141</b>
<b>Supplemental Figure 1. ....</b>	<b>92</b>
<b>Supplemental Figure 2. Additional PCA and clustering analyses.....</b>	<b>93</b>
<b>Supplemental Figure 3. IvyGAP molecular subtyping. ....</b>	<b>94</b>
<b>Supplemental Figure 4. Structure-based gene signature. ....</b>	<b>95</b>
<b>Supplemental Figure 5. GSEA hallmark gene set enrichment results from CT stratified molecular subtypes. ....</b>	<b>96</b>
<b>Supplemental Figure 6. Analysis of established prognostic gene signature expression with all samples.....</b>	<b>97</b>
<b>Supplemental Figure 7. Enriched gene sets in IvyGAP CT genes associated with increased risk.....</b>	<b>98</b>
<b>Supplemental Figure 8. Survival analysis using the new survival prediction gene signature. ....</b>	<b>99</b>
<b>Supplemental Figure 9. A panel of bladder cancer cell lines models the genomic diversity of primary bladder cancer tumors.....</b>	<b>142</b>
<b>Supplemental Figure 10. Heatmap of bladder cancer cell lines hierarchically clustered to identify molecular subtypes.....</b>	<b>142</b>
<b>Supplemental Figure 11. Microenvironment factors influence EdU incorporation and differentiation. ....</b>	<b>144</b>
<b>Supplemental Figure 12. LYVE-1 increases bladder cancer cell number and percentage of cells in S phase in plates pre-coated with collagen I. ....</b>	<b>146</b>

<b>Supplemental Table 1. Tumor structure definitions.....</b>	<b>100</b>
<b>Supplemental Table 2. New prognostic gene signature statistics.....</b>	<b>101</b>
<b>Supplemental Table 3. Genetic characterization of major oncogenes and tumor suppressor genes in urinary bladder cancer cell lines.....</b>	<b>143</b>

## Abbreviations

ACT	-	Adoptive cell transfer
BCG	-	Bacillus Calmette-Guérin
CAR	-	Chimeric antigen receptor
CIS	-	Carcinoma in situ
CNS	-	Central nervous system
CRT	-	Chemoradiotherapy
CT	-	Cellular tumor
CT	-	Computed tomography
CTLA-4	-	Cytotoxic T-lymphocyte associated protein 4
ECM	-	Extracellular matrix
EdU	-	5-Ethynyl-2'-deoxyUridine
EGF	-	Epidermal growth factor
EGFR	-	Epidermal growth factor receptor
EMT	-	Epithelial to mesenchymal transition
FDA	-	U.S. Food and Drug Administration
FGFR-TACC3	-	FGFR3-transforming acid coiled-coil containing protein 3
FGFR3	-	Fibroblast growth factor receptor 3
FPKM	-	Fragments Per Kilobase of transcript per Million
G-CIMP	-	CpG island methylator phenotype
GBM	-	Glioblastoma multiforme
HBV	-	Hyperplastic blood vessels
HDAC	-	Histone deacetylase
HER2	-	Human epidermal growth factor receptor 2
HGF	-	Hepatocyte growth factor
IAP	-	Inhibitor of apoptosis proteins
IDH	-	Isocitrate dehydrogenase
Ig	-	Immunoglobulin
IMRT	-	Intensity-modulated radiation therapy
IORT	-	Intraoperative radiation therapy
IT	-	Infiltrative tumor
IvyGAP	-	Ivy Glioblastoma Atlas Project
KPS	-	Karnofsky Performance Scale
KRT	-	Cytokeratin
KRT	-	Cytokeratin
LE	-	Leading edge
LHRH	-	Luteinizing hormone-releasing hormone
LYVE-1	-	Lymphatic vessel endothelial hyaluronic acid receptor 1
MEMA	-	MicroEnvironment MicroArray
MEP	-	Microenvironment perturbation
MGMT	-	O <sup>6</sup> -methylguanine-DNA methyltransferase
MIBC	-	Muscle invasive bladder cancer
MMR	-	Mismatch repair
MRI	-	Magnetic resonance imaging
MVP	-	Microvascular proliferation
Myc	-	Myelocytoma virus
NOS	-	Not otherwise specified
NRG	-	Neuregulin
PAN	-	Pseudopalisading cells around necrosis
PCA	-	Principal component analysis

PD-1	-	Programmed cell death protein-1
PDGF	-	Platelet-derived growth factor
PDL-1	-	Programmed death ligand-1
PET	-	Positron emission tomography
PFA	-	Paraformaldehyde
PNET	-	Primitive neural ectodermal tumor
PNZ	-	Perinecrotic zones
RSV	-	Rous sarcoma virus
RT	-	Room temperature
SM	-	Smooth muscle
TCGA	-	The Cancer Genome Atlas
TME	-	Tumor microenvironment
UPK	-	Uroplakin
WHO	-	World health organization (WHO)

## **Acknowledgements**

I humbly and graciously thank my mentor, Dr. Joe Gray, and co-mentor, Dr. Jim Korkola, for their continued support and guidance throughout my doctoral research endeavors. Dr. Gray inspires me to be innovative in all approaches from basic to translational science and push the boundaries of what I believe possible. Dr. Korkola has been great in providing advice and encouragement. His understanding of basic science as it relates to medicine reminds me to remain hungry for knowledge. Most importantly, I'm grateful for them being a wonderful example of the 21<sup>st</sup> century scientist – someone who harnesses the knowledge of experts in different areas by bringing teams together to bridge the gap between basic and translational science to reach a common goal.

I am also extremely grateful to my thesis advisory committee, Drs. Rosie Sears, Dr. Shih-Wen Luoh and Dr. Laura Heiser. It has been awe-inspiring to witness their collective multidisciplinary insight of science and medicine and I appreciate their high standards in encouraging me to a better investigator.

As an extension of the Gray lab, Dr. Laura Heiser and her group have had an instrumental impact on my career in providing me the support and patience necessary to flourish in programming, a new language that I will continue to hone. I owe a big thanks to Elmar Bucher, for providing me the “red pill”, and encouraging my nascent programming skills. Mark Dane and Daniel Derrick are owed thanks for supporting my work in *R* by helping me troubleshoot and discuss general approaches.

Thank you to all Gray/Korkola/Heiser lab members for having such a wonderful impact on me personally and professionally. In particular, I thank the former affiliates,

Drs. Theresa Koppie and Trevor Levin for inspiring me to become passionate about the understudied field of bladder cancer.

Additionally, I thank the Neuwelt lab in providing me a second scientific home to expand beyond my comfort zone into the field of brain tumors. Drs. Neuwelt and Muldoon possess the right balance of constructive criticism and encouragement, while Dr. Ambady ensures clinical relevance. I also sincerely thank Cymon Kersch, my fellow MD/PhD classmate and partner in tackling the molecular underpinnings of glioblastoma, who inspires me daily with her enthusiasm for science, medicine, and life regardless of the circumstances.

I also acknowledge my fellow OHSU MD/PhD and Biomedical Engineering (BME) classmates, the MD/PhD program, the BME department as well as the OCSSB.

Finally, I would like to thank the NIH NCI Ruth L. Kirschstein predoctoral F31 fellowship for their generous financial support.

### **Dedication**

I would like to dedicate this work to my mother, Corina Castillo. Your sacrifices throughout my entire life have made this endeavor possible.

## **Abstract**

Advancing precision medicine in the treatment of cancer is complex and requires extensive molecular profiling to identify therapeutic targets and appropriately stratify patients into groups that differ in therapeutic vulnerability. The Cancer Genome Atlas (TCGA) has molecularly defined several cancer types and identified distinct subtypes. However, in some cases identification of molecular subtypes have failed to translate clinically. In particular, glioblastoma (GBM) and muscle-invasive bladder cancer (MIBC) are two such cancers that have molecular subtypes defined, though little clinical advancements have occurred as a result. Over the past three decades, there have been few treatment options and little change in overall survival for these cancers, with less than a 5% five-year survival rate for GBM and metastatic MIBC. Intra-tumoral heterogeneity and tumor microenvironment (TME) signals further complicate the ability to adopt precision medicine approaches for these cancers. We hypothesize that more accurate molecular subtyping and patient stratification can be achieved by taking into account intra-tumoral heterogeneity and microenvironment signals. This will allow for the ability to predict which treatments will work best for different groups of patients.

Precise management of GBM will require stratification of tumors into subtypes that differ in outcome and therapeutic vulnerability. We hypothesize that stratification into subtypes and prognostic groups can be achieved by taking GBM intra-tumoral heterogeneity into account. Our approach utilizes open-source transcriptional profiles of predefined histological structures from human GBM to develop methods to mitigate the impact of heterogeneity on transcriptomic-based stratification. We show that histologic architecture strongly influences tumor classification when assessing established gene signatures for subtyping and prognostic marker development, and that using mixed structure samples gives misleading results. We identify cellular tumor as a GBM



structure from which transcriptional subtyping and prognostic strategies can be applied to more accurately stratify patient cohorts. We analyzed this specific architecture to create an improved risk stratification tool. Our results suggest that biomarker performance for diagnostics, prognostics, and prediction of therapeutic response can be improved by analyzing transcriptional profiles in pure cellular tumor.

TME signals and differentiation state plasticity are two overlooked potential targets to aid in predictions of therapeutic response in the treatment of MIBC. Signals from the TME cooperate with tumor cell genotype (mutations, translocations, copy number), and phenotype (differentiation state) to select for the cell type most fit to survive the conditions of the environment. Understanding the interplay between TME signals that stimulate a pro-proliferative phenotype, and induce differentiation state plasticity has implications in identifying predictors of outcome and targets for therapeutic intervention. We hypothesize that distinct TME signals stimulate proliferation and differentiation state plasticity in human bladder cancer cell lines in the presence and absence of drug treatment. To test our hypothesis, we utilized a novel platform, microenvironment microarray (MEMA) technology, to identify candidate microenvironment signals that have effects on cellular proliferation and differentiation state in bladder cancer cell lines. Our results suggest that response to microenvironment signals is dependent on genotype, and cells have the ability to exhibit differentiation state plasticity and interpret microenvironmental cues as pro-proliferative, which may enhance tumorigenesis. This knowledge can enable the development of targeted therapies aimed at inhibiting the transduction of microenvironment signals and differentiation state changes. This collective work has the potential to improve predictions of outcome and advance GBM and MIBC into the modern era of precision medicine.

## **CHAPTER 1. INTRODUCTION TO CANCER AND ADVANCEMENT INTO THE AGE OF PRECISION MEDICINE**

### **1.1 Defining cancer**

Cancer is the second most common cause of death in the United States, and represents a major health concern. Cancer is a term that describes malignant cells that have the propensity for uncontrollable growth and division or are resistant to cell death. Malignant neoplasms, or new cancerous growths, have varying degrees of invasiveness and typically invade surrounding tissues or spread to distant organs via blood or lymphatic vessels. There are over 100 recognized cancer types and are generally classified based on the tissue of origin. The main types of cancer include carcinomas, central nervous system cancers, sarcomas, leukemias, and lymphomas. Carcinomas refer to cancer cells that are epithelial in origin and arise in skin or the lining of internal organs. Central nervous system cancers originate in the brain and spinal cord. Sarcomas are cancers of mesenchymal origin that begin in connective tissue such as bone, cartilage, fat, or muscle. Leukemias begin in the blood marrow from abnormal white blood cells or leukocytes. Lymphomas commence in lymphocytes, a type of leukocyte<sup>1</sup>.

### **1.2 Cancer in Ancient Times**

Fossilized tumors of the bone, ancient manuscripts, and mummified humans in ancient Egypt include some of the earliest chronicles of cancer. Evidence of bony skull destruction signifying head and neck cancer and growths indicative of osteosarcoma have been recognized in mummies<sup>2</sup>. The earliest descriptions of cancer were recorded in the Edwin Smith Papyrus, which contained notes on trauma surgery from an ancient Egyptian textbook written around 2500 BC<sup>3-5</sup>. It describes tumors of the breast treated by surgical resection with a fire drill and adds that the disease is incurable<sup>3-5</sup>.

### **1.3 Origin of the term cancer**

The Greek physician, Hippocrates (460 - 370 BC), is known as the “Father of Medicine” and is credited for the origins of the term cancer. Hippocrates referred to cancer by the word karkinos, Greek for crab, likely based on the finger-like projections of a malignant tumor reminiscent of a crab. Celsus (28 - 50 BC), a Roman physician, later translated the Greek term to cancer, meaning crab in Latin. Later, Galen (130-200 AD), another Greek physician, described tumors with the term oncos, the Greek word for swelling. Galen’s term is the origin for the word oncology, the modern study of cancer<sup>2,6,7</sup>.

### **1.4 The Advent of Cancer Biology**

In 1838, the German pathologist Johannes Müller developed the blastema theory, the notion that cancer is made up of budding elements (blastema), or a collection of cells. This theory founded the study of cancer histopathology. Around the same time, in 1839, Theodor Schwann and Matthias Schleiden introduced cell theory, the idea that all living organisms are comprised of uni- or multi-unit cells and that the most basic unit of life is the cell. In 1855, Müller’s student Rudolph Virchow, supplemented cell theory by adding that all cells, even diseased cells such as cancer, originated from other cells. Virchow continued to study diseased tissues and associated histopathology to illness, which allowed a cellular insight into cancer pathology and assisted cancer surgery. Tissue removed during surgery could now be examined and a diagnosis made based on pathology. The tissue could also be examined by the pathologist to determine whether the surgery excised the cancer completely with clean margins. Today, pathologists continue to assist in diagnosis of cancers and determine whether there are clean

margins. Due to these contributions, Virchow is known as the founder of cellular pathology<sup>8,9,10</sup>.

### **1.5 Seed and soil hypothesis**

In 1889, an English surgeon, Stephen Paget proposed the seed and soil hypothesis after realizing that specific cancers spread through the bloodstream and exhibited organotropism, or a predilection of certain cancers to distinct organs. Paget reasoned that for cancer metastasis to be non-random, cancer cells (seeds) can only live and grow in an environment (soil) conducive for life and growth. Nearly a century later, Paget's hypothesis was finally confirmed by modern cellular and molecular biology techniques. This hypothesis led to the thorough appreciation of metastatic disease and helped recognize that surgery alone was limited and that systemic treatment before or after surgery may help minimize the seeding of cancer to distant sites. Paget is credited as being the founder of tumor microenvironment research<sup>11,12</sup>.

### **1.6 Cancer is a Genetic Disease**

In 1902, Theodor Boveri, a German biologist, proposed that cancer was a result of genomic insults. Boveri pioneered experiments in the field of cytology by studying chromosomal segregation in sea urchin embryos. He found that an improper number of chromosomes caused embryonic cells to die or endure abnormal differentiation. Boveri rationalized that chromosome abnormalities may be causative of cancer since cancer also had chromosome anomalies. Further sea urchin embryo experiments with chemical carcinogens caused chromosome impairment demonstrating that genomic damage causes cancer. Boveri further postulated that cancer is a consequence of cell proliferation due to chromosomal damage, and predicted the presence of oncogenes,

tumor suppressor genes, and heritable oncogenic mutations. Boveri's postulates led to the somatic mutation theory of cancer<sup>13,14</sup>.

### **1.7 Rous sarcoma virus**

In 1911, Francis Peyton Rous discovered the Rous sarcoma virus (RSV) by demonstrating that cancer in chickens was transmissible by a virus. Rous took cell-free filtrate from a chicken sarcoma and injected it into healthy chickens. The injected chickens soon grew sarcomas, showing for the first time that a virus could transmit cancer. RSV could now be used as a model to explore the molecular mechanisms of cancer initiation and progression. Following RSV, several other tumor-inducing viruses were soon identified leading to the Epstein-Barr virus discovery in 1964, the first oncogenic human virus known. In 1966, Rous was awarded the Nobel prize for his revolutionary work. Rous' pioneering work has established the basis of modern virology and oncology<sup>15</sup>.

### **1.8 Two-hit hypothesis**

The somatic mutation theory of cancer eventually led to the two-hit hypothesis by Alfred Knudson. The two-hit hypothesis is the concept that cancer is a consequence of at least two mutations in a cell's DNA that affect both alleles of a particular gene. This general idea was initially proposed in the multi-mutation theory on cancer by Carl Nordling in 1953, with the exception that a series of multiple cumulative mutations were suggested. D.J. Ashley revisited Nordling's theory in 1969 and concluded that cancer resulted in the accumulation of about 3 to 7 mutations. Subsequently, in 1971, Knudson applied a statistical analysis to retinoblastoma cases where children either inherited or sporadically developed a tumor of the retina. Knudson observed that inherited retinoblastoma frequently occurred bilaterally, and younger in age when compared to

sporadic cases, suggesting a predisposition to the disease. In inherited retinoblastoma, children would inherit the initial mutation, and any additional mutations would cause cancer. In sporadic retinoblastoma, at least two mutations had to occur before the disease would develop. These results suggested that a minimum of two “hits” needed to occur to cause cancer. Knudson's work indirectly led to the identification of critical genes involved in cancer called tumor suppressor genes.

### **1.9 The Discovery of Viral Oncogenes**

Continued studies with RSV led to the discovery of a viral oncogene, v-src. Focus forming transformation assays were developed in 1958 and were utilized in RSV mutant and non-mutant strains. Some RSV strains demonstrated that they had the ability to replicate and transform chicken fibroblasts, while others strains could only replicate or transform cells, but not both. These studies showed that virus replication and oncogenic transformation were not interdependent events, indicating that a distinct gene caused transformation. In 1970, Dominique Stehelin, a post-doctoral researcher in the lab of Michel Bishop and Harold Varmus, compared non-mutant RSV with normal replicative and transforming abilities to mutant RSV strains that could replicate but not transform. Through this work, Stehelin identified src as the gene responsible for transformation. This established src, later named v-src, as the first oncogene identified, which demonstrated the initial evidence that expression of a single altered gene had the ability to cause cancer<sup>16-18</sup>.

### **1.10 The Discovery of Proto-Oncogenes**

Bishop and Varmus conducted experiments to identify related genes to src in other species. Surprisingly, they found src in all avian cells, but also in higher organisms, including human cells. In 1976, hybridization assays between v-src and normal chicken

DNA helped discover a cellular non-oncogenic variant of src in many avian species, c-src. This discovery introduced the idea of proto-oncogenes, where c-src is the proto-oncogene, or the wild-type non-oncogenic version, that mutates to v-src and acquires constitutive activity. This concept suggests that cancer may be induced by alterations in normal genes. Oncogenic viruses, such as RSV and others, are believed to have incorporated a proto-oncogene from the hosts genome during viral replication, and later acquired a mutation in the transduced gene, resulting in a viral oncogene. Bishop and Varmus were awarded the Nobel prize for their discovery in 1989<sup>16,17</sup>.

### **1.11 The Discovery of Human Oncogenes**

The v-src oncogene became the model for identifying other transforming genes harbored in oncogenic viruses. For example, the first two ras genes, H-ras (associated with bladder cancer) and K-ras (associated with pancreatic, lung, and colorectal cancer) were identified based on studies of two oncogenic viruses, the Harvey sarcoma virus and Kirsten sarcoma virus. During the 1960's, these viruses were discovered initially in rats by Jennifer Harvey and Werner Kirsten, respectively. In 1982, activated and transforming human ras genes were discovered in human cancer cells by several groups. N-ras, a third ras gene was then discovered by Robin Weiss' group and Michael Wigler's group, named based on its initial identification in human neuroblastoma cells. A nearly identical gene was found in normal human DNA. Cloning and sequencing identified the gene as c-ras, the normal proto-oncogene. It was later appreciated that ras family genes are the most common oncogenes in cancer, having alterations in up to 25% of all human cancers. In 1977, the myc gene was first identified in the avian myelocytoma virus (v-myc). Homology between v-Myc and an over-expressed gene in various human cancers, c-Myc, led to its discovery. Further homology studies helped discover the human genes n-Myc and l-Myc. Oncogenic c-Myc is most frequently

discussed in reference to Burkitt lymphoma, a cancer with chromosomal translocations of chromosome 8 and 14. This translocation places the highly active immunoglobulin (Ig) promoter region upstream of c-Myc, resulting in c-Myc overexpression. These findings suggested that human cancers were driven by human oncogenes<sup>19-24</sup>.

## **1.12 Tumor suppressor genes**

Shortly after the discovery of oncogenes, DNA tumor viruses (e.g. SV40, adenovirus, papillomavirus) were found to express oncoproteins (e.g. SV40 Large T-antigen, E1A, E7) that interact with cell proteins and inhibit their ability to control the cell cycle. Tumor suppressor genes were the name later designated for the genes encoding the targeted cell proteins. The normal role of tumor suppressor genes is to down-regulate cell division to allow for DNA repair and initiate cell death when DNA is too damaged for repair or when otherwise appropriate. Therefore, inactivating tumor suppressor genes removes critical regulatory proteins and results in uncontrolled cell growth and cancer. Somatic cell hybridization experiments performed by Henry Harris in 1969 provided the initial understanding into the function of tumor suppressor genes. Tumor cells were fused with normal cells generating hybrid cells with chromosomes from both parental cells types. Hybrid cells rarely formed tumors in animals, leading to the conclusion that genes originating from normal parental cells had the ability to suppress tumor development<sup>13,25,26</sup>.

### **1.12.1 Rb gene**

A more extensive molecular definition and functional awareness of tumor suppressor genes came from later studies in retinoblastoma, which helped identify Rb as the first tumor suppressor gene. Chromosome morphology studies in retinoblastoma showed that Rb was a negative regulator of tumorigenesis. Chromosome 13q14 was



visible deleted in certain retinoblastomas, indicating that loss the Rb gene, not activation, led to tumor formation. Further studies in gene-mapping in the late 1970's suggested that tumor development was a result of normal Rb genes. In 1986, Rb was isolated as a molecularly clone and was found to be undoubtedly deleted or mutated in retinoblastomas. Direct confirmation that Rb is a tumor suppressor came from introducing normal Rb into retinoblastoma cells, which reverted tumor cells back to a normal phenotype. Additionally, Rb protein was identified as a target of oncoviral proteins from the DNA viruses SV40, adenoviruses, and human papillomaviruses<sup>26-28</sup>.

Since the original identification in retinoblastoma, deleted or inactivated Rb has been identified in many common cancers such as bladder, breast, and lung carcinomas. Classification of Rb as a tumor suppressor gene paved the way for identification of other tumor suppressor genes that may play a role in cancer development<sup>26,29</sup>.

#### 1.12.2 p53 gene

p53 was the second tumor suppressor gene identified and is altered in over 50% of all human cancers. p53 becomes activated by cellular stresses, such as oncogene activation, DNA damage, and hypoxia and initiates cell cycle arrest, DNA repair, and cell death by apoptosis to prevent damaged cells from proliferating. Alternatively, inactivating p53 leads to uncontrolled proliferation culminating in tumor development<sup>30</sup>.

In 1979, six groups independently identified a 53 kD nuclear protein that associated with the Large T antigen of the SV40 oncovirus in human and mouse cells now known as p53. Many groups then began studying p53 to characterize its function and classification. There were numerous indications that p53 was indeed an oncogene. Several studies from 1982-84 with the murine and human p53 suggested that it was an

oncogene due to the fact that it was able to transform cells upon transfection of the gene. p53 was also found to be overexpressed in many types of cancer cells and knockout of p53 prompted arrest of cell proliferation. The association with oncoviral protein also indicated the likelihood that p53 was an oncogene. The interpretation of the findings from p53 experiments largely reflected what was known at the time in cancer research. It seemed appropriate at the time to classify p53 as an oncogene as they were thought to be vital to cancer development. On the other hand, tumor suppressor were overlooked for the classification of p53 due to the lack of evidence for their existence<sup>26,29,30</sup>.

Nearly a decade after its' discovery, p53 was rightly classified as a tumor suppressor by applying the two-hit hypothesis test. Recall that statistical analysis of retinoblastoma cases helped establish the two-hit hypothesis, which became the method for distinguishing between a mutant gene as an oncogene or a tumor suppressor gene. If both alleles of the gene were altered, it was categorized as a tumor suppressor gene. In contrast, the gene was classified as an oncogene if only one allele was altered. In 1989, one TP53 copy of a tumor was lost and the other was sequenced, finding that the remaining copy was mutated, whereas in the normal tissue it was not. In other tumors, it was found that there was either loss or mutations in the TP53 gene indicating that p53 was in fact a tumor suppressor, not an oncogene. In addition, p53, like Rb, was identified as a target of oncoviral proteins from the DNA viruses SV40, adenoviruses, and human papillomaviruses. Further studies in p53 demonstrated that it is the most frequently mutated gene in tumors<sup>31</sup>.

Over the last few decades since its discovery, several functions have attributed to different p53 alterations. Different studies have shown that missense mutations in p53

can abolish tumor suppressor function, but may also provide p53 oncogenic gain-of-function abilities. Some mutant forms of p53 are able to inactivate the endogenous wild-type p53 protein in a dominant-negative fashion by forming a heterotetramer complex. These findings suggest that dominant-negative mutations in one p53 allele should be sufficient to inactivate p53 function in a cell. Further studies show that specific mutant forms in one copy of p53 can exert a dominant-negative function and inactivate wild-type p53 through the formation of a heterotetramer complex. These results indicate that in some cases one “hit” is sufficient to cause tumorigenesis. Furthermore, dominant-negative p53 mutants may play a pivotal role in accelerating glioblastoma development. The average age of patients that harbor dominant-negative p53 mutations is significantly lower than those that do not possess these mutants. Thus far, there is evidence that p53 mutants contribute to a wide array of functions such as tumor proliferation, survival, replication, somatic cell reprogramming, genomic instability, inflammation, disruption of tissue architecture, migration, invasion, angiogenesis, and metastasis. Despite several decades worth of research on p53, there is still more to learn about the roles that p53 and its mutants play in tumorigenesis<sup>26,29,32–34</sup>.

### **1.13 The tumor microenvironment (TME)**

The TME includes a collection of seemingly normal cells that surround a tumor and contribute to tumorigenic traits. Blood and lymph vessels, immune cells, and fibroblasts, as well as soluble signaling molecules and extracellular matrix make up components of the TME. Studies in many cancer types have implicated the TME in promoting tumor progression. Through multiple signals, a tumor can alter the TME to create favorable conditions for proliferation. The TME can, in turn, signal to the tumor and modulate survival, proliferation and differentiation, via transducing signals into cells through a variety of cell surface receptors. Intra-tumoral heterogeneity allows

subpopulations of cells to differentially respond to TME signals. Fully recognizing the contribution of the TME to tumorigenesis and can aid in identifying new therapeutic targets and developing novel drugs<sup>35-38</sup>.

## **1.14 Cancer Treatments**

### **1.14.1 Surgery**

Advances in cancer treatment underwent slow development from initial references of cancer treatment until today. Ancients realized that cancer would usually recur once removed, and intervention may do more harm than good. Galen wrote that surgical cures for breast cancer were possible and depended on the full resection of the tumor early in the disease. At the time, surgery was primitive without general anesthesia and was encumbered by complications such as severe pain and blood loss. Knowledge of the surgical experience prior to the age of anesthesia came in 1812 from the novelist Fanny Burney who graphically recounted her traumatic mastectomy experience in 1811<sup>2,6,39</sup>.

Major advancements in the treatment of cancer didn't arrive until 1846 with the advent of anesthesia. General anesthesia enabled surgeons Theodor Bilroth in Germany, W. Sampson Handley in London, and William Halsted in Baltimore, to perform extensive tumor resections that included the primary tumor and the regional lymph nodes. Halstead introduced the radical mastectomy as the standard of care in 1894 and continued to refine it in the United States. This practice was based in part on work by Handley, who believed that the primary tumor spread outward by invasion<sup>40,41</sup>.

Radical mastectomy was a gruesome and highly disfiguring operation. Not only were the tumor and lymph nodes removed, but the surrounding muscles of the chest

wall and extended lymph nodes were removed as well, based on the belief that the patient could be cured with a greater excision. This remained the standard of care treatment of breast cancer until the 1970's with 90% of patients treated with radical mastectomy between 1890 and 1975. This extreme surgery was unnecessary in many cases. For women with local disease, the tumor hadn't invaded surrounding tissue necessitating such an extensive surgery. For women with metastatic disease, the disease was incurable with surgery alone. A better understanding of cancer biology was needed to reduce undue harm and improve outcomes over surgery alone<sup>42-45</sup>.

In 1889, Stephen Paget developed the seed and soil hypothesis (see previous section) suggesting that cancer cells from a primary tumor metastasized through the bloodstream and demonstrated organotropism. The full appreciation of this hypothesis was delayed, but eventually became a defining element in acknowledging the limitations of cancer surgery. It ultimately led to the development of systemic treatments used after surgery to kill cells that had spread, allowing less destructive operations. Today, systemic treatments may be used prior to surgery as well<sup>8,11,12</sup>.

In the 1970s, clinical trials revealed that most women with breast cancer can undergo less extensive surgery and have equally effective outcomes. Current surgical treatment for most women with breast cancer include removing the primary tumor by lumpectomy, and then follow with radiation therapy<sup>44</sup>.

Throughout the end of the 20<sup>th</sup> century, surgeons continued to develop greater technical skills in maximizing the extent of tumor resection while minimizing the amounts of normal tissue removed. This progress was made possible by enhanced knowledge of cancer biology, better surgical instruments, chemotherapy, and radiation. Until the end of

the 20<sup>th</sup> century, surgery was frequently required to obtain tissue samples for testing by pathologists to diagnose cancer. Beginning in the 1970's, many operations for diagnostic purposes are unnecessary due to the advancement in imaging modalities such as ultrasound (sonography), computed tomography (CT scans), magnetic resonance imaging (MRI scans), and positron emission tomography (PET scans). CT scans and ultrasound can be used to guide biopsy needles into tumors to obtain tissue samples for pathologic testing<sup>44,46,47</sup>.

Today, surgeons have the ability to visualize and perform laparoscopic surgery (inside the abdomen) or thorascopic surgery (inside the chest) by using specialized surgical instruments through narrow tubes that are placed in small incisions in the skin. Endoscopic surgery is similar, but differs in that the tubes are placed in natural orifices and can be used to remove some tumors from the colon, esophagus, or bladder<sup>48,49</sup>.

Lasers, as opposed to scalpels, can also be used to cut or vaporize tumor tissue of cervix, larynx, liver, rectum, skin and other organs. Recently, even less invasive ways of killing tumors are being investigated including cryosurgery and radiofrequency ablation. Cryosurgery uses liquid nitrogen spray to freeze and kill abnormal cells, and radiofrequency ablation transmits radio waves to a small antenna positioned in the tumor to kill cancer cells by heating<sup>49-51</sup>.

#### 1.14.2 Hormone Therapy

In 1878, George Thomas Beatson, a British physician, discovered that rabbits ceased the production of breast milk following the removal of the ovaries, or oophorectomy. This indicated that one organ (the ovaries) controlled the ability of a separate organ (the breasts) to produce a secretion (breast milk). Beatson decided to

test oophorectomy in women with advanced breast cancer, finding that oophorectomy frequently resulted in improvement. He also surmised that the ovaries were the cause of breast cancer. Beatson essentially identified the stimulating effect of estrogen, the female ovarian hormone, on breast cancer, even before it was discovered. This work established the modern use of hormone therapy to treat or prevent breast cancer, such as tamoxifen (blocks estrogen receptor) and the aromatase inhibitors (blocks estrogen production)<sup>52</sup>.

Following Beatson's discovery, Charles Huggins, a urologist, in 1941 described dramatic regression of metastatic prostate cancer following castration (orchiectomy), or removal of the testicles. Based on this observation, a hormonal influence on prostate cancer was established. Following Huggins discovery, an effective treatment for prostate cancer was realized in androgen deprivation therapy through surgical (orchiectomy) or medical castration (luteinizing hormone-releasing hormone (LHRH) agonists). Huggins was awarded the Nobel Prize in 1966 for discovering in hormones could be used to control the spread of some cancers<sup>53</sup>.

The contributions of Beatson and Huggins to the field of cancer biology has led to the understanding of the influence of hormones on cancer growth. This has directed the development of a variety of new drugs for cancer treatment.

### 1.14.3 Radiation Therapy

In 1896 a German physics professor, Wilhelm Conrad Roentgen is credited as the discoverer of the X-ray. Worldwide excitement led to plans for X-ray use in diagnostics within months, and within 3 years, radiation was used for cancer treatment. In 1901, Roentgen received the first Nobel Prize awarded in physics. In the early 20th

century, soon after radiation was used for diagnosis and therapy, researchers discovered that radiation could cause cancer as well as cure it. Many early radiologists developed leukemia from exposing themselves to radiation routinely. They would use their skin to test the optimum radiation strength of the machines by identifying a dose that produced a pink reaction (erythema) similar to a sunburn. This was called the erythema dose and indicated an estimate of the proper daily fraction of radiation.

Recent radiation physics and computer technology advancements made it possible to direct radiation more precisely leading to several types of radiation therapy described below:

- i. *Conformal radiation therapy (CRT)* – uses CT images and computers to precisely map the cancer location in 3 dimensions. Radiation beams are matched to the tumor shape and delivered from several directions. A plastic mold is fitted to the patient to ensure the body is kept still and in the same position for each treatment<sup>54</sup>.
- ii. *Intensity-modulated radiation therapy (IMRT)* – similar to CRT, but the beams can vary in intensity allowing more control of dosing so that normal tissues are less affected<sup>55</sup>.
- iii. *Conformal proton beam radiation therapy* – similar to CRT, but uses proton beams instead of X-rays causing less damage to tissues it passes through. Can deliver more radiation while potentially reducing damage to normal tissue with this method<sup>54</sup>.



- iv. *Stereotactic radiation therapy* – encompasses several techniques that deliver a large and precise radiation dose to a small area. The brain is the most common site treated with this technique<sup>54,56</sup>.
  
- v. *Intraoperative radiation therapy (IORT)* – cancer is removed surgically immediately followed by radiation to adjacent tissues. Commonly used in abdominal, and pelvic tumors as well as in cancers that tend to recur, such as bladder cancer<sup>57,58</sup>.

Currently research is being conducted to identify radiosensitizers that make cancer more sensitive to radiation therapy. Ideal agents would make the tumor more sensitive while having a minimal or no effect on normal tissues. Research is also being done to identify formulations that protect normal cells from radiation<sup>54</sup>.

#### 1.14.4 Chemotherapy

The development of chemotherapy for cancer treatment was a result of knowledge obtained after military people were exposed to mustard gas during World War II. Exposed people had considerably reduced leukocyte count due to bone marrow cell toxicity. Investigators asked whether similar compounds to mustard gas would be effective anti-cancer therapies. This led to the identification of nitrogen mustard (mustine), which was effective against lymphoma. In the 1940's, Alfred Gilman and Louis Goodman, two pharmacologists at Yale, studied mustard agents for the treatment of lymphoma. They demonstrated efficacy of mustard agents in mice models of lymphoma. In 1943, in collaboration with Gustav Linskog, a thoracic surgeon, Gilman and Goodman injected nitrogen mustard into a non-Hodgkin's lymphoma patient. The patient's tumors significantly reduced after treatment, marking the beginning of the era of cytotoxic

treatment of cancer. The results of this study were published in 1946, resulting in nitrogen mustard becoming a popular treatment for lymphomas in the United States. Nitrogen mustard became the prototype for the development of other, more effective mustard gas derivatives known as alkylating agents. Examples of alkylating agents include the tetrazines and cisplatin, which have the ability to kill rapidly growing cells through damaging DNA by alkylation<sup>59,60</sup>.

Another approach to chemotherapy agents was investigated by Harvard Medical School pathologist, Sidney Farber. He considered folic acid, an essential vitamin in DNA metabolism, as a target for anticancer effects. Farber developed a folate analogue, aminopterin, that was antagonistic to normal folate and in 1948 showed that this could induce remissions in children with acute lymphoblastic leukemia. Aminopterin preceded methotrexate, a folate analogue used today for the treatment of cancer. In 1956, methotrexate proved extremely effective in metastatic cancer against a rare tumor, choriocarcinoma, by curing it. Other examples of chemotherapies include plant alkaloids extracted from *Vinca rosea* that were reported to be effective in leukemia patients. This led to the introduction of the vinca alkaloids, vinblastine and vincristine in the 1960's. Researchers continued to investigate others therapies and their ability to block cell growth and replication in cancer, which initiated the era of chemotherapy<sup>61-64</sup>.

Intense research efforts went into identifying other agents with anticancer properties. In 1978 cisplatin, an alkylating agent, was approved by the U.S. Food and Drug Administration (FDA) for the treatment of testicular cancer, ovarian cancer, and bladder cancer. Cisplatin was wildly successful in treating testicular cancer and effectively considered a cure. The approval for cisplatin in bladder cancer made cisplatin the first chemotherapy drug approved for bladder cancer and is still used today. Another

alkylating agent, temozolomide, was identified as effective against melanomas and certain brain cancers. In 1999, the FDA approved temozolomide for refractory anaplastic astrocytomas, and in 2005 for newly diagnosed adult glioblastomas (GBM).

Temozolomide is still the first line chemotherapeutic agent for GBM<sup>65-67</sup>.

In the early 20th century, only small localized cancers that could be entirely removed by surgery were considered curable. Later, radiation therapy was introduced after surgery to destroy remaining cancer cells not able to surgically excise. Finally, chemotherapy was introduced to kill cancer cells spread beyond the local tumor environment beyond the reach of the surgery or radiation. Chemotherapy used after surgery is called adjuvant therapy. Sometimes chemotherapy is used before surgery and is called neoadjuvant therapy.

The introduction of chemotherapy has proven successful in the treatment of many cancers. Long-term remission or cures have been attributed to chemotherapy. However, this has not come without compromise. The side effects associated with some chemotherapies are sometimes intense and dose limiting due to the non-specificity of these drugs to cancer cells. The intent of chemotherapy use is to affect rapidly dividing cancer cells; however, normal dividing cells are also affected resulting in toxicities. This makes the use of chemotherapies a fine balance between killing tumor cells while managing potentially life-threatening side effects.

Over the last two decades, chemotherapy has been aimed at the use of combination chemotherapy, with differing mechanisms of action to effectively treat the cancer and reduce side effects. Treatment approaches in conjunction with early detection has improved patient survival and demonstrated a decline in mortality. There is now the trend to identify who will respond best to certain chemotherapies based on

genetic markers. Ongoing clinic trials stratify patients based on their genetics and test new treatment options against standard treatments so that benefits and risks are appropriately understood<sup>68,69</sup>.

#### 1.14.5 Immunotherapy

There are multiple descriptions of tumors shrinking or disappearing following an infection or elevated febrile episode dating back to ancient times up until the early 18<sup>th</sup> century. Histologic principles first had to be established before these accounts were able to be validated.

Two German physicians, W. Busch and F. Fehleisen, independently observed tumor regression in patients after accidental infections by erysipelas. In 1868, Busch intentionally infected a cancer patient with bacteria and the tumor shrank. Fehleisen followed suit in 1882 witnessing the same result from a streptococci-causing erysipelas. In 1891, an American surgeon, William Coley, independently observed regression of a sarcoma after he injected an inoperable patient with streptococcal organisms. Over the next several decades, Coley injected over 1000 cancer patients with bacteria or bacterial products known as Coley's Toxins, bringing the field of cancer immunology to life. He and fellow doctors injected Coley's Toxins into cancer patients and reported exceptional results, particularly in bone and soft-tissue sarcomas. However, many colleagues were in disbelief of Coley's results, fueled by the lack of good scientific protocols and inconsistencies in reproducibility. These controversies along with the advent of radiation therapy and chemotherapy led to the gradual disappearance of Coley's Toxins from use, as well as cancer immunotherapy for the time being<sup>70-72</sup>.

In 1976, there was a resurgence of Coley's principles and cancer immunotherapy when the use of bacteria was finally justified. Morales et al. validated the effectiveness of

the bacterium *Bacillus Calmette-Guérin* (BCG) in the treatment of superficial bladder cancer. A 1959 study by Old et al demonstrated the anti-tumor effects of BCG in a mouse model and provided the basis for the 1976 clinical trial. Coley and Old have each been denoted as the “Father of Immunotherapy” due to their foundational contributions to the field<sup>73-75</sup>.

Today, cancer immunotherapies are defined as a type of treatment that uses biological agents to exploit the innate ability of the immune system to combat cancer. These biological agents can now be produced in the laboratory and used as cancer immunotherapies, many of which function with different mechanisms of action. These treatments can exert their function directly by helping the immune system attack the cancer or indirectly through general stimulation of the immune system<sup>9,76,77</sup>.

Types of immunotherapy that function directly include:

- i. *Checkpoint inhibitors* - T cells can distinguish between healthy cells and malignant cells through activation or deactivation of various receptors on the T-cell surface. Cancer cells can escape immune detection by mimicking healthy cells through the expression of cell surface molecules that interact with T cell receptors. This results in the immune system remaining inactive against the cancer cells. Checkpoint inhibitors are drugs that help the immune system respond to the presence of a tumor cell and kill it. These drugs work by inhibiting the inappropriate interaction between T cells and cancer cells, thereby releasing T cells' inhibition to kill cancer cells. These drugs do not target the tumor directly, but block the ability of cancer cells to evade immune system attack. Three main checkpoint targets include PDL-1 (programmed death ligand-1), programmed cell death protein-1 (PD-1), and cytotoxic T-lymphocyte associated protein 4 (CTLA-

4). Inhibiting these checkpoints has been the primary focus for the treatment of bladder cancer, and have many inhibitor agents approved. These treatments hold promise in being effective in many other cancer types, and are currently being tested in clinical trials. Limitations of these inhibitors include their associated adverse events, cost, and access. Immune-related adverse events are the most worrisome of the limitations and can be severe and life-threatening due to the overstimulation of the immune system or the induction of autoimmunity. Adverse events frequently include rash and gastrointestinal complications, but may also result in pulmonary, renal, endocrine, and hepatic dysfunction<sup>78-80</sup>.

- ii. *Adoptive cell transfer (ACT)* - A treatment that attempts to boost the natural ability of the patients' T-cells to fight cancer. T-cells are isolated from the tumor and those that show the most activity against the cancer are grown in large batches in the lab for 2 to 8 weeks. During this time, chemotherapy or radiation therapy may be used to reduce immune cells and enhance ACT efficacy by eliminating cells that compete for homeostatic cytokines necessary for survival of the transferred cells. After these treatments, the T-cells that were grown in the lab are given back and hopefully attack the cancer. There are several types of adoptive cell transfer protocols, with the greatest advancements seen in chimeric antigen receptor (CAR) T-cell therapy, which uses a patients' own T-cells that are engineered in the lab to express a receptor for a specific antigen of interest on tumor cells. The modified cells are then reintroduced to the patient and home to the tumor cells expressing the antigen. Limitations to CAR T-cell therapy include toxicities and cost of over \$250,000 per infusion. Toxicities can be severe and include neurologic, cardiovascular, hepatic, renal, gastrointestinal, and

musculoskeletal effects. Despite toxicity profiles, in 2017 the FDA approved two CAR T-cell therapies, Kymriah™ (tisagenlecleucel) and Yescarta™ (axicabtagene ciloleucel), the first gene therapies approved in the United States. Kymriah™ was approved for patients less than 25 years old with refractory or relapse acute lymphoblastic leukemia, and Yescarta™ was approved to treat adults with refractory or relapse large B-cell lymphoma. Research is still being conducted to demonstrate the efficacy of CAR T-cell therapy in the treatment of solid tumors<sup>81-85</sup>.

- iii. *Monoclonal antibodies* - Therapeutic monoclonal antibodies are immune system proteins created in a lab and designed to attach to specific target antigens on cancer cells. Due to this specificity, therapeutic monoclonal antibodies are also considered targeted therapies. Some monoclonal antibodies bind to cancer cells and recruit the immune system. Other monoclonal antibodies bind cancer cells and directly stop them from growing or cause them to die. Certain antibodies are conjugated to drugs or toxins and deliver them to cancer cells. Rituximab (Rituxan) and trastuzumab (Herceptin) in the late 1990's were the first therapeutic monoclonal antibodies approved that specifically target CD20 on lymphoma cells and HER2 on breast cancer cells, respectively. Since then, many other monoclonal antibodies have been developed to target blood and solid cancers. The specificity of monoclonal antibodies makes them an attractive therapeutic option and is one of the main advantages for their use as a cancer treatment. Limitations of monoclonal antibodies include adverse reactions, such as infusion-related reactions and tumor lysis syndrome. Infusion-related reactions are any symptoms experienced by the patient during infusion of the antibodies or during the first day of treatment, and can be mild or extend to life-threatening

anaphylaxis. Tumor lysis syndrome can occur after administration of monoclonal antibodies causes large amounts of tumor cells to die resulting in acute renal failure and associated electrolyte imbalances, which may be fatal. More common adverse reactions include chills, malaise, headache, vomiting, diarrhea, and rashes. Other limitations of monoclonal antibodies in the treatment of cancer include the high production cost, which is estimated to be double that of other standard drugs. Monoclonal antibodies for the treatment of cancer continue to be developed to offer more specific, less toxic, and more cost-effective treatment<sup>76,77,86</sup>.

- iv. *Treatment vaccines* – Boosts your immune system’s response to cancer cells. Treatment vaccines do not refer to preventative vaccines.

Types of immunotherapy that function indirectly include:

- I. *Cytokines* - Proteins that play important roles in the body’s normal immune response and in the immune system’s ability to respond to cancer and include interferons and interleukins. Interferon-alpha and interleukin-2 are the main cytokines being used as anti-cancer therapies. Interleukin-2 is normally produced by activated T-cells in response to infection and as a cancer therapy can stimulate T-cells to target cancer cells and B-cells to produce anti-cancer antibodies. Interferon-alpha may boost the immune response by enhancing the production of dendritic cells, natural killer cells and macrophages to attack cancer cells, and may also inhibit cancer growth or promote cell death. Cytokine therapy been approved for leukemias and lymphomas, melanoma, and renal cell carcinoma, and is being used in clinical trials for bladder cancer<sup>87-89</sup>.



- II. *BCG* - An immunotherapy approved in 1976 to treat superficial bladder cancer. It is the weakened form of *Mycobacterium bovis* that causes tuberculosis in cows. *BCG* causes an immune response against bladder cancer when inserted directly into the bladder with a catheter. Research is being studied on its effectiveness in other types of cancer.

#### 1.14.6 Targeted Therapy

Prior to the late 1990's, most drugs used for the treatment of cancer, excluding hormone therapy, worked by destroying cells that were undergoing replication and were extremely toxic. These chemotherapy drugs had the greatest effect on cancer cells due to their rapid proliferative profile, but had toxicity limitations because they affected normal proliferating cells. It became clear that targeted therapies were needed to increase specificity and reduce toxicities. The concept of targeted therapies refers to targeting a genetically distinct alteration in cancer cells that is absent in normal cells, thereby enhancing specificity of cancer cell death while protecting normal cells. Specific targets for the use of targeted therapies include aberrant growth signaling, pro-angiogenic signaling, loss of inhibitory or cell death signaling, as well as other signals that give cancer cells a growth, survival, or mobility advantage<sup>69,90,91</sup>.

##### 1.14.6.1 *Growth signal inhibitors*

Growth factors bind to cell surface receptors and signal to a cell when to grow and divide. The role of growth factors in fetal growth and tissue repair was first appreciated in the 1960's. Subsequently, researchers identified overexpression or altered forms of growth factors contribute to carcinogenesis with the molecular mechanisms not fully understood. During the 1980s, it was discovered that many growth factors, growth factor receptors, and proteins responsible for transducing their

intracellular signal were products of oncogenes. This discovery led to the development of targeted therapies to block unrestrained cell growth. The earliest of these targeted therapies include the monoclonal antibodies trastuzumab (Herceptin; targets HER2), and cetuximab (Erbix; targets EGFR), as well as the tyrosine kinase inhibitors gefitinib (Iressa; targets EGFR), and imatinib (Gleevec; targets Bcr-Abl). Monoclonal antibodies specific to growth factor receptors can block signaling by inhibiting normal ligand binding or by keeping the receptor in its' inactive conformation. Tyrosine kinase inhibitors can interrupt growth signaling by binding to the activate site of tyrosine kinases and compete with ATP binding, substrate binding, or both, and can also affect enzyme activity by binding to an allosteric site. Limitations of these targeted therapies include specificity, delivery, and resistance. Depending on the dose, there may be off-target binding and rapid turnover or degradation. Resistance can also be a problem when cells adapt to inhibition of one pathway through upregulation of the same pathway or activation of orthogonal pathways. These limitations need to be considered when developing new targeted approaches and designing clinical trials<sup>86,92,93</sup>.

#### 1.14.6.2 *Angiogenesis inhibitors*

Angiogenesis is the physiological formation of new blood vessels from pre-existing vessels and has roles in wound healing and repair. In contrast, under a pathological setting such as cancer, angiogenesis supports de novo formation of blood vessels to provide the growing mass with its own blood supply. However, these blood vessels are abnormally formed and tortuous. Anti-angiogenesis substances are forms of targeted therapy that inhibit the new formation of blood vessels in tumors. This concept of inhibiting angiogenesis in cancer was first suggested by Judah Folkman in the early 1970s, but the first angiogenesis inhibitor, bevacizumab (Avastin), wasn't approved for clinical use until 2004. Bevacizumab is used to treat advanced colorectal, kidney, and

lung cancers, as well as adult patients with glioblastoma that progressed following prior therapy. There are two main anti-angiogenesis classes: (i) antibodies or small molecules that target pro-angiogenic factors of tumor cells, such as VEGF, bFGF or PDGF, and (ii) endogenous inhibitors of angiogenesis such as thrombospondin-1, angiostatin, interferons, endostatin, arresten, canstatin and tumstatin that function by inhibiting angiogenesis by targeting vascular endothelial cells. Bevacizumab and other inhibitors of angiogenesis are currently being studied as treatment for many other types of cancer. However, cancer cells can adapt to a hypoxic setting without an adequate blood supply, or produce blood vessels via alternative pathways and survive. To be clinically relevant and successful, multiple therapies would have to be used to inhibit angiogenesis through canonical or non-canonical pathways, as well as inhibit the ability to adapt to a hypoxic environment<sup>94-96</sup>.

#### 1.14.6.3 *Apoptosis-inducing drugs*

Apoptosis, or programmed cell death, is a physiological process of cellular suicide committed to remove damaged, mutated, or aged cells. Apoptosis is initiated when DNA is too damaged to be repaired as a result of various DNA-damaging agents such as radiation or chemotherapy. If a cell doesn't activate apoptosis and die when it should, such as in the case of irreparable DNA damage, the cell will survive with mutations potentially leading to aberrant functions that can cause cancer. Overexpression of anti-apoptotic proteins, inhibition of pro-apoptotic proteins, or the combination of the two can result in cancer. Therefore, apoptotic pathways represent potential targets for therapeutic intervention. Several agents targeting some aspect of apoptosis are being tested in pre-clinical and clinical trials as single agents or combination therapy. Molecules currently being tested include antisense oligonucleotides or small molecule inhibitors against anti-apoptotic genes such as Bcl-2

and inhibitor of apoptosis proteins (IAPs), BH3-mimetics, and histone deacetylases (HDAC) inhibitors. Antisense oligonucleotides are single-stranded synthetic DNA that have the ability to bind target mRNA and inhibit expression of the encoded gene and can enhance sensitivity to cytotoxic drugs. Main limitations for these drugs is that they are rapidly degraded. The development of oblimersen sodium (G3139), an 18-base anti-BCL-2 mRNA agent has had the most promise, and was the first proof of principle for oligonucleotides in inhibiting tumors. Oblimersen is currently being tested in phase I and phase II clinical trials for hematologic and solid cancers that have relapsed or are unresponsive to standard therapy. Activity of IAPs affect cell death by controlling initiator and effector caspases. Overexpression of IAPs have been associated with a poor prognosis and chemoresistance in many cancers, making them a good drug target. Currently, small molecule inhibitors of IAP are being tested in phase I and phase II clinical trials for their efficacy in advanced solid cancers. Small molecule BH3-mimetics are a new class of drugs that antagonize anti-apoptotic Bcl-2 family members by mimicking pro-apoptotic BH3-only Bcl-2 family members. Navitoclax was the first oral BH3-mimetic developed and proved effective against chronic lymphoblastic leukemia. However, in clinical trials navitoclax demonstrated dose limiting thrombocytopenia due to platelet toxicity. This led to the development of a drug with less platelet toxicity, venetoclax. Clinical trials of venetoclax are currently being tested in hematologic cancers to enhance response while minimizing toxicities. HDACs are good potential drug targets in cancer due to their control of gene expression, and the recognition that HDAC overexpression is a critical event in tumorigenesis. The FDA has approved the HDAC inhibitors vorinostat (SAHA) and romidepsin (Istodax) for the treatment of cutaneous T-cell lymphoma, as well as belinostat (Beleodaq) and romidepsin for peripheral T-cell

lymphoma. These HDAC inhibitors are further being investigated for ability to inhibit other hematologic and solid tumors in phase I and II clinical trials<sup>97,98</sup>.

### **1.15 The Omics Era**

Sequencing the human genome along with computational and technological advancements in the 21<sup>st</sup> century have enabled the birth of the omics era. Omics is the overarching word that refers to the collective study of specific fields of biology with the suffix -omics. Omic technologies are concerned with the comprehensive detection of genes (genomics), mRNA (transcriptomics), proteins (proteomics), epigenetic modifications (epigenomics), and metabolites (metabolomics). The integration of this information is referred to as systems biology, which takes a holistic perspective of the complex interactions of a biological system. Using a systems biology approach to understanding cancer has implications in prevention, diagnosis, and treatment<sup>99-103</sup>.

### **1.16 The Promise of Precision Medicine**

Precision medicine refers to the custom management of disease often using extensive omic analyses and a systems biology approach to identify optimal treatment options for an individual patient. Precision oncology is the precision medicine approach applied to cancer patients and involves omic profiling of their tumor to identify drug targets. This approach allows the ability to predict which treatments will work best in different groups of patients and who among them are at the highest risk for rapid progression. To be successful in cancer treatment, we must move from a one-size fits all approach traditionally used in medicine to a precision medicine approach where the right therapy is selected for the right patient at the right time based on their omic profile. A prime example demonstrating the need to move toward precision medicine is EGFR in GBM. EGFR is overexpressed in GBM making it a good target for inhibition with targeted

small molecule tyrosine kinase inhibitors. However, targeted inhibition of EGFR in GBM has been unsuccessful due to variable EGFR expression within a GBM, adaption to EGFR pathway inhibition, and activation of redundant alternative signaling pathways. This example supports the idea that individual cases need to be considered to develop the best treatment plans for the best outcomes to be observed. If successful, precision oncology holds promise in improving quality of life and extending overall survival<sup>99,104–108</sup>.

### **1.17 Molecular Classification of Cancers**

Realizing the potential of precision medicine in cancer is dependent on optimal clinical classification, which has previously been hindered by a lack of molecular insight. Accordingly, The Cancer Genome Atlas (TCGA) was developed to identify molecular alterations involved in cancer and classify patients based on their omic profile. Through this mission, TCGA has profiled 33 cancer types beginning with GBM in 2008 and extending to others, including bladder cancer. The hopes are that the information obtained through TCGA will enable the development of precision medicine approaches to treating cancer<sup>109,110</sup>.

### **1.18 Towards advancing precision medicine – two tales**

Realizing the potential of precision medicine in cancer is dependent on optimal clinical classification, which has previously been hindered by a lack of molecular insight. Accordingly, TCGA was developed to identify molecular alterations involved in cancer and classify patients based on their omic profile and identify molecular subtypes. Through this mission, TCGA has profiled 33 cancer types beginning with GBM in 2008 and extending to others, including bladder cancer in 2014. The hope is that TCGA information and molecular subtype classification will enable the development of precision medicine approaches to treating cancer. In some cancers, identification of molecular

subtypes has failed to translate clinically. GBM and muscle-invasive bladder cancer (MIBC) are two prime examples that demonstrate little clinical advancements despite having molecular subtypes defined. Treatment options and overall survival for these cancers has minimally changed for these cancers over the past three decades, with less than a 5% five-year survival rate for GBM and metastatic MIBC. Furthermore, potential therapeutic vulnerabilities have been identified for each of these cancers, but clinical trials with targeted therapies aimed at the vulnerabilities have failed to demonstrate effectiveness. This is likely due to the lack of integration of knowledge about intra-tumoral heterogeneity and the tumor microenvironment. Precision medicine approaches in GBM and MIBC are direly needed to observe changes in overall survival and have the potential to be successful if intra-tumoral heterogeneity and the tumor microenvironment are taken into account<sup>111–116</sup>.

## **1.19 Glioblastoma multiforme (GBM)**

### **1.19.1 Gliomas**

GBM is the most common, aggressive and lethal malignant primary brain tumor, accounting for 46.1% of all malignant primary brain and CNS tumors diagnosed in the United States<sup>117</sup>. GBM is a glioma, which are the most common type (80%) of malignant primary brain and central nervous system (CNS) tumor, and are comprised of cells that have similar histologic features of glial cells (astrocytes, oligodendrocytes, and ependymal cells)<sup>117–120</sup>. Adult diffuse gliomas are diffusely infiltrating tumors and are classified by the world health organization (WHO) as grade II and III astrocytomas and oligodendrogliomas, as well as grade IV glioblastomas (GBM)<sup>121</sup>.

### 1.19.2 Site

The majority of adult GBM tumors (95%) occur in supratentorial locations (frontal, temporal, parietal, and occipital lobes), though in rare occasions may occur in the cerebellum, brainstem, and spinal cord. In order of incidence, GBM most frequently occurs in the frontal lobe, followed by multiple lobes simultaneously, temporal lobes, and parietal lobes<sup>122,123</sup>. In contrast to adults, pediatric GBM occurs more frequently (10-30%) in central locations such as the ventricles, brain stem, and cerebellum<sup>124,125</sup>.

### 1.19.3 Epidemiology

In the United States, the average annual age-adjusted incidence rate is 2-3 new GBM diagnoses per 100,000 people per year, or approximately 13,200 new cases per year. GBM is uncommon in children and in adults increases in frequency with age. At diagnosis, the median age is 64 years, peaking in incidence between 45 and 75 years of age. GBM affects more men at a rate of approximately 1.5 times that of women and is 2-3 times more common in Caucasians than other race groups<sup>126,127</sup>.

### 1.19.4 Prognosis

GBM is an incurable disease with an exceptionally poor prognosis. A population-based study in the U.S. showed that median survival for GBM has improved from 4.9 months to 11.5 months for the periods of 1980 to 1994 and 2005 to 2009, respectively. Currently, the median overall survival for GBM is only about 14-15 months, with less than a 5% 5-year survival rate. These extensions in overall survival, albeit minimal, are



likely attributed to the introduction of temozolomide therapy into the treatment regimen in 2005 leading to its current widespread use<sup>126,127</sup>.

#### 1.19.5 Prognostic Factors

While all patients with GBM have a dismal prognosis, there are some factors that help identify better or worse prognosis within the disease. Prognostic factors for GBM include extent of surgical resection of the tumor, Karnofsky Performance Scale (KPS) score, age, O<sup>6</sup>-methylguanine-DNA methyltransferase (*MGMT*) promoter methylation, and isocitrate dehydrogenase 1 (*IDH1*) mutation. *MGMT* promoter methylation and *IDH1* mutation status are intriguing prognostic factors as they indicate genetic differences between tumors and will be discussed in further detail in subsequent sections. The KPS score classifies patients based on their functional abilities or impairments on a scale of 0 to 100. The higher the score, the greater the functionality; the lower the score, the greater the impairment. KPS score and age are more obvious prognostic factors as they indicate the ability to recover after treatment. Extent of surgical resection is also an obvious prognostic factor as a patient would likely live longer with removal of more of the tumor. In general, a younger patient with an extensive tumor resection, *IDH1* mutation, *MGMT* promoter methylation, and a high KPS score prior to surgery would have the best prognosis of all GBM patients. In contrast, an older patient, with a minimally resected tumor, *IDH1*-WT, *MGMT* promoter un-methylated, and a low KPS score would have the worst prognosis of all GBM patients<sup>128–131</sup>.

#### 1.19.6 Risk factors

Accepted risk factors for developing GBM are rare genetic mutations, a family history, and exposure to ionizing radiation. However, the majority of cases are not attributed to these factors. Rarely, GBM is a consequence of hereditary tumor

predisposition syndromes such as Li-Fraumeni syndrome (inherited mutations in the tumor suppressor genes *TP53* or *CHEK2*) and constitutional mismatch repair-deficiency or Turcot syndrome (inherited biallelic mutations in mismatch repair genes *MSH2/6*, *MLH1*, *PMS2*). In these cases, there are usually multiple family members with a history of early-onset cancers. In other GBM cases, there is a clear family history of brain cancers with no known genetic cause. Exposure to ionizing radiation is the only known risk factor for developing GBM, aside from genetic considerations. It's estimated that ionizing radiation increases the risk of developing GBM by 2.5%<sup>120,126–128</sup>.

#### 1.19.7 Symptoms

Patients with GBM have progressive neurological symptoms that depend on location and size of the tumor. Symptoms can be a direct effect of tumor tissue undergoing necrosis and destroying brain tissue, leading to focal neurologic deficits (40-60%) and cognitive impairment. These types of focal effects are highly dependent on the region of the brain the tumor resides. For instance, patients who present with personality changes (20-40%) are due to their tumor being in their frontal lobe imparting cognitive impairment, while patients who have hearing and visual symptoms have their tumor in the temporal lobe. Other focal neurologic symptoms include memory loss, motor weakness, and speech difficulty. Symptoms may also be due to a mass effect causing secondary pathological effects as a result of increased tumor size. Consequently, there is increased edema and intracranial pressure, which leads to a displacement of intracranial contents resulting in headaches, the most common symptom in 50-60% of GBM patients. Headaches may also be accompanied by nausea and vomiting. New onset seizures are also symptoms in GBM patients<sup>126,132,133</sup>.

#### 1.19.8 WHO classification of CNS tumors

Historically, classification of brain tumors was based on histology and level of differentiation. In 2016, the WHO updated its 2007 classification parameters to incorporate molecular features into the classification scheme of CNS tumors, signifying a shift in century-old diagnostic principles to the molecular era. The new classification is based on the idea of an integrated or layered diagnosis, combining phenotype and genotype classification. The integrated diagnosis layer is the top layer and is only applicable if all of the information of the lower layers is available. The second layer is for histological classification of cell type (e.g. astrocytoma or oligodendroglioma). The third layer involves grading into grade I to IV based on the state of differentiation and level of malignancy. The last layer considers molecular features (e.g. IDH-wildtype or IDH-mutant)<sup>121</sup>.

Accordingly, GBM is designated grade IV due to being undifferentiated with a high level of malignant characteristics (highly invasive, necrosis, mitotic figures, and vascular endothelial hyperplasia), and is divided into the following three groups:

- i. GBM, IDH-wildtype - corresponds similarly with the clinically defined primary GBM group representing 90% of cases.
- ii. GBM, IDH-mutant - corresponds closely to the clinically defined secondary GBM group representing 10% of cases.
- iii. GBM, NOS (not otherwise specified) - a diagnosis given when there is insufficient molecular information to make a firm diagnosis.

#### 1.19.9 Primary and secondary GBM

GBM has traditionally been divided into primary and secondary types based on clinical characteristics and distinct genetic modifications. Primary or *de novo* GBM arises

with no known clinical or histological precursor and primarily affects patients over 55 years of age (mean age = 64 years). Primary GBM is also typified by the presence of several genetic alterations such as *PTEN* and *TERT* promotor mutations, overexpression of EGFR and MDM2, as well as *CDKN2A* (p16/INK4a) deletion. Secondary GBM tends to occur in younger patients (mean age = 45 years) with a history of a precursor low grade diffuse glioma lesion. Genetic aberrations characteristic of secondary GBM include mutations in *IDH1/2*, *ATRX*, and *TP53*, as well as amplification of platelet-derived growth factor (PDGF) signaling by over expression of PDGFA and PDGFRA. Loss of heterozygosity of the 10q chromosomal arm occurs in both primary and secondary GBM with 70% and 65% of patients affected, respectively<sup>134–136</sup>.

#### 1.19.10 Glioma - CpG island methylator phenotype (G-CIMP)

G-CIMP, a promoter hypermethylator phenotype, may be an additional method to further classify secondary GBM. Studies using a GBM tumor tissue database identified this phenotype in younger patients with IDH1 mutant tumors who had a better prognosis compared with similarly classified patients without G-CIMP. Independent of tumor grade and histology, demethylation signifies glioma progression with G-CIMP-high tumors evolving to G-CIMP-low at recurrence<sup>129,137,138</sup>.

#### 1.19.11 Macroscopic and Histologic Features of GBM

As the multiforme designation suggests, GBM displays diverse macroscopic and histologic features (Figure 1). At the macroscopic level, both multifocal and multicentric disease can be appreciated. Frequently GBM will be displayed as a single, large, irregularly shaped tumor with thick margins surrounded by vasogenic edema, a central necrotic core, and the potential for a hemorrhagic element. In multifocal disease, tumor foci are noticeably linked by abnormal white matter, which represents microscopic

dissemination of tumor cells. In multicentric disease, no connections between tumor foci can be appreciated. Grossly there are heterogeneous features of hemorrhagic, necrotic (soft and yellow), cystic (firm and white), and gelatinous regions identified. Histologically there is a diversity of patterns with pleomorphic cell populations featured throughout the tumor. GBM displays high cellularity with a range of cell architectures such as small undifferentiated tumor cells, large multinucleated tumor cells, pseudopalisading cells around regions of necrosis, proliferative vascular endothelial cells, and glomeruloid vascular structures. Microscopic infiltration into normal brain structures and a high Ki-67 labeling index, indicating proliferative activity, are also characteristic features of GBM<sup>121,136,139</sup>.

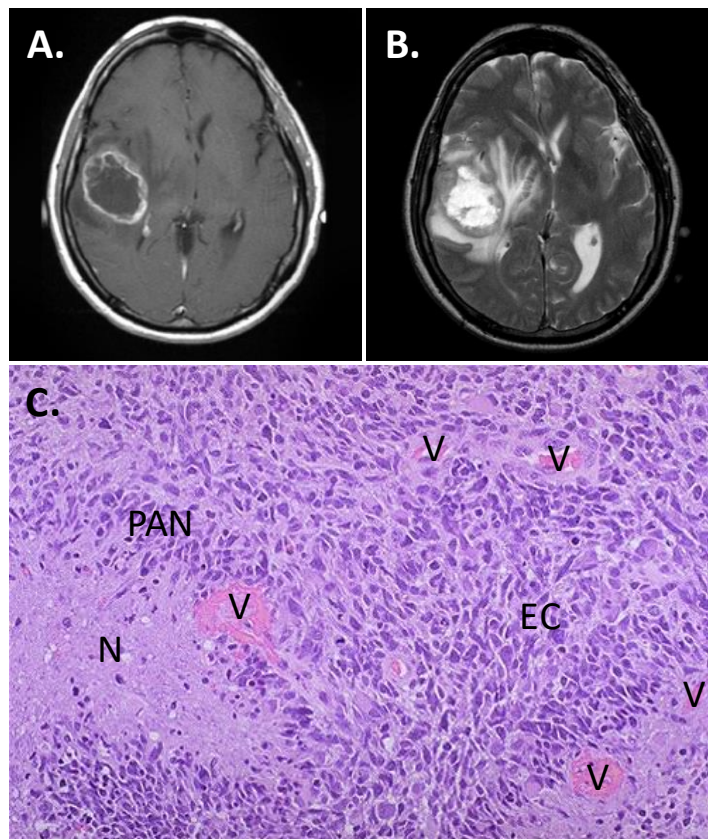


**Figure 1. Macroscopic and histologic view of glioblastoma.**

(A) Post-gadolinium contrast T1-weighted MRI showing a large mass in the superior part of the right temporal lobe with irregularly enhanced margins. (B) T2-weighted MRI demonstrating an intense signal in the center of the mass, suggestive of necrosis. (C) Hematoxylin and eosin staining of a glioblastoma section showing enhanced cellularity (EC), necrosis (N), pseudopalisading cells around necrosis (PAN), and prominent vascularity (V). (A and B) Adapted from Glioblastoma NOS Case courtesy of A.Prof Frank

#### 1.19.12 Histological GBM variants

There are several histological variants of glioblastoma recognized with distinct histologic features. Giant cell GBM, gliosarcoma, and epithelioid GBM are all IDH-wildtype GBM. Other patterns include GBM with primitive neuronal component, small cell GBM and granular cell GBM. Giant cell glioblastoma display large cells that are up to 400 µm diameter that are multinucleated with greater than 20 nuclei per giant cell. A stromal reticulin network occasionally will be present and these cells have a high frequency of TP53 mutations. Gliosarcoma exhibit gliomatous and sarcomatous features. This variant has similar genetic alterations as traditional GBM, though with infrequent MGMT promoter methylation and *EGFR mutations*. Epithelioid GBM display large epithelioid cells that have an eosinophilic-rich cytoplasm, prominent nucleoli, chromatin with vesicular components, and may have rhabdoid cells present. This variant lacks classic IDH-wildtype genetic features such as *EGFR* amplifications and chromosome 10 loss. GBM with primitive neuronal component was previously referred to as GBM with primitive neural ectodermal tumor (PNET)-like component, and has well-demarcated nodules with neuronal differentiation exhibited in primitive cells. This GBM variant occasionally has MYC or MYCN amplification with approximately 25% developing from a low-grade glioma precursor and are IDH-mutant. Small cell GBM features uniformly small cells that resemble oligodendrogliomas, which regularly amplify *EGFR*. Granular cell GBM is characterized by lysosome-rich cells that are granular or macrophage-like<sup>121,140</sup>.

#### 1.19.13 Treatment

GBM is treated through a multimodal approach consisting of surgical debulking of the tumor, followed by adjuvant radiation therapy and concomitant temozolomide chemotherapy<sup>141</sup>.

The primary goal of surgery is to resect as much of the tumor as possible while preserving neurological function. Debulking surgery usually reduces symptoms associated with the mass effect of the tumor such as increased intracranial pressure, seizures and neurological deficits, thereby improving the quality of remaining life and possibly prolonging life. The extent of surgical resection usually depends on the location of the tumor and how crucial that site is to normal function. However, complete resection is impossible due to the highly infiltrative nature of GBM cells, which invade normal brain tissue and create undefined tumor margins<sup>141,142</sup>.

Several intraoperative techniques are used to improve the extent of surgical resection while preserving normal brain function. For tumors involved in the speech, sensory or motor cortex, an awake craniotomy may be performed along with frameless computer guided stereotaxis and cortical stimulation to identify the location of these cortices and avoid them during resection. This technique incorporates previously acquired MRI and CT scans with a neuronavigational system to identify intracranial locations. Alternatively, intracranial navigation can assist the resection in real time by employing intraoperative CT or MRI scanners. The latter technique does not rely on preoperative data, and can identify residual tumor after initial resection and can guide further resection. Despite the attempt for complete resection and advancements in technology to assist in complete resection, recurrences are almost always inevitable<sup>143-</sup>

146.

Seminal studies in GBM have shown that radiation therapy following surgery extends survival compared with surgery alone. Therefore, the treatment protocol for GBM patients includes post-operative radiation therapy to kill any remaining tumor cells that were unresectable during surgery, including infiltrating tumor cells that may be present beyond the visible tumor margin<sup>147</sup>. Unfortunately, some tumors may exhibit radio-resistance and recur. There are also side effects associated with radiation therapy and include radiation-induced necrosis and permanent neuronal damage<sup>141,148</sup>.

Following surgery, median survival was improved in GBM patients treated concomitantly with temozolomide and radiation therapy (14.6 months) compared to radiation therapy alone (12.1 months; Figure 2). Other chemotherapy regimens other than temozolomide have been tested in clinical trials, but temozolomide has demonstrated superiority. Therefore, the standard chemotherapy treatment for GBM is temozolomide and is administered concurrently with radiation therapy, as well as 6 to 12 cycles after radiation therapy. Temozolomide is given the first 5 days of each 28-day cycle, followed by a recovery period of 23 days. Side effects of temozolomide treatment include nausea, vomiting and dose-limiting myelosuppression<sup>65,149</sup>.



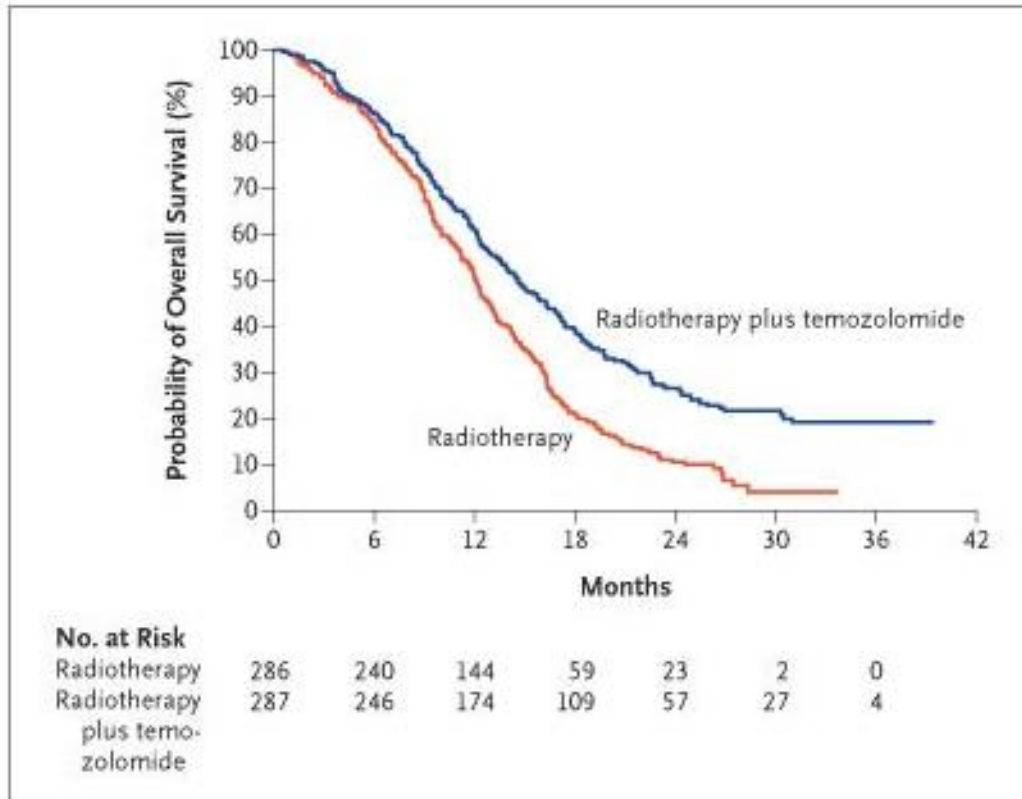


**Figure 2. Kaplan-Meier estimates of overall survival by treatment group.**

The radiotherapy plus temozolamide group demonstrated a longer overall survival as compared to the radiotherapy alone group with a hazard ratio for death at 0.63 (95% confidence interval, 0.52-0.75;  $p < 0.001$ ). Adapted from “Radiotherapy plus concomitant and adjuvant temozolomide for glioblastoma” by R. Stupp, et.al., 2005, *N Engl J Med*, Volume 352 (Issue 10), p.987-96. Copyright [2005] by Massachusetts Medical Society<sup>150</sup>.

Aside from the standard of care approaches to treat the tumor, GBM management also includes supportive care, which entails treating worsening symptoms due to the tumor or the standard treatment. Thorough management includes treating cerebral edema, seizures, cognitive impairment, mood disorders, as well as other symptoms previously described<sup>133,141,151</sup>.

#### 1.19.14 GBM Molecular Subtypes

In 2008, TCGA began a series of systematic studies of different cancer types, and GBM was the first to be investigated. The initial study involved the analysis of 206 GBMs at the genomic and transcriptomic level, which allowed the detection of somatic modifications that commonly converged on three signaling pathways. The common pathways altered include the p53 stress response pathway (87% of GBMs), Rb cell cycle control signaling pathway (78% of GBMs), and receptor tyrosine kinase/RAS/PI3K signal transduction pathway (88% of GBMs). Despite the convergence on common pathways, extensive inter-tumor genomic heterogeneity was also appreciated. In 2010, Verhaak and colleagues reported the results of employing an iterative consensus clustering method to group the cohort of patients in the TCGA analysis based on similar molecular features and resolved the inter-tumor heterogeneity, leaving intra-tumor heterogeneity unresolved. This resulted in the classification of GBM into four distinct molecular subtypes based on gene expression and are identified as proneural, neural, classical, and mesenchymal (Figure 3)<sup>115,116</sup>.

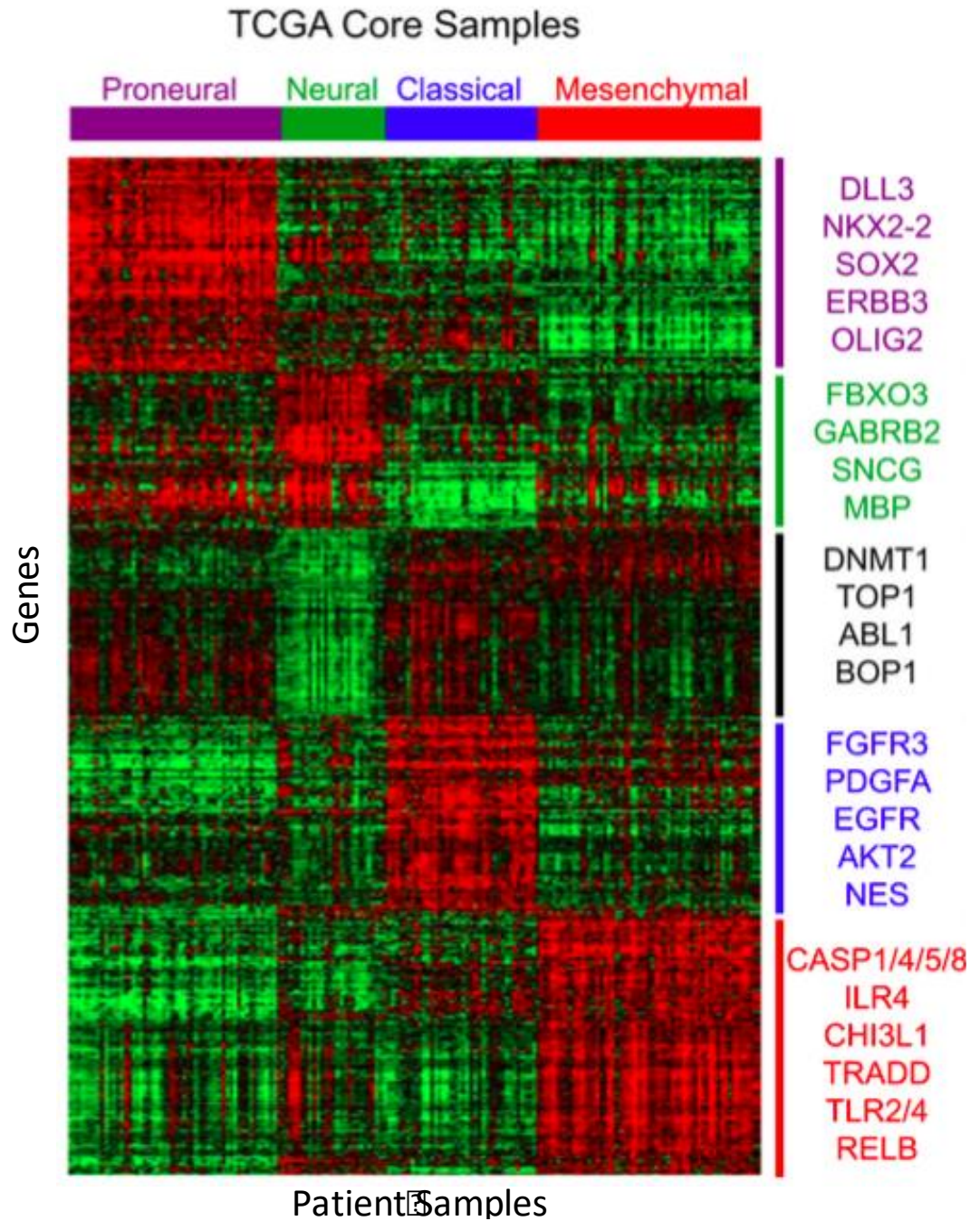


**Figure 3. GBM molecular subtypes as defined by TCGA.**

Heatmap of TCGA patient samples (x-axis) ordered based on molecular subtype predictions and an 840-gene list (y-axis) was clustered using 173 TCGA GBM samples. Prominent genes in each cluster are labeled on the left. Adapted from "An integrated genomic analysis identifies clinically relevant subtypes of glioblastoma characterized by abnormalities in PDGFRA, IDH1, EGFR and NF1" by R. Verhaak, et.al., 2010, *Cancer Cell*, Volume 17 (Issue 1), p.98. Copyright [2009] by the Elsevier Inc<sup>115</sup>.

The proneural subtype is characterized by *PDGFRA* amplifications, as well as *IDH1* and *TP53* mutations. Modifications in *PDGFRA* and *TP53* were seen in other subtypes, but the majority were seen in the proneural subtype. IDH1-mutant GBM are nearly exclusive to proneural tumors, and harbor a DNA hypermethylation profile termed G-CIMP as defined in a previous section, which provide a survival advantage of this subtype over others. Interestingly, proneural tumors are also enriched in oligodendrocyte proneural genes<sup>115,137,138</sup>. The classical subtype is typified by *EGFR* amplification and loss of *CDKN2A*. Classical tumors distinctively lack *TP53* mutations and have similar enrichment patterns as astrocytes<sup>115,152</sup>. The mesenchymal subtype typically has *NF1* deletion or mutations, and mutations in *PTEN* and *TP53*. Notably, this subtype has enrichment of genes expressed in cultured astroglia cells<sup>115,116</sup>. Distinct molecular aberrations have not been identified for the neural subtype. However, this subtype has been found to have similar gene expression to normal astrocytes and oligodendrocytes<sup>115</sup>. Recent studies attempting to validate GBM molecular subtypes, as well as single cell profiling of GBM tumors indicate that the neural subtype is not a true subtype<sup>153,154</sup>.

The molecular subtypes identified through the auspices of TCGA are a valuable reference for GBM<sup>110</sup>. However, these subtypes have yet to find clinical utility. While molecular subtypes were able to resolve general inter-tumor heterogeneity, intra-tumor heterogeneity remains unresolved<sup>155</sup>. Recent regional and single-cell studies have shown that indeed various subtypes had the ability to co-exist within an individual tumor<sup>153,154</sup>. The assigned subtype likely reflects the dominant expression profile of the tumor sample isolated at a particular location and time. Furthermore, regional biopsy sampling may confound subtyping in cases where samples are obtained from the most convenient location, not necessarily the most malignant region due to it residing in an

eloquent location. Additionally, sampling may have been directed by MRI intensity, which tends to coincide with vasculature leakiness, not the region of proliferating tumor<sup>156,157</sup>.

#### 1.19.15 Resistance to standard treatment

The mechanism of action of temozolomide is DNA alkylation by methylating purines at the N7 and O6 position on guanine and N3 position on adenine<sup>158–160</sup>. Temozolomide cytotoxicity is induced primarily by O-6-methylguanine, which erroneously hydrogen bonds with thymine during DNA replication. Failure of the DNA mismatch repair (MMR) system to identify an appropriate complementary base, ultimately results in single and double stranded DNA breaks, which blocks progression of the cell cycle and triggers apoptosis. However, cells can escape apoptosis and lead to temozolomide resistance if deficient in the MMR system or if MGMT is expressed. MGMT expression confers resistance due to its ability to transfer the methyl group of O-6-methylguanine to a sulfur in MGMT's own catalytic pocket, which repairs guanine and inactivates MGMT. Each MGMT copy can transfer only one methyl group making repair dependent on the level of MGMT expression. Accordingly, epigenetic silencing of MGMT via MGMT promoter methylation is associated with longer overall survival in patients treated with the standard of care<sup>161,162</sup>. The addition of the MGMT inhibitor O-6-benzylguanine to temozolomide treatment has been investigated to induce sensitization, but inhibition of MGMT has not been successfully sustained through this approach<sup>163,164</sup>.

Furthermore, temozolomide treatment induces mutations in the setting of silenced MGMT and deficient MMR, which may lead to a hypermutator phenotype frequently observed in recurrent tumors<sup>165,166</sup>. Currently, the prognostic significance of the hypermutator phenotype is not fully understood. Additionally, GBM mesenchymal cells display resistance to radiation and recurrent tumors typically display a shift to the

mesenchymal subtype<sup>160,167</sup>. However, it is not yet appreciated how non-mesenchymal tumors develop radiation resistance and recur as mesenchymal.

#### 1.19.16 Heterogeneity

Glioblastoma is the archetypal heterogeneous tumor displaying a high degree of both inter- and intra-tumoral heterogeneity<sup>168,169</sup>. Studies investigating inter-tumor heterogeneity have led to the molecular subtyping classification previously described. Intra-tumoral heterogeneity, on the other hand, has not been studied in depth and is not well understood<sup>155</sup>. Spatially distinct GBM samples analyzed in bulk or at the single cell level have revealed that morphologic, genotypic and phenotypic diversity exists<sup>153,154,170</sup>. This intra-tumoral heterogeneity contributes to clonal adaptations to the microenvironment with individual clones demonstrating unique proliferative, differentiation, and therapeutic responses. The heterogeneous responses in a single tumor likely underlie the failure of standard treatment to achieve long-term survival. The interplay between inter and intra-tumoral heterogeneity highlights the need for non-reliance on single-agent chemotherapy. Spatiotemporal sampling of GBM has demonstrated that a single-site biopsy is insufficient in capturing an accurate assessment of the heterogeneous genetic alterations in the bulk tumor<sup>171,172</sup>. A precision oncology approach will be necessary to effectively target spatially heterogeneous clonal aberrations and extend overall survival.

#### 1.19.17 Recent Advancements in Treatment

Numerous immune-based therapies are currently being investigated for the treatment of gliomas and include immune checkpoint inhibitors, peptide vaccines, dendritic cell vaccines, and engineered T-cell therapy. In particular, immune checkpoint blockade has proven its value in treating patients with a number of cancer types. Robust responses have been witnessed in tumors that have high mutational loads and are

deficient in MMR genes, such as non-small cell lung cancers and melanomas. This has garnered enthusiasm for the use of immune checkpoint blockade in treating GBM due to the presence of a hypermutator phenotype and MMR deficiency in some tumors.

On May 23, 2017, pembrolizumab (Keytruda®), a PD-1 inhibitor, was granted accelerated approval by the FDA for the treatment of unresectable or metastatic solid tumors that are microsatellite instability-high, or MMR-deficient and progressed after treatment<sup>173,174</sup>. This approval was granted for any tumor site or histology, making this the first tissue and site independent approval by the FDA<sup>175</sup>. Immune checkpoint inhibitors are now being evaluated for newly diagnosed GBM (CheckMate-498, and CheckMate-548) and for recurrent GBM (CheckMate-143)<sup>176,177</sup>. However, results have been discouraging and calling to question appropriate patient selection. PD-L1 and lymphocyte marker expression have been used as biomarkers to predict response to immune checkpoint blockade, though have proven unsuccessful<sup>178,179</sup>. It is thought that immunohistochemistry techniques are inconsistently utilized rendering the biomarkers unsuitable for use. Additionally, pembrolizumab is currently being employed in recurrent malignant glioma patients (grades II–IV) with a hypermutator phenotype (MK-3475)<sup>180</sup>. The results of this trial will help identify whether immune checkpoint blockade is effective in the hypermutator phenotype. Although immune checkpoint blockade has proven unsuccessful in gliomas thus far, it is important to not disregard these therapies as useful and further explore how to properly select patients for maximal effectiveness in clinical trials.

Optune® is another type of treatment recently FDA approved for the treatment of newly diagnosed adult GBM patients (22 years old or older) in combination with temozolomide after standard of care management<sup>181,182</sup>. For the treatment of recurrent

GBM, Optune® is intended to be used alone as an alternative to standard therapy. Optune® is a portable device that uses 4 adhesive patches applied to the scalp, called transducer arrays, to produce electric fields known as tumor treating fields (TTFields). Transducer arrays connect to the device and battery, which are conveniently carried in a back or shoulder bag. TTFields work by interfering with cancer cell division and may destroy them. The recommendation is that the device be worn at least 18 hours per day for best treatment responses<sup>182–185</sup>.

The EF-14 phase 3 clinical trial using Optune® in conjunction with temozolomide for newly diagnosed GBM showed a progression-free survival and overall survival advantage versus treatment with temozolomide alone. The open-label trial enrolled 695 patients from 83 centers and assigned 466 patients to the TTFields plus temozolomide arm and 229 patients to the temozolomide arm alone, while balancing patient characteristics between the groups. Median progression-free survival was 6.7 months for the TTFields plus temozolomide group as compared to 4.0 months for the temozolomide alone group. Similarly, a survival advantage was seen in the TTFields plus temozolomide arm with a median overall survival of 20.9 months versus 16.0 months in the temozolomide arm alone. No significant increases in systemic adverse events were identified in the TTFields plus temozolomide arm as compared to the temozolomide arm alone. However, Optune® treatment was associated with mild to moderate skin irritation beneath the transducer arrays. Limitations of the study include the lack of a placebo control, as well as the requirement of patients receiving the TTField therapy to continuously carry the Optune® device and have it applied to a shaved scalp. Clinical trials will continue to evaluate the benefit of other Optune® combinations besides temozolomide<sup>181–186</sup>.



#### 1.19.18 Remaining impediments in advancing precision medicine in GBM

Advancing precision medicine in the treatment of GBM will require stratification of tumors into subtypes that differ in outcome and therapeutic vulnerability. Successful stratification would improve clinical decision-making, design of clinical trials, and patient outcomes. Unfortunately, immense intra-tumoral heterogeneity in GBM has hindered the development of stratification strategies<sup>155</sup>. GBMs high degree of heterogeneity contributes to inherent and acquired resistance to therapy and doesn't allow single site sampling to capture the repertoire of genetic aberrations that exist within a tumor<sup>153,168</sup>. Advancement into the precision medicine era for GBM will be accomplished when we are able to clearly identify the diversity of genetic drivers within a GBM and treat the patient accordingly with a treatment combination that targets those drivers.

## 1.20 Bladder Cancer

### 1.20.1 Natural History of Bladder Cancer

Bladder cancer is the sixth most prevalent cancer in the United States and will contribute to an estimated 81,190 new cases and 17,240 deaths in 2018<sup>1</sup>. Males are disproportionately affected at a 4-fold higher rate than women, though the gender bias is not fully understood. Risk factors for bladder cancer include tobacco smoking, exposure to carcinogenic industrial compounds such as aromatic amines, arsenic-contaminated water, previous cyclophosphamide chemotherapy, and a family history. The most common clinical presentation of bladder cancer is gross or microscopic hematuria, or blood in the urine. Approximately 95 percent of cases originate from the inner epithelial lining of the bladder, or urothelium, making the majority of bladder cancers urothelial carcinomas. Urothelial carcinomas are broadly classified as non-muscle invasive (NMIBC; tumor stages CIS, Ta, T1) based on the confinement of the tumor to the urothelium, or muscle-invasive bladder cancer (MIBC; tumor stages T2-T4), the more aggressive form of the disease, based on the invasion of the tumor into the surrounding muscle. Approximately 25% of patients are diagnosed with MIBC or metastatic disease at the time of diagnosis resulting in a worse prognosis. The majority of deaths are due to MIBC, (34% 5-year survival) and progression to metastasis results in even poorer survival (5% 5-year survival). In advanced disease, MIBC spreads beyond the bladder and metastasizes to distant sites such as lymph nodes, bone, liver, lung, or peritoneum<sup>187-191</sup>.

### 1.20.2 Standard of Care in Urothelial Carcinoma

Treatment of urothelial carcinoma is dependent on invasiveness, histological grade and clinical stage<sup>192</sup>. NMIBC treatment consists of transurethral resection of the bladder tumor followed non-systemic mitomycin C, a DNA crosslinker, applied directly

into the bladder, also known as intravesical chemotherapy. Low grade NMIBC patients undergo surveillance or repeated treatment with intravesical chemotherapy. Moderate- to high-grade NMIBC patients typically receive intravesical BCG immunotherapy to stimulate an immune response in the tumor microenvironment. For over 30 years, the first-line standard of care for patients with MIBC is a regimen of cytotoxic chemotherapy, surgical cystectomy along with an extended bilateral pelvic lymphadenectomy. Randomized-control trials have demonstrated a survival benefit with neoadjuvant combination chemotherapy along with radical cystectomy over surgery alone. Due to these studies, neoadjuvant chemotherapy is recommended prior to surgery to shrink the tumor and reduce the risk of recurrence. Despite the demonstrated survival benefit, widespread administration of neoadjuvant chemotherapy is not yet practiced prior to surgery with reports showing approximately only 20% of patients with MIBC get neoadjuvant chemotherapy. In these settings, chemotherapy is administered as an adjuvant therapy after surgery. Reasons for non-administration of neoadjuvant therapy include toxicity concerns and delay of surgery. For patients who are able to tolerate neoadjuvant or adjuvant treatment, cisplatin-based combination chemotherapy is recommended and includes methotrexate, vinblastine, doxorubicin and cisplatin (established in 1985). Another cisplatin-based treatment includes gemcitabine plus cisplatin, which is a better option in older patients or when limiting toxicities is of interest<sup>193,194</sup>.

### 1.20.3 The tumor microenvironment as a pro-proliferative cue

Bladder cancer tumors frequently exhibit heterogeneous cellular differentiation states that correlate with outcome. Hence, differentiation state plasticity in bladder cancer may allow subsets of cells to thrive in certain TME settings and contribute to aggressiveness. Currently, the extent to which extrinsic factors, within the TME,

promotes proliferation and facilitates differentiation in MIBC remains unclear.

Additionally, there has been a lack of comprehensive studies to examine proteins in the ME that may have effects on MIBC proliferation. Understanding interactions between MIBC and the TME may aid the development of new therapeutic strategies<sup>35-38</sup>.

#### 1.20.4 Bladder cancer differentiation states

The bladder urothelium is comprised of an epithelial lining of cells with 3-5 layers corresponding to the basic architecture of basal, intermediate, and luminal umbrella cells<sup>195,196</sup>. Each cell type represents a unique stage in differentiation corresponding to early, mid, and terminal differentiation, which are typically distinguished by their unique cytokeratin (KRT) expression. Basal cells are cuboidal, rest on the basement membrane, and represent an early differentiation state. KRT5/17 and CD44 expression identify basal cells of the urothelium. KRT14 is expressed in early stem/progenitor cells in the basal population. Basal cells give rise to larger intermediate cells that form several layers of the urothelium. Some studies show that the loss of KRT14 and remainder of KRT5 demark the intermediate cell population, while other studies suggest that KRT 8/18 expression better identify this population. Intermediate cells give rise to large, flat superficial umbrella cells that are adjacent to the bladder lumen. Expression of KRT20 and uroplakin (UPK) 1A/2 identify this terminally differentiated population of luminal umbrella cells<sup>197,198</sup>.

MIBCs are frequently heterogeneous with individual cells within a tumor exhibiting distinct differentiation state phenotypes. This heterogeneity allows subpopulations of cells within the tumor to differentially respond to TME cues and adapt to their environment differently. Even clonal populations of cells can have a differential response when exposed to different environmental signals. Cells can adapt to their environment by becoming plastic and intrinsically altering their differentiation. Moreover,

any of these cell types can undergo malignant transformation and give rise to proliferative tumors with diverse phenotypes and propensities to metastasize. Recent studies using a KRT14 Cre reporter mouse followed by lineage-tracing in bladder urothelium demonstrated that KRT14 marks progenitor cells that have the capacity to give rise to all urothelial layers. Patient bladder tumors with high expression of KRT-14 have a poorer prognosis, suggesting that cellular differentiation state affects disease progression, treatment efficacy, or both. To prevent disease recurrence and progression, it is crucial to understand the molecular interactions between a heterogeneous population of tumor cells and their environment and how this allows subpopulations of cells to proliferate and thrive<sup>197,199–201</sup>.

#### 1.20.5 Molecular subtypes

Over the past several years, TCGA and other groups have described distinct molecular subtypes in MIBC based on molecular signatures. In 2013, TCGA identified 4 mRNA expression-based molecular subtypes using a 131-tumor set. In 2017, TCGA further refined their molecular subtyping and identified 5 subtypes by extending their 131-tumor set to 408 (Figure 4). The 5 subtypes were concordant with the 4 initial subtypes described. They were able to identify the well-established luminal and basal subtypes of bladder cancer while further delineating the luminal subtype and identifying a new neuronal subtype. The 5 MIBC expression subtypes include: luminal-papillary (n = 142, 35%), luminal-infiltrated (n = 78, 19%), luminal (n = 26, 6%), basal-squamous (n = 142, 35%), and neuronal (n = 20, 5%). Though, due to purity concerns, some of the subtypes identified may be a consequence of increased signal from other cell types in the tumor microenvironment<sup>112,113</sup>.

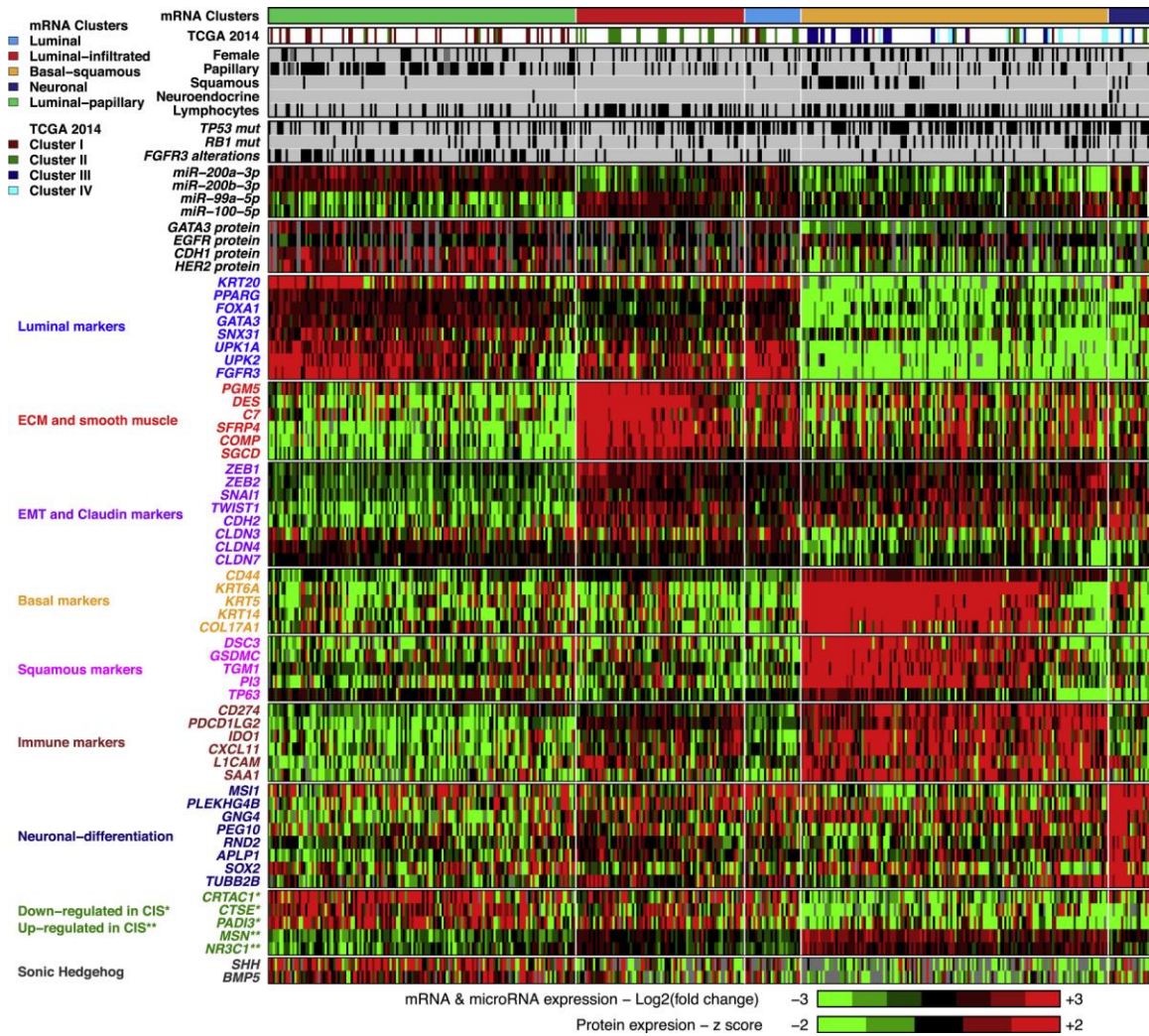


**Figure 4. MIBC molecular subtypes as defined by TCGA.**

Heatmap of MIBC TCGA patient samples (x-axis) ordered based on molecular subtype predictions using normalized expression for miRNAs and proteins, and z-score of log<sub>2</sub> expression for selected genes (y-axis). Molecular subtypes (top, left to right) include luminal-papillary, luminal-infiltrated, luminal, basal-squamous and neuronal. Adapted from "Comprehensive Molecular Characterization of Muscle-Invasive Bladder Cancer" by A.G. Robertson, et.al., 2017, *Cell*, Volume 171, p.540-556. Copyright [2017] by the Elsevier Inc.

In general, samples from the luminal subtypes had increased expression of uroplakins (UPK1A and UPK2) as well as differentiation markers FOXA1, GATA3 and PPARG. Distinct clustering of the 3 luminal subtypes is confounded by purity differences, which may have contributed to their ultimate separation into subtypes. In favor of being truly distinct subtypes, there were differences in wild-type p53, EMT, and stromal gene

signatures among the 3 luminal subtypes. Though, this may be a consequence of varying levels of contamination from the tumor microenvironment<sup>112,202</sup>.

The luminal-papillary subtype was enriched in tumors with papillary histology, lower stage and higher purity. *FGFR3* mutations, amplification, overexpression, and TACC3 fusions were prominent features of this subtype. These tumors also had low carcinoma in situ (CIS) expression scores and active SHH signaling. These features collectively imply that luminal-papillary tumors developed from a precursor papillary NMIBC. Of the 5 subtypes, luminal-papillary tumors have the best survival outcome with 5-year survival rates at approximately 60%, indicating a low risk for progression. Preclinical studies suggest that these tumors do not respond well to cisplatin-based neoadjuvant chemotherapy. However, the high frequency of *FGFR3* alterations suggests that patients with these tumors may benefit from FGFR3 tyrosine kinase inhibitors<sup>112</sup>.

The luminal-infiltrated subtype has the lowest purity with lymphocytic infiltrates, and high expression of smooth muscle and myofibroblast genes, indicating that gene signatures from non-tumor cell types may be a driver of this subtype. There is also increased expression of EMT genes and the immune markers CD274 (PD-L1) and PDCD1 (PD-1). Initial studies on the luminal-infiltrative subtype show that this subtype is resistant to cisplatin-based chemotherapy and sensitive to immune checkpoint inhibition with anti-PDL1 treatment. Ongoing studies are continuing to test this hypothesis.

The luminal subtype most highly expressed markers of terminally differentiated luminal umbrella cells (*UPK1A*, *UPK2*, *KRT20*). Treatment efficacy in this subtype has not been fully explored. Future clinical trials should consider testing the efficacy of

cisplatin-based neoadjuvant chemotherapy to immune checkpoint inhibition, as well as other targeted therapies rationally employed based on mutation and expression profiles.

The basal-squamous subtype was more common in females and characterized by high expression of basal and stem-like markers, squamous differentiation markers, immune infiltration, *CIS signature*, *TP53* mutations, and loss of SHH signaling. This subtype collectively had low purity as evidenced by large amounts of lymphocytic infiltration and the highest expression of immune genes. Surprisingly, several samples (n=20) were classified as the basal-squamous subtype, though they lacked expression of both basal and squamous markers. They were classified as such due to the lack of luminal marker expression and similarly high immune marker expression to other basal-squamous samples. These samples are likely not basal-squamous, but a distinct subtype on their own. These samples should be identified as mesenchymal due to the lack of basal-squamous, and luminal marker gene expression, and the presence of EMT gene expression. Future studies should focus on achieving greater tumor cell purity in tissues such that greater resolution of tumor cell intrinsic biology can be achieved to fully separate out samples that don't share similar biology and follow-up with rational treatment options<sup>112</sup>.

The neuronal subtype (n=20) had high expression of neuroendocrine markers as well as neuronal differentiation and development genes. However, only 3 samples had identifiable neuroendocrine histology present. Half of the samples subtyped as neuronal had either *TP53* and *RB1* mutations, or a *TP53* mutation and *E2F3* amplification, consistent with small cell neuroendocrine cancers and an unregulated proliferative state. The majority of neuronal samples (n=17) had p53 or cell-cycle pathway genes altered. The neuronal subtype is important to recognize clinically as the neuronal subtype has



the poorest survival (~15% 5-year survival) of the 5 subtypes identified in MIBC.

Research should be done on how to identify this subtype using a straightforward, rapid approach since the classic neuroendocrine features are typically absent. The efficacy of etoposide plus cisplatin therapy should be tested in clinical trials for this subtype in MIBC due to this being the preferred treatment for neuroendocrine cancers originating from different tissues<sup>112</sup>.

Classifying MIBC into molecular subtypes have moved the field forward tremendously in being able to broadly classify samples and associate outcomes. However, the influence of non-tumor cells to the molecular signature may confound subtyping. Methodologies are needed to either increase tumor purity or amplify the molecular signature from the tumor cells themselves so that we can more accurately subtype MIBCs and begin to identify the molecular drivers of each subtype and their therapeutic vulnerabilities.

#### 1.20.6 Recent Advancements in Treatment

Over the last three decades there have been limited options in the treatment of MIBC with combination cisplatin-based chemotherapy playing a prominent role in treatment. However, many patients with advanced disease are not candidates for cisplatin-based chemotherapies due to comorbidities such as impaired kidney function, hearing loss, or heart failure. Cisplatin ineligible patients or those who failed cisplatin-based therapy have traditionally had few options and frequently succumb to their disease. With the advent of immune checkpoint inhibitors over the last decade, the treatment landscape in multiple malignancies, including MIBC, has drastically changed. Excitingly, within the past 2 years five new immune checkpoint inhibitors have been approved for the treatment of advanced MIBC. These inhibitors include atezolizumab

(Tecentriq®), durvalumab (Imfinzi™), and avelumab (Bavencio®), monoclonal antibodies against PDL-1 on tumor cells. Approved inhibitors also include nivolumab (Opdivo®) and pembrolizumab (Keytruda®), monoclonal antibodies that block PD-1 on immune cells. Results of clinical trials and toxicity profiles associated with each inhibitor will be discussed below<sup>79,203</sup>.

In May 2016, the FDA granted accelerated approval of atezolizumab (Tecentriq®) in the second-line setting for patients with locally advanced or metastatic MIBC that became worse during or after treatment with cisplatin-based therapy. The conditional approval was based on the results of the open-label Phase II IMvigor210 study and was subject to confirmation. Unfortunately, on May 10, 2017 it was announced that atezolizumab failed to meet the primary endpoint of improved overall survival compared with chemotherapy in the randomized Phase III IMvigor211 study, which enrolled pretreated metastatic MIBC patients pre-stratified according to PD-L1 expression. The results are disappointing, however, atezolizumab did demonstrate activity against platinum-refractory MIBC and warrants further study to identify the population that would best benefit from this therapy. Atezolizumab also represents a good alternative to other second-line chemotherapies based on equivalent efficacy and a favorable toxicity profile<sup>79,204,205</sup>.

Before the announcement that atezolizumab failed the Phase III endpoint as a second-line therapy in MIBC, on April 17, 2017, the FDA granted an accelerated approval of atezolizumab as a first-line treatment for patients with locally advanced or metastatic MIBC who are ineligible to receive cisplatin-based chemotherapy. The expanded approval of atezolizumab as a first-line treatment was based on the results of the single-arm phase II IMvigor210 trial with 119 patients. The overall

response rate was 23.5% (n=28/119) for patients who received atezolizumab, including partial and complete responses of 16.8% (n=20/119) and 6.7% (n=8/119), respectively. Common side effects of atezolizumab treatments include fatigue, diarrhea, and severe itching, or pruritus. Immune system-related side effects may also be caused by the treatment. Side effect severity lead to nine patients discontinuing the drug<sup>204,206</sup>.

On May 1, 2017, durvalumab (Imfinzi™), and May 9, 2017, avelumab (Bavencio®) was approved for patients with locally advanced or metastatic bladder cancer whose disease has progressed during or after platinum-containing chemotherapy or within 12 months of neoadjuvant or adjuvant chemotherapy. Durvalumab approval was based on the 182-patient phase 1/2 Study 1108 whose disease had progressed after treatment with platinum-containing chemotherapy. The objective response rate in the study was 17%. Side effects of durvalumab commonly included fatigue, musculoskeletal pain, and constipation, and less commonly infection and immune-related side effects. Avelumab approval was based on objective response, or reduction in tumor size, in the single-arm open-label 242-patient JAVELIN Solid Tumor trial. The overall response rate was 13.3% (n=32/242) at 13 weeks and increased to 16.1% (n=39/242) at six months. The most common side effects of the avelumab included fatigue, musculoskeletal pain, and nausea. Forty-one percent (n=99/242) of patients had serious adverse reactions, including urinary tract infection and secondary bacterial infections of the blood, blood in the urine and urinary tract, and intestinal obstruction. Adverse reactions to avelumab led to the deaths of 6% (n=14/242) of patients in the trial. Avelumab is currently being evaluated as a first-line treatment in patients with locally advanced or metastatic MIBC in the ongoing phase III JAVELIN Bladder 100 trial<sup>79,207,208</sup>.

Nivolumab (Opdivo®) was approved in February 2017 for patients with surgically unresectable locally advanced or metastatic bladder cancer that progressed or recurred after treatment with platinum-based chemotherapy. Approval was based on a Checkmate-275, a multicenter, single-arm phase II clinical trial of 270 patients. Nivolumab treatment resulted in an objective response rate of 19.6% (n=53/270), a complete response of 2% (n=6/270), and a 17% (n=46/270) partial response. Fatigue, diarrhea and skin rashes were common side effects. Fourteen patients discontinued nivolumab treatment due to side effects and three deaths were a result of treatment causing pneumonitis, acute respiratory failure and cardiovascular issues<sup>80,209,210</sup>.

On May 18, 2017, the FDA approved pembrolizumab (Keytruda®) for use in the second-line setting in patients with locally advanced or metastatic urothelial cancer whose disease has progressed during or after platinum-based therapy. The second-line setting pembrolizumab approval was based on the KEYNOTE-045 study, a randomized phase III study for second-line treatment of locally advanced or metastatic urothelial carcinoma. This multicenter study demonstrated a clear improvement in overall survival with pembrolizumab compared with investigator's choice chemotherapy for pretreated patients with urothelial carcinoma. Pembrolizumab as a single-agent demonstrated a median overall survival of 10.3 versus 7.4 months for chemotherapy and patients receiving pembrolizumab had fewer treatment related side effects. The FDA also granted accelerated approval to pembrolizumab for patients with locally advanced or metastatic bladder cancer in the front-line setting for patients who are treatment-naive and ineligible for cisplatin. The accelerated approval was based on the KEYNOTE-052 study, a single-arm, open-label trial in 370 patients who were not eligible for cisplatin-containing chemotherapy. The response rate was approximately 29% at the median

follow-up of 7.8 months. Common side effects in the two trials included fatigue, musculoskeletal pain, decreased appetite, nausea, and diarrhea<sup>211–213</sup>.

Immune blockade represents a promising leap forward in treating MIBC, though there is still much work to be done in correctly identifying patients who will most benefit from this type of treatment. Unfortunately, excitement for immune checkpoint inhibition in MIBC has been dampened by atezolizumab's inability to meet endpoint expectations in clinical validation studies. This failure has raised doubts for the success of the other four PD-1/L1 drugs approved to treat MIBC, despite success in other cancer types.

Continued work is being done to compare efficacy of PD-1 versus PD-L1 inhibition. To further advance this burgeoning field of MIBC treatment, studies need to be done on immunotherapy and chemotherapy combination effectiveness, the optimal treatment sequence, how to overcome resistance mechanisms and toxicities, and how to achieve a prolonged response duration. Furthermore, clinically useful molecular signatures need to be developed to identify the optimal treatment for patients. The recently redefined molecular subtypes may help in recognizing therapeutic vulnerabilities in subsets of patients.

#### 1.20.7 Remaining impediments in advancing precision medicine in MIBC

Recurrence and resistance are difficult to predict and we don't fully understand how the TME and cellular heterogeneity contribute to aggressiveness in MIBC. Each urothelial carcinoma is comprised of varying amounts of cells from each differentiation state depending on the level of heterogeneity. Recently, there has been interest in the molecular profiling of MIBC, both to understand the biology of these tumors and to develop novel therapies. Molecular subtypes are based in part on differentiation state and differentiation state is tied to prognosis. Therefore, developing a prognostic gene

signature based on tumor differentiation seems rational. There has been some effort in moving forward with this idea using the subtype classification defined by the TCGA. However, there have only been two specifically distinct differentiation states fully appreciated and able to distinguish based on gene expression - basal and luminal. Though, there are 5 distinct subtypes the TCGA has defined. These additional subtypes are seemingly based on the presence or absence of a response from the TME. Smooth muscle, ECM and immune infiltrate seem to be driving some of the additional subtypes identified. While it is important to understand how and why some tumors have more or less of these components and try to correlate them with survival and therapeutic response, it's arguable that it is more important to identify tumor cell specific signatures and how the cancer cell in its' specific TME is driving this response. It's also plausible that samples were taken without regard for histology and more stroma was present in a subset of samples, as suggested by the purity estimates. Macrodissection or microdissection of tumor cells from MIBC may help in better distinguishing subtypes of MIBC that differ in intrinsic biology, therapeutic response, and survival.

## CHAPTER 2. ATIENT STRATIFICATION IN GLIOBLASTOMA IS IMPROVED BY ACCOUNTING FOR VARIATIONS IN GENE EXPRESSION CAUSED BY DIFFERENT HISTOLOGICAL STRUCTURES.

The contents of this chapter are part of a submission for publication and will also be present in the dissertation of Cymon N. Kersch due to co-authorship of this study. This study was entirely collaborative with both Cymon and I equally contributing to each portion.

### 2.1 Abstract

Precise management of glioblastoma multiforme (GBM) will require stratification of tumors into subtypes that differ in outcome and therapeutic vulnerability. To date, stratification strategies have been hampered by immense intra-tumoral heterogeneity. We have used open-source transcriptional profiles of predefined histological structures from human GBM to develop methods to mitigate the impact of heterogeneity on transcriptomic-based stratification. We show that histologic architecture strongly influences tumor classification when assessing established gene signatures for subtyping and prognostic marker development, and that using mixed structure samples gives misleading results. We identify cellular tumor as a GBM structure from which transcriptional subtyping and prognostic strategies can be applied to more accurately stratify patient cohorts. We analyzed this specific architecture to create an improved risk stratification tool. Our results suggest that biomarker performance for diagnostics, prognostics, and prediction of therapeutic response can be improved by analyzing transcriptional profiles in pure cellular tumor.

### 2.2 Introduction

Glioblastoma multiforme (GBM), a grade IV glioma, is the most common and aggressive malignant primary brain tumor, with a median survival of only 18.1 months<sup>149</sup>.

Efforts to improve survival are hindered by the current inability to stratify GBMs into groups with differential sensitivity to various therapies (chemoradiotherapy [CRT], immunotherapies, and targeted therapies) and to identify patients with the highest risk of rapid disease progression. Being able to identify patient cohorts with similar GBM tumors would improve clinical decision-making, design of clinical trials, and patient outcomes.

Stratification of GBM is particularly challenging because these tumors display complex multilayered inter- and intra-tumoral heterogeneity<sup>168,169</sup>. Current clinical stratification methods include: extent of resection, Karnofsky Performance Score (KPS), age, O<sup>6</sup>-methylguanine-DNA methyltransferase (MGMT) promoter methylation, and isocitrate dehydrogenase 1 (IDH1) mutation, none of which capture the intricate molecular and heterogeneous landscape of GBM<sup>123,135,161,162,214,215</sup>. However, modern 'omic' technologies, such as high-throughput genomic, transcriptomic, and proteomic profiling enable new approaches for tumor subset identification. Omic analyses of GBM samples from The Cancer Genome Atlas (TCGA) defined four molecular subtypes: classical, neural, proneural, and mesenchymal<sup>115</sup>. However, these subtypes and subsequent prognostic gene signatures have not found clinical utility.

We explore the hypothesis that GBM's intra-tumoral heterogeneity has impeded the development of robust molecular tools for patient stratification due to sampling regions that differ in histological structure. GBM tumors are clinically defined by their diverse histologic structures, with grade IV gliomas distinguished from grade III by the histological presence of necrosis and/or microvascular proliferation<sup>121,135</sup>. Nearly all omic studies investigating GBM have used samples collected with little regard for histological structure other than necrosis<sup>114</sup>. This methodology captures histologically diverse tissue architecture composed of cancer cells, stromal cells, vasculature, immune infiltration, and some necrosis. Samples that contain a mixture of these elements may obscure detection of key tumorigenic processes enriched or depleted in specific tumor



microenvironments. Furthermore, this histologic heterogeneity may interfere with inter-patient comparisons when biopsies are composed of inconsistent tissue architecture.

We show that characterizing transcriptional patterns in intra-tumoral heterogeneity enables identification of a more consistent histologic region that can be assayed to improve inter-patient comparisons. Specifically, we demonstrate that (1) histologic structures within a tumor are molecularly distinct and that variations in histology confound results of established gene signatures created from mixed samples, and (2) focusing specifically on the dense cellular tumor structure improves both GBM subtyping into biologically distinct cohorts and patient risk stratification that are more strongly associated with clinical outcome. These advances will guide the future development of personalized medicine approaches for GBM and enhance prognostics to identify patients with the highest risk of rapid progression.

## **2.3 Results**

### **2.3.1 Histologic structures in GBM tumors are molecularly distinct, explaining in part intra-tumoral heterogeneity.**

We analyzed RNA-sequencing and corresponding clinical data from the Ivy Glioblastoma Atlas Project (IvyGAP) to assess the extent to which transcription profiles varied between histological structures<sup>216</sup>. The IvyGAP dataset is comprised of two companion databases: (1) RNAseq and In Situ Hybridization data from histologically identified tumor structures and (2) clinical information including patient demographics, pathology, and survival. Briefly, this database was generated by analyzing tissue blocks with usable RNA obtained at tumor resection (Supplemental Figure 1A). Pre-defined histologic structures including: infiltrative tumor (IT), leading edge (LE), cellular tumor (CT), perinecrotic zones (PNZ), pseudopalisading cells around necrosis (PAN), hyperplastic blood vessels (HBV), and microvascular proliferation (MVP), were outlined

on H&E stained tumor sections and microdissected on adjacent sections at the Allen Brain Institute (Figure 5A; Supplemental Figure 1B-C; Supplemental Table 1). The number of different structures sampled varied between patients. Dissected structures underwent RNA sequencing and results were archived as Fragments Per Kilobase of transcript per Million (FPKM) mapped reads. We used the FPKM data from 34 newly diagnosed GBM in the present analyses.

We analyzed histological structure specific transcriptional profiles from the IvyGAP database using principal component analysis (PCA) and correlation network analysis<sup>217-219</sup>. The first two principal components in the PCA explained 50.9% of the variance in the 1000 most variable genes in the dataset and separated samples by structure, but not by other clinical features associated with GBM such as KPS, age, MGMT promoter methylation, and IDH1 mutation (Figure 5B; Supplemental Figure 2A-G). This finding suggests that sample variance was driven by histologic structure and not by other patient characteristics. Transcript-to-transcript correlation network analysis corroborated PCA results, confirming that samples within a region were more highly correlated than samples from different regions, even in cases where samples were from the same patient (Figure 5C)<sup>217,218</sup>.

Samples from several of the 7 histologically-defined structures had overlapping clusters in PCA and network analyses, indicating that their transcription profiles were similar. We used the gap statistic method, k-means clustering, and hierarchical clustering to show that the original 7 histologic structures could be collapsed to 4 molecularly distinct structures having high tumor cellularity (CT), tumor invasion (LE/IT), vascular involvement (HBV/MVP) and necrosis (PAN/PNZ)(Figure 5D, Supplemental Figure 2H,I). The analyses that follow focus on these four structures.

### 2.3.2 Distinct biological processes are enriched in tumor structures.

We analyzed whole transcriptome measurements of each of the four transcriptionally distinct structures using Gene Set Enrichment Analysis (GSEA) of gene ontology (GO) to identify biological processes enriched in each structure relative to the rest of the tumor (Figure 6)<sup>220–224</sup>. The LE/IT structure, where the ratio of tumor cells to central nervous system (CNS) cells is low, had enrichment of normal CNS processes such as neuron development, synaptic signaling, and regulation of ion and neurotransmitter homeostasis. Thus, transcriptomic analysis of the bulk tumor edge captures CNS processes, rather than cancer specific biology. The vascular architecture (HBV/MVP), as expected, was associated with angiogenesis, regulation of blood pressure, vascular permeability, cell junction assembly, and extracellular structure organization. This region also was enriched in immune processes including regulation of phagocytosis, leukocyte migration and activation, and cytokine production, suggesting this is an inflammatory microenvironment in GBM. The PNZ/PAN architecture also was associated with enhanced immune processes, such as monocyte and lymphocyte differentiation, and leukocyte migration and chemotaxis. Additionally, the PNZ/PAN region was characterized by biological networks associated with necrosis, cellular starvation, hypoxia, and oxidative stress.

The CT structure has the highest density of neoplastic cells and the transcription profiles of this structure varied between patients, suggesting that analysis of transcription profiles from CT might enable more precise identification of biologically distinct GBM cohorts. The variation between patients decreased our ability to identify biological processes associated with the overall CT structures. However, there was a trend toward enhancement of traditional cancer processes including DNA replication and repair, chromatin remodeling, and stem cell proliferation.

The diversity of biological networks interacting in spatially distinct histological structures highlights the complexity of GBM tissue. These studies suggest that efforts to compare tumors using samples containing unknown quantities of these structures may be compromised. Instead, comparing tumors using gene expression profiles measured for a consistent structure across patients, particularly the CT, may be an effective inter-tumoral comparison method.

### 2.3.3 Molecular subtype classification depends on structure, with CT best able to distinguish subtypes.

Existing GBM molecular subtypes (mesenchymal, classical, neural, and proneural) are not strongly associated with clinical endpoints<sup>115</sup>. Thus, this gene classifier has not translated clinically. Additionally, several analyses have reported classification of a single tumor into multiple subtypes<sup>153,155,225</sup>. We reasoned that both of these issues might be related to histological heterogeneity within and between tumors.

Our analyses of subtype gene expression profiles showed that histological architecture significantly influenced subtype classification of samples, using subtype criteria defined by TCGA (Figure 7A; Supplemental Figure 3A). Neural and proneural subtype-defining genes were strongly expressed in LE and IT samples, while mesenchymal subtype genes were highly expressed in HBV and MVP samples. This suggests that a biopsy taken from the tumor edge might be classified as neural or proneural, while a biopsy from the same tumor taken from a highly vascular region might be classified as mesenchymal. To test this, we subtyped all samples from each structure, using single-sample GSEA. We found that, in many cases, a single patient would be classified as every subtype depending on the structure analyzed. To avoid this problem, we focused on using solely the CT since this structure showed the most variability in subtype gene expression (Supplemental Table 1). Our analyses

demonstrated that all four subtypes could be distinguished in CT (Figure 7B,C; Supplemental Figure 3B). Furthermore, these results suggested three main subtypes exist: proneural, classical, and mesenchymal (Figure 7C). This result supports the idea that the original neural subtype may have been an artifact<sup>226</sup>.

The finding that analyses limited to CT structures could stratify molecular subtypes needed to be validated in an independent dataset. Doing so was complicated since all other GBM gene expression databases, to our knowledge, have been created from mixed-structure samples. Therefore, we created a novel gene expression classifier, using lasso logistic regression on each of the 4 transcriptionally distinct tumor structures in the IvyGAP database, to identify expression profiles that distinguish the 4 structures (Supplemental Figure 4A,B)<sup>227</sup>. Applying this new gene classifier to tissue composed of mixed structures identifies the predominant structure in a sample. We applied this structure classifier to GBM samples from TCGA and identified 40 samples predicted to be composed of predominantly CT (Supplemental Figure 4C)<sup>116</sup>. Clustering these 40 predicted CT samples revealed proneural, classical, and mesenchymal cohorts, similar in pattern to the IvyGAP CT samples (Figure 7D).

#### 2.3.4 Molecular subtype classification using CT distinguishes tumors with unique biology.

We applied GSEA to the proneural, classical, and mesenchymal cohorts identified in the CT samples from the IvyGAP database to identify enriched hallmark gene sets in each subtype<sup>220,228</sup>. The proneural and mesenchymal, but not classical and neural, cohorts had significantly enriched gene sets (Figure 7E; Supplemental Figure 5). Cell cycle checkpoints (G2M and E2F hallmark gene sets) and MYC signaling (MYC targets hallmark gene set) were enriched in proneural tumors, while the mesenchymal tumors were highly inflammatory (enriched inflammatory response, IL6/JAK/STAT3

signaling, coagulation, and IFN $\gamma$  response gene sets). These patterns were corroborated in the CT-predicted TCGA samples (Supplemental Figure 5).

### 2.3.5 Survival prediction using an established prognostic gene signature is driven by tumor structure.

We applied an established multigene predictor of GBM outcome to transcriptomic profiles from structurally distinct samples and observed that predicted outcome was confounded by structure (Figure 8A, Supplemental Figure 6A)<sup>229</sup>. Specifically, this analysis predicted that samples rich in LE and/or IT would have good prognoses, while samples rich in PNZ, PAN, HBV, and/or MVP have poor prognoses, independent of patient origin. In other words, an individual could be assigned either a good or poor prognosis based on the histological structure analyzed (Figure 8B, Supplemental Figure 6B)<sup>229</sup>. Using the metagene score to separate all IvyGAP samples into high versus low-risk groups showed no survival difference in Kaplan-Meier analysis. This result was observed due a single endpoint being associated with multiple samples that predict opposite outcomes.

We performed independent Kaplan-Meier analyses on samples within each structure to test whether applying the survival prediction gene signature to a specific structure could accurately stratify patients. CT showed a minor trend in correctly stratifying patients, but only analysis of HBV samples was statistically significant ( $p < 0.05$ ). However, analysis of HBV samples inverted the survival curve, alarmingly predicting opposite outcomes; patients predicted to have a poor prognosis had longer overall survival.

Our analyses suggest that applying this existing gene signature to a mixed structure sample could assign a prognosis based on the structure composition of the sample more than aggressiveness of the neoplastic cells, with highly vascular and

necrotic tumors having a worse prognosis. Guided by this, we next asked whether patients could be better stratified according to outcome using gene expression profiles measured for the cancer cell rich CT structures.

### 2.3.6 A novel prognostic gene signature, created utilizing CT transcriptomics, identifies highest-risk GBM patients.

We performed stepwise multivariate Cox proportional hazards regression on IvyGAP CT samples to create a novel prognostic model and risk score equation for GBM (Figure 9A; Supplemental Table 2). We included known prognostic factors including age, MGMT status, and IDH1 mutation in the model. The final risk score calculation included MGMT status, age, and expression of 6 genes: PGAM4, ETNK2, MIA, GMPS, BCL7B, and IBSP.

We assessed hazard ratios in samples from IvyGAP and validated these using the CT samples in the TCGA dataset in order to determine whether our prognostic signature improved survival prediction over MGMT methylation status alone. In both datasets, stratification of patients into moderate versus highest-risk groups was statistically significant and better than MGMT expression alone (Figure 9B,C). When we applied the gene signature to all samples from IvyGAP and TCGA (not only CT samples), the model correctly stratified patients, again improving stratification over MGMT expression alone (Figure 9D,E). These results suggest that our survival prediction model, created based on CT gene expression, can be applied to samples containing either pure CT or mixed structures. The model also effectively identified medium and low risk groups (Supplemental Figure 7).

We asked whether genes associated with high-risk had enriched biological patterns that could highlight key tumorigenic processes. To test this, we ranked the entire transcriptome in order of the Wald statistic calculated during multivariate Cox

regression analysis. We then used GSEA to probe this ranked list for established gene signatures enriched in transcripts with the greatest Wald statistic. Hallmark pathways, including oxidative phosphorylation, MYC targets, MTORC1 signaling, Glycolysis and DNA repair, were associated with high-risk genes (Supplemental Figure 7a).

Furthermore, enrichment of genes at chromosomal locations Chr13q12, ChrXp11, Chr16p12, Chr3q22, and Chr3q25 were associated with high-risk status (Supplemental Figure 7b).



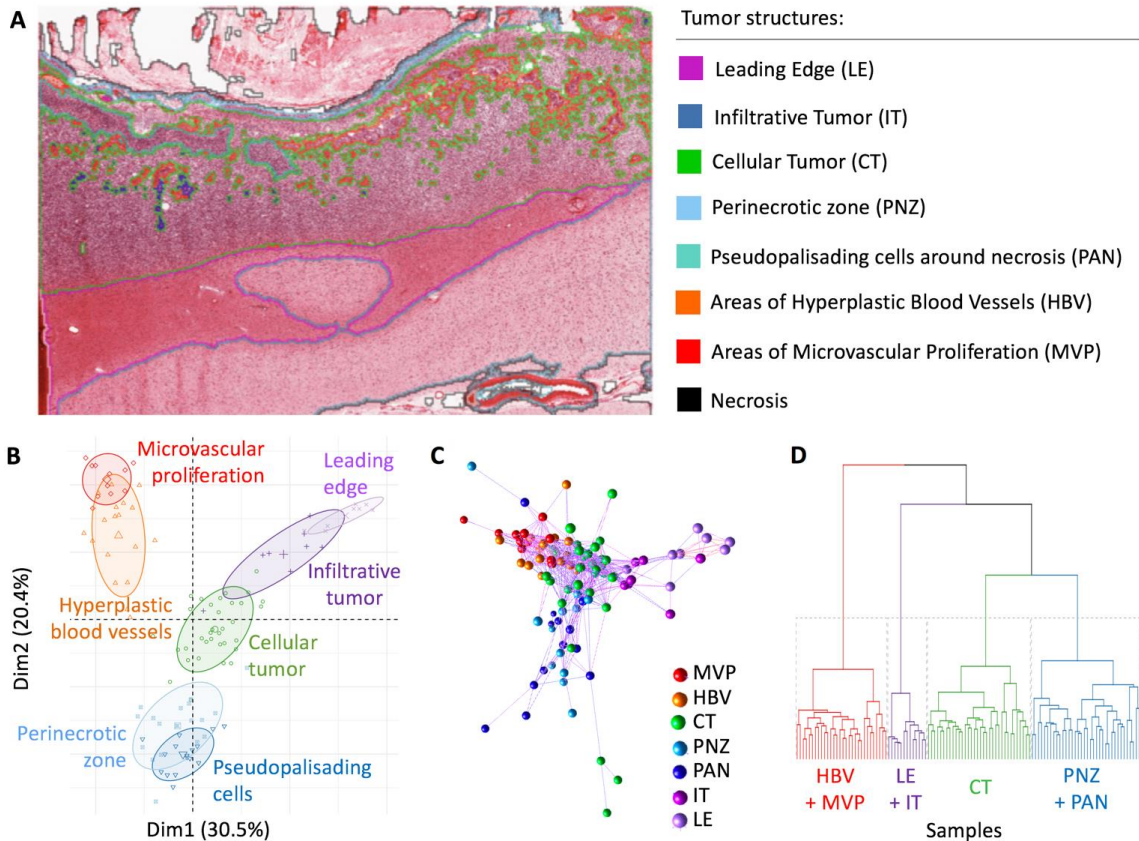
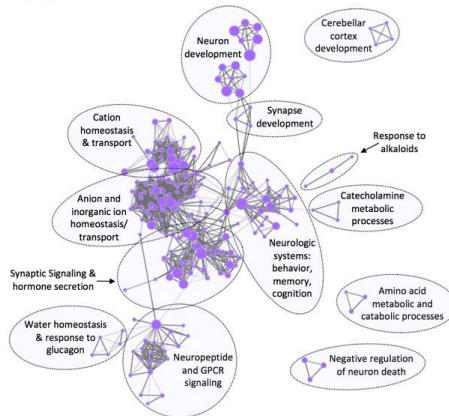


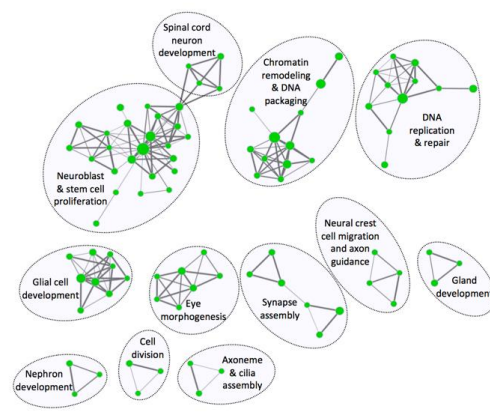
**Figure 5. Variation in GBM sample gene expression is primarily explained by histologic structure.** (a) Representative image demonstrating the histologic structures identified by the Allen Brain Institute (ABI), outlined by different colors. The ABI microdissected these structures, performed RNAseq on the dissected structures, and then archived the FPKM level data in the Ivy Glioblastoma Atlas Project (IvyGAP) database. See Supplemental Table 1 for higher magnification structure images and definitions. (b-d) Analysis of the 1000 most variable genes in the IvyGAP data set. (b) Principle component analysis (PCA) of dimensions 1 (Dim1) and 2 (Dim2) demonstrate that most variation in the data is explained by the histologic structure from which the RNA was extracted. Each sample is represented as a symbol, and colored by the structure the sample is from; ellipses are drawn around samples from the same structure (ellipse level=0.66). (c) Correlation network analysis shows samples from a histologic structure are clustered. Nodes represent samples, color represents the structure samples came from, and edge length depicts the degree of correlation between samples. (d) Dendrogram of hierarchically clustered (k = 4) samples demonstrating structures with the most similarity.

## Biological Processes Enriched in GBM Structures

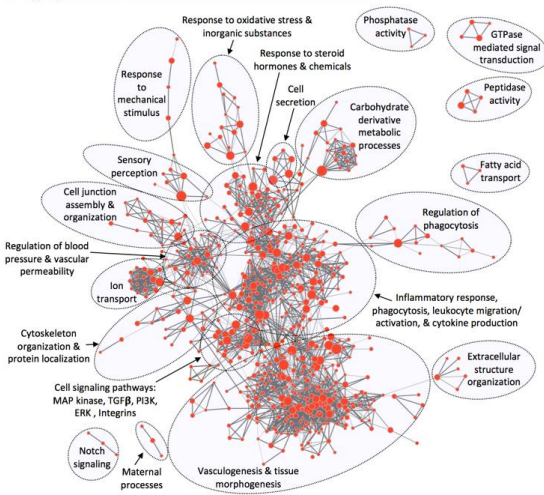
### A Leading Edge & Infiltrative Tumor



### B Cellular Tumor



### C Hyperplastic Blood Vessels & Areas of Microvascular Proliferation



### D Perinecrotic Zones & Pseudopalisading Cells

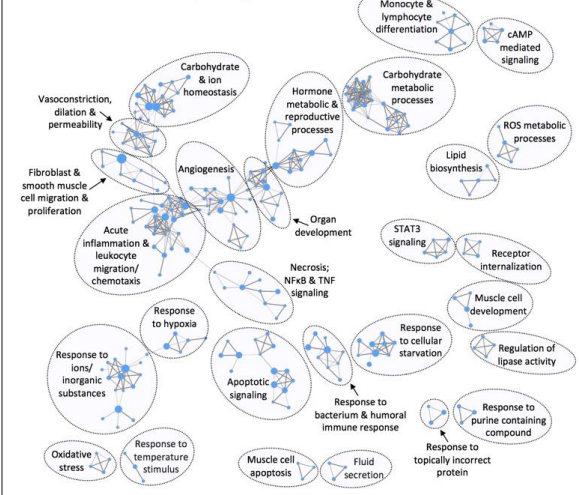


**Figure 6. Biological processes enriched in tumor structures.**

Gene Set Enrichment Analysis (GSEA) followed by enrichment map visualization shows gene ontology (GO) biological processes enriched in (a) leading edge (LE) and infiltrating tumor (IT), (b) cellular tumor (CT), (c) hyperplastic blood vessels (HBV) and microvascular proliferation (MVP), as well as (d) perinecrotic zones (PNZ) and pseudopalisading cells around necrosis (PAN) relative to the rest of the tumor. Nodes represent GO terms. Clusters of functionally related enriched GO terms were manually circled and labeled. Node color represents the structure enriched (Purple: LE/IT; Green: CT; Dark orange: HBV/MVP; Blue: PNZ/PAN). Node size within each structure quadrant is proportional to the number of genes within each GO term. Edge thickness signifies the overlap between GO terms (number of genes shared between two gene sets); thicker edges depict connections between nodes that share more genes than thinner edges. For visualization purposes, significance thresholds were set highly conservative for the LE/IT and HBV/MVP structures (p-value cutoff 0.005, false discovery rate (FDR) q-value cutoff 0.001), conservative for PNZ/PAN (p-value cutoff 0.005, FDR q-value cutoff 0.1), and very loose for CT (p-value cutoff 0.1, FDR q-value cutoff 0.4).

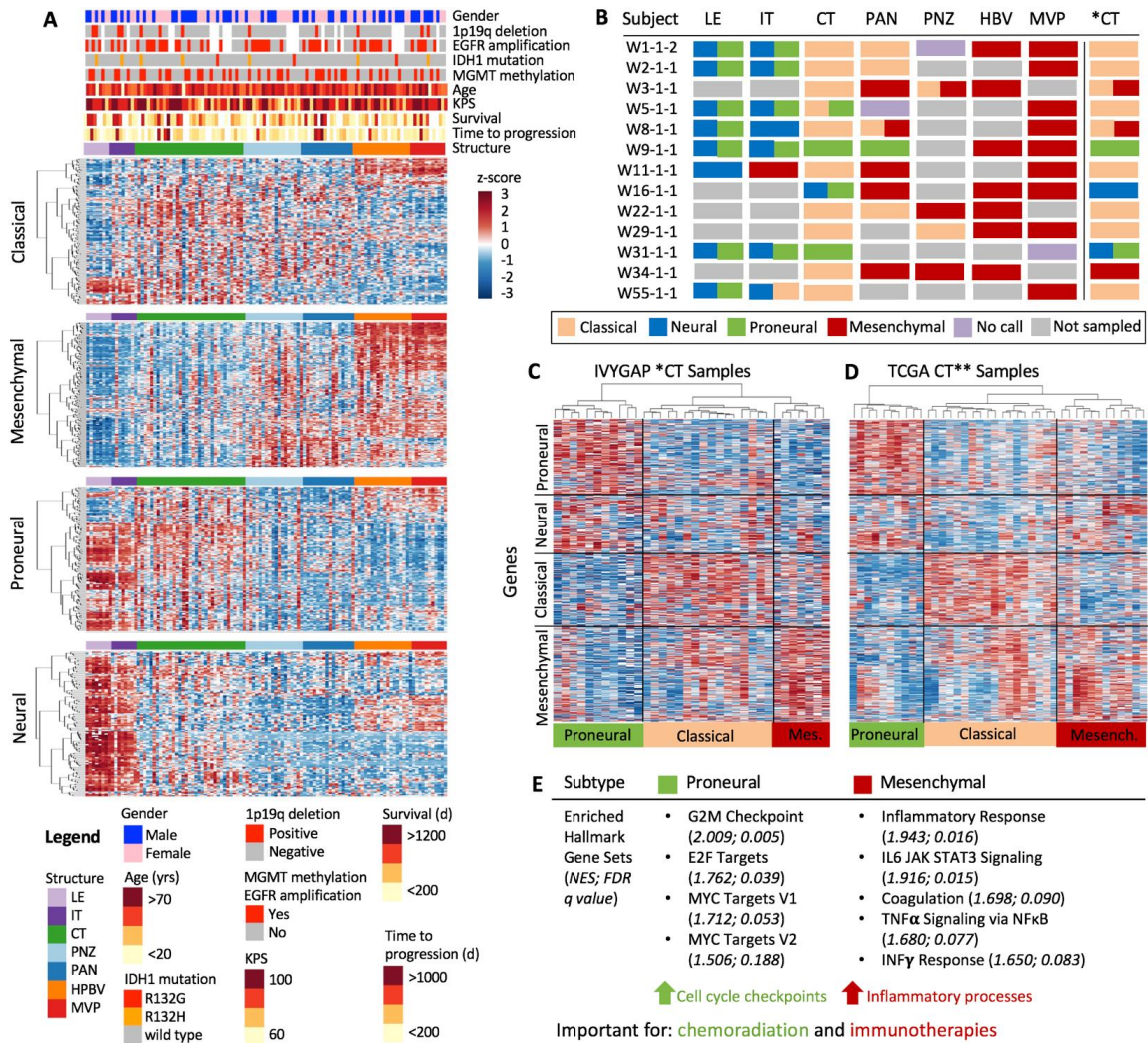


**Figure 7. Molecular subtype classification depends on the structure sampled, with Cellular Tumor (CT) able to distinguish biologically distinct subtypes.**

(a) Expression of subtype gene set (y-axis) in IvyGAP samples from each region (x-axis) show that sample structure is a main contributor to expression of subtype gene signatures. Genes corresponding to each subtype were organized independently by unsupervised hierarchical clustering. (b) Subtype classification for samples corresponding to subjects with  $\geq 4$  samples from different regions. All sample calls are shown in Supplemental Figure 3b. CT\* represents subtype analysis using only CT (z-scored data across CT samples only). (c) Unsupervised hierarchical clustering of IvyGAP CT samples (z-scored data across CT samples only) showing 3 main clusters with signatures of proneural, classical, and mesenchymal GBM subtypes. (d) Unsupervised hierarchical clustering of TCGA samples predicted to be composed predominantly of CT, also showing 3 main clusters with signatures of proneural, classical, and mesenchymal subtypes. (e) Enrichment of hallmark gene sets in the GBM subtypes (stratified based on the CT sample analysis) showing statistically significantly enriched processes in proneural and mesenchymal tumors (none were statistically significant in classical or neural). Proneural and mesenchymal tumors have enrichment of cell cycle checkpoints and immune processes, respectively. NES: normalized enrichment score; FDR: false discovery rate.

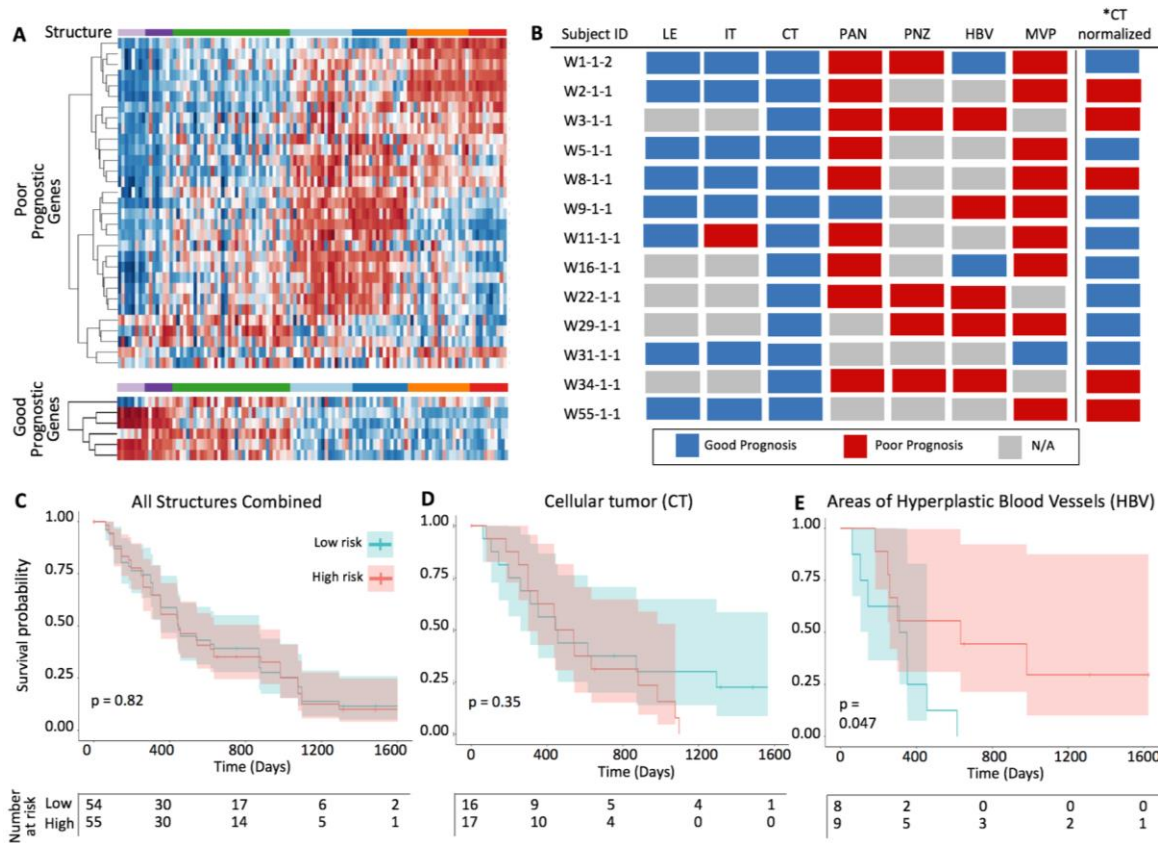


**Figure 8. Established prognostic gene signature expression is driven by tumor structure.**

(a) A survival prediction gene set, composed of genes associated with poor or good prognosis, shows differential expression based on tumor structure, with opposite expression in the IT/LE compared to the PAN/PNZ/HBV/MVP. The prognostic gene sets were organized independently by unsupervised hierarchical clustering. (b) Prognostic prediction for samples from subjects with  $\geq 4$  samples from different structures, with prognosis determined based on sample metagene score. A single patient (subject) can be predicted to be either high or low risk depending on which structure in their tumor is analyzed. All sample calls are shown in Supplemental Figure 6b. (c) Kaplan-Meier survival analysis of all IvyGAP samples. No difference is observed when all structure data is combined. (d) Analysis of survival prediction using a metagene score based on only CT samples. Results in a Kaplan-Meier curve show a minor, but correct trend in stratification of longer versus shorter survivors. (e) Analysis of survival prediction using a metagene score based on only HBV samples results in a statistically significant Kaplan-Meier curve that incorrectly, and oppositely, stratified long versus short survivors. For survival analysis, metagene scores were used to risk stratify (poor prognosis: metagene score  $> 0$ ; good prognosis: metagene score  $< 0$ ). Differences between survival curves was evaluated using the log-rank test. All tests were two-tailed; p-values  $< 0.05$  were considered significant.

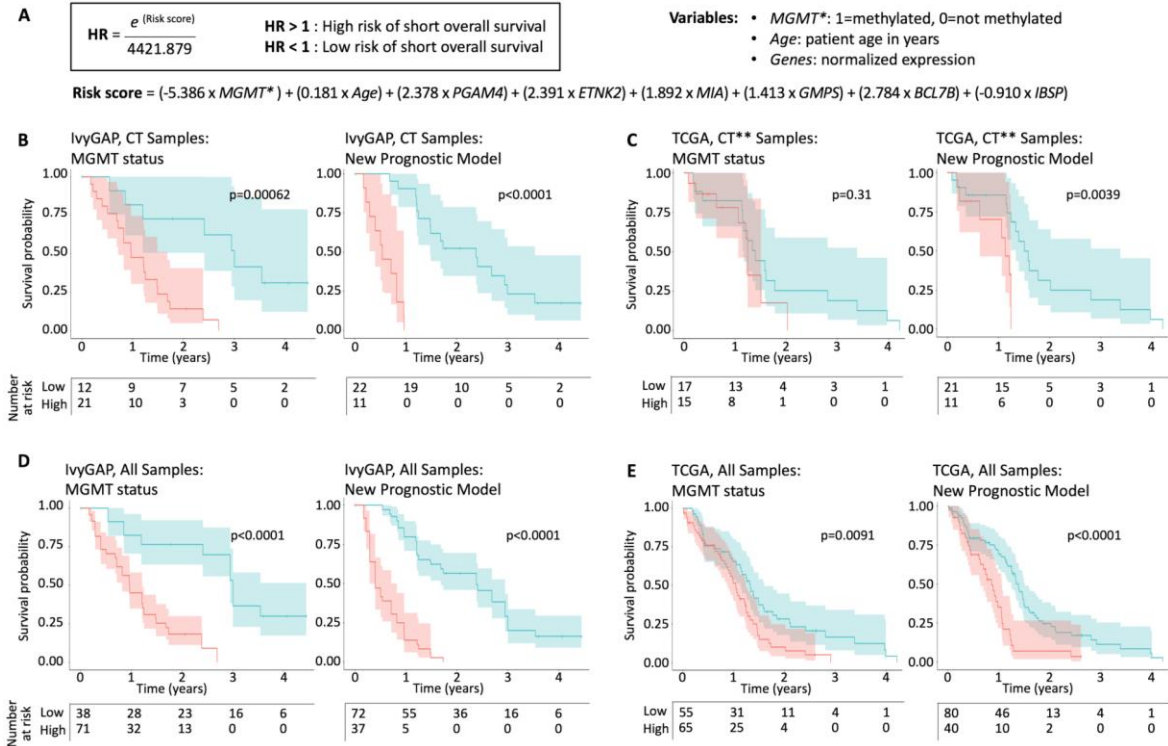
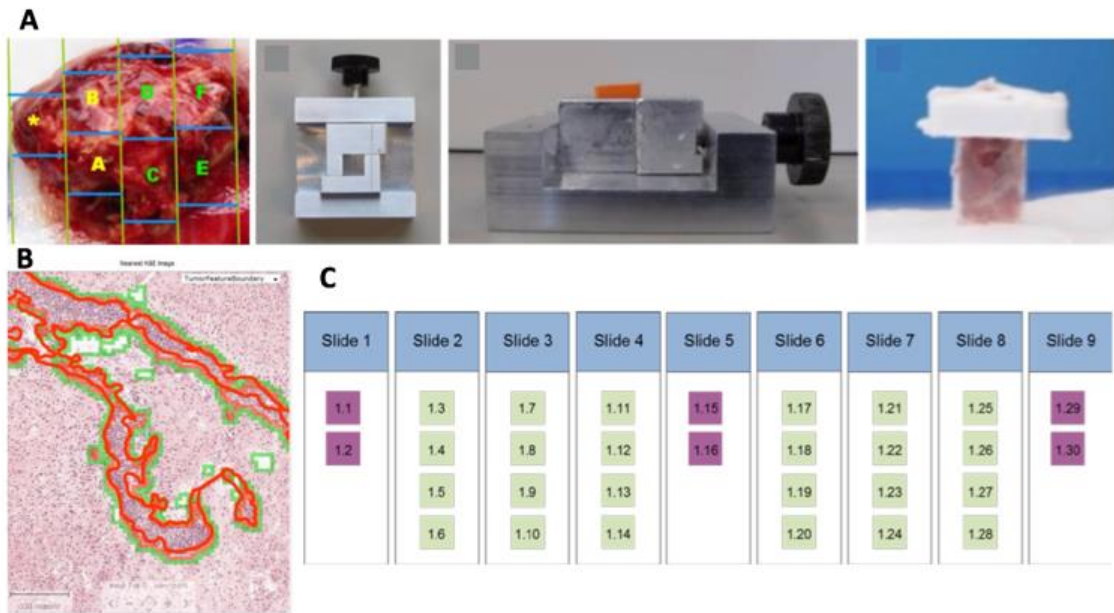


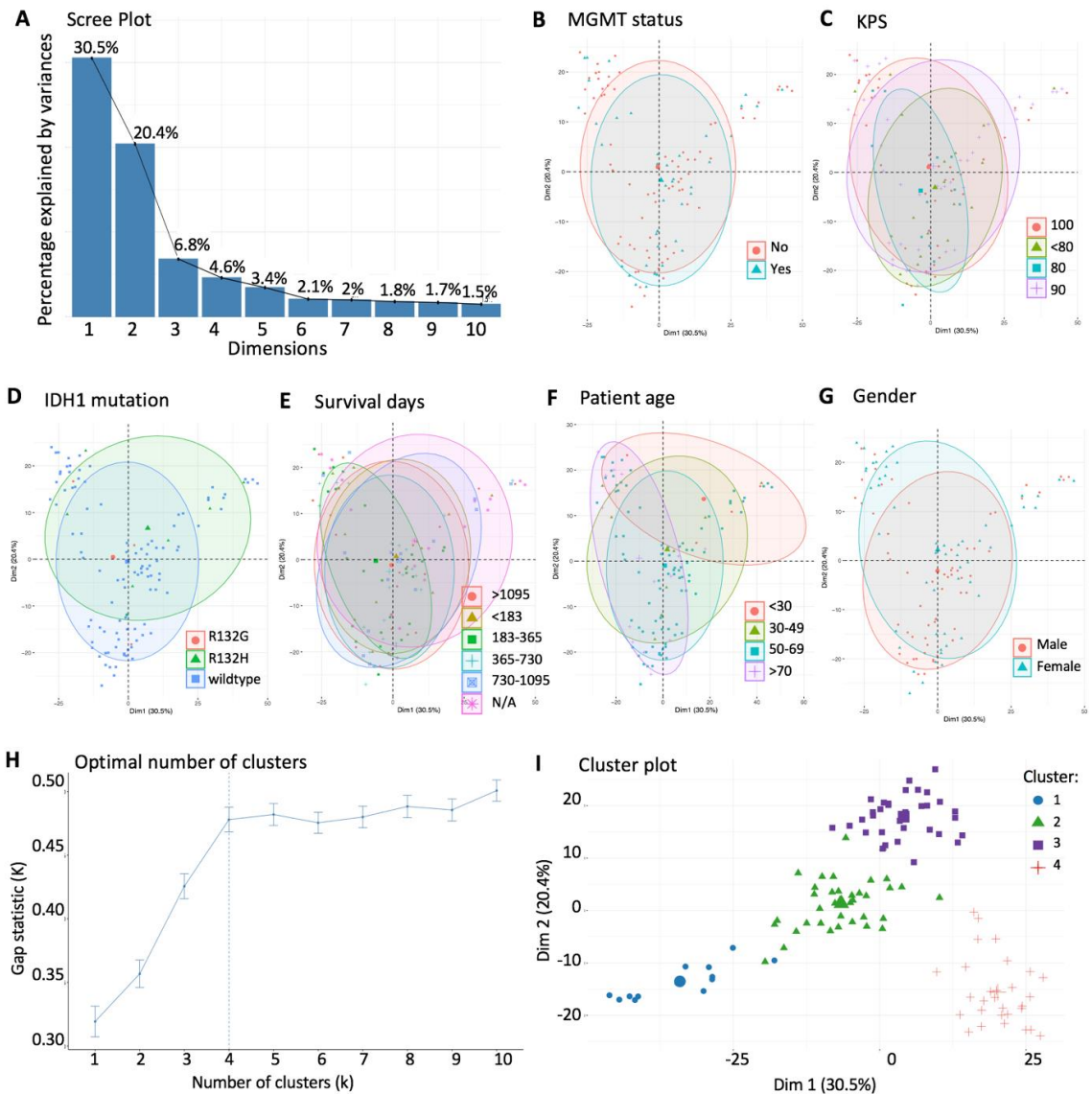
**Figure 9. Novel prognostic gene signature created utilizing solely Cellular Tumor (CT) sample gene expression data.**

(a) Risk score and hazard ratio (HR) prediction equation created using a novel prognostic model for GBM. The risk score is calculated as the sum of the product of the defined weighting factors with the corresponding predictors, MGMT promoter methylation status (0: not methylated; 1: methylated), patient age (in years), and normalized expression values of 6 genes: PGAM4, ETNK2, MIA, GMPS, BCL7B, and IBSP. Kaplan-Meier survival analysis of (b) IvyGAP CT samples, (c) CT-predicted TCGA samples, (d) all IvyGAP samples, and (e) all TCGA samples dichotomized into high and low risk groups based on MGMT promoter methylation status (left) and predicted HR (right). For MGMT promoter methylation status, survival was evaluated by separating samples into methylated (low risk) or unmethylated (high risk) groups. For assessing survival using the new prognostic model, tertiles of HR values were used to risk stratify (high risk:  $HR > \text{quantile}^{(2/3)}$ ; low risk:  $HR < \text{quantile}^{(2/3)}$ ). Differences between survival curves was evaluated using the log-rank test. All tests were two-tailed; p-values < 0.05 were considered significant. Shading on survival lines correspond to 95% confidence intervals. \*MGMT promoter methylation status. \*\* Samples predicted to be predominantly CT as classified using the structure-based lasso logistic regression classifier.



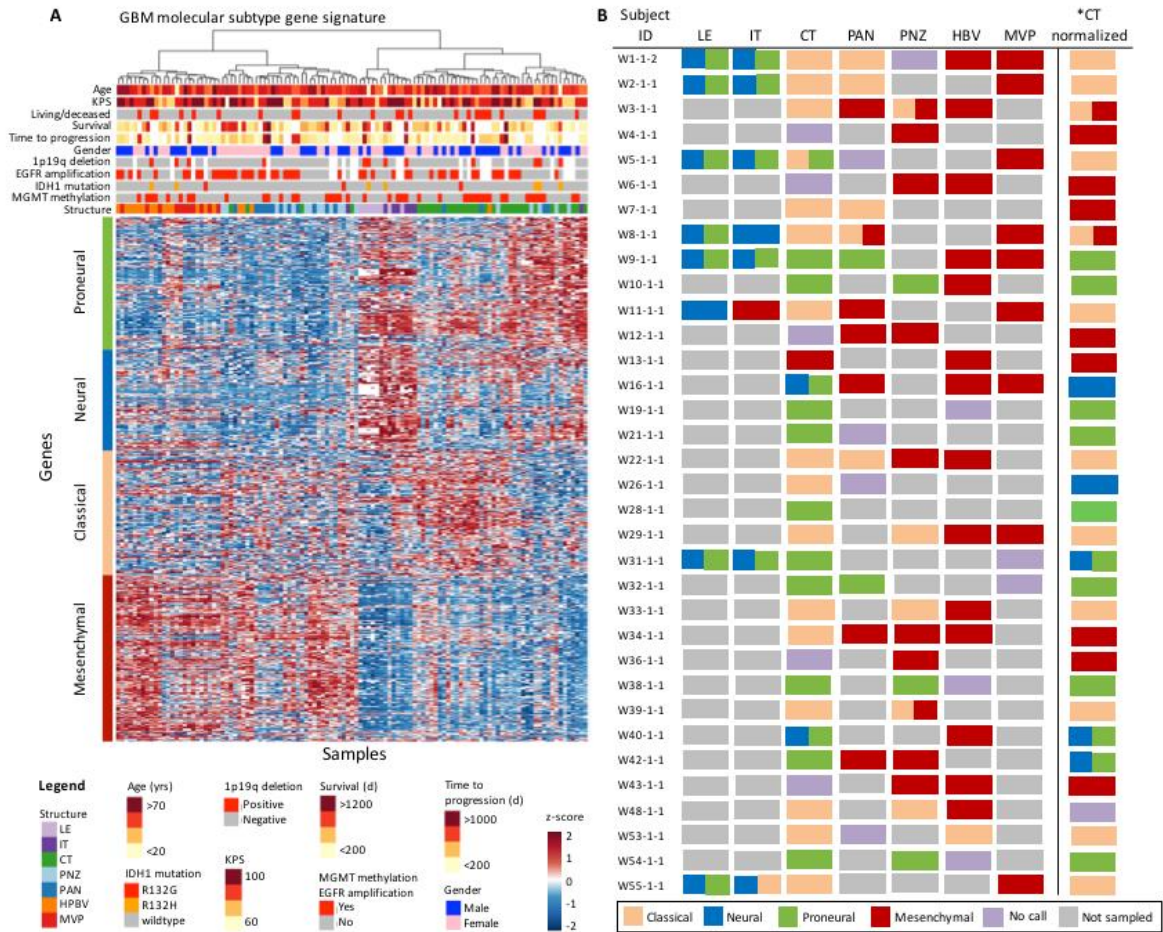
**Supplemental Figure 1.**

(a) Tissue collection, subsectioning, and freezing done by the Allen Brain Institute (ABI). (b) Example of histologic structure identification done by the ABI. (c) Slide layout for serial sections for structure alignment, completed by the ABI. Images: ABI, technical white paper.



**Supplemental Figure 2. Additional PCA and clustering analyses.**

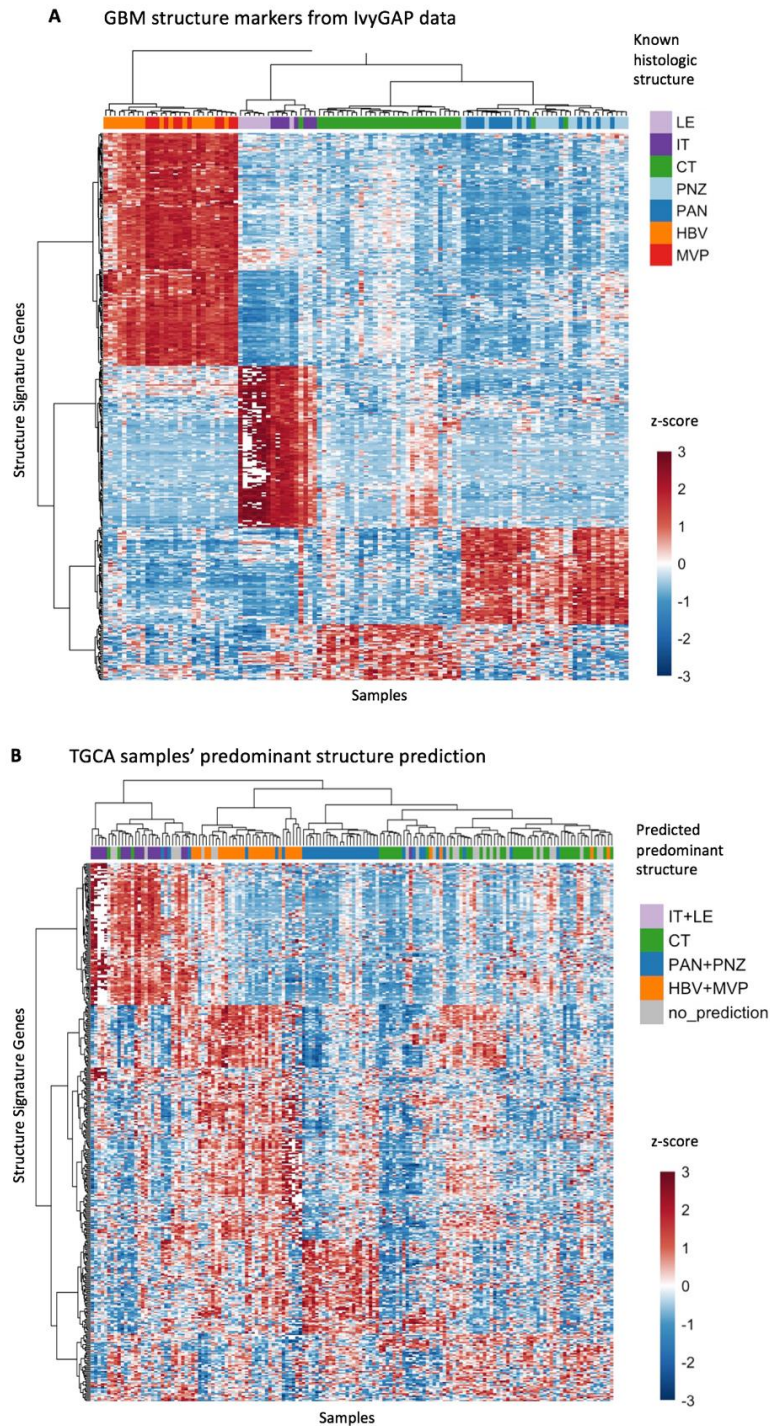
(a) Scree plot showing percent of variance described by each principle component (dimension) in analysis of the top 1000 most variable transcripts. PCA labeling clinical patient stratifiers (b) MGMT methylation status, (c) Karnofsky Performance Score (KPS), (d) IDH1 mutation status, (e) overall survival days, (f) patient age at time of diagnosis, and (g) gender of the samples (each symbol represents and individual sample). No alternative labeling explains variance in the data set as well or better than histologic structure seen in figure 1. (h) Gap statistic method identifying optimal number of clusters for k=1-10. (i) K-means clustering using k=4 and visualization of clusters using PCA.



**Supplemental Figure 3. IvyGAP molecular subtyping.**

(a) Expression of subtype gene set (y-axis) in the IvyGAP samples from each region (x-axis) showing sample structure is a main contributor to expression of subtype gene signatures. Samples were organized by unsupervised hierarchical clustering using Ward's method and the Euclidean distance metric. (b) Subtype classification calls for structures from all samples. CT\* represents subtype calls using CT z-scored data across only the CT samples.





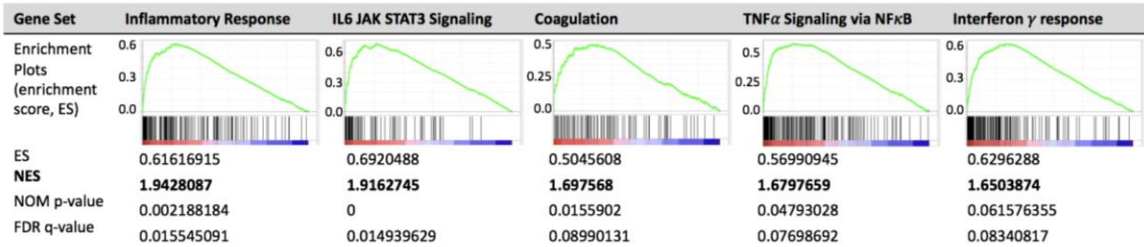
**Supplemental Figure 4. Structure-based gene signature.**

(a) Heatmap displaying z-score normalized expression of the structure-based genes signature, which was created by logistic regression modeling on the IvyGAP data with known tumor structures. (b) Heatmap of the structure-based signature genes in the TCGA GBM data. The predominant structure was predicted by applying the model learned by logistic regression from the IVGAP data to the TCGA GBM data. (a,b) Samples and genes were organized by unsupervised hierarchical clustering, which results in a nearly perfect separation of the structure (a). Genes are on the y-axis, samples on the x-axis.

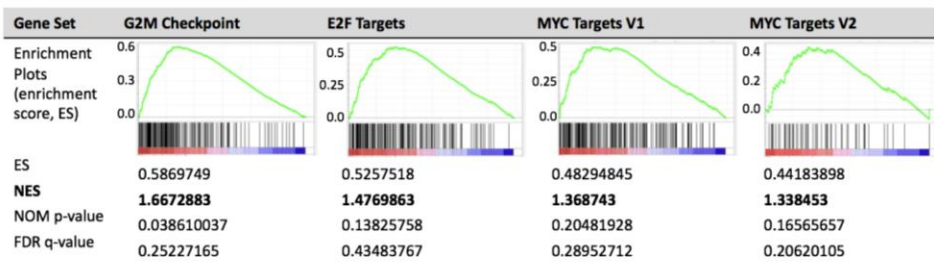
**A IvyGAP Proneural Tumors**



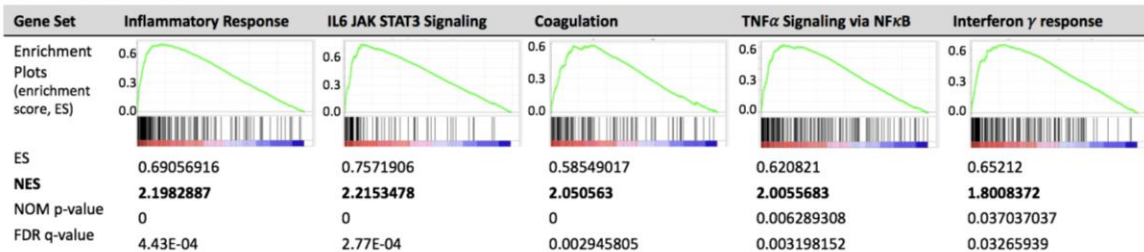
**B IvyGAP Mesenchymal**



**C TCGA Proneural Tumors**

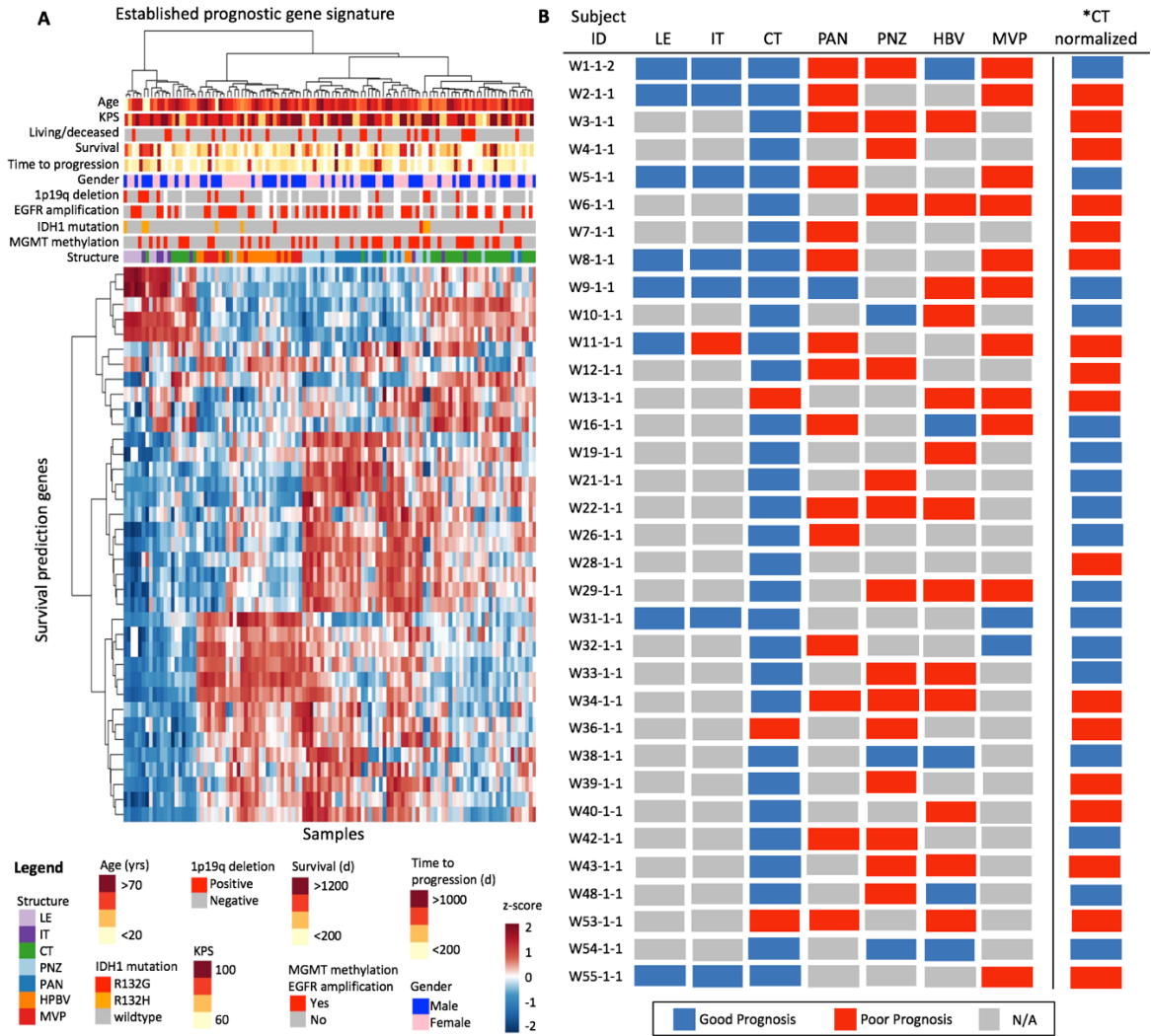


**D TCGA Mesenchymal**



**Supplemental Figure 5. GSEA hallmark gene set enrichment results from CT stratified molecular subtypes.**

Enrichment plots of top enriched hallmark gene sets in IvyGAP CT samples from (a) Proneural versus REST (all samples not classified as proneural), and (b) Mesenchymal versus REST (all samples not classified as mesenchymal) analyses. The top enriched hallmark gene sets in IvyGAP CT samples were also enriched in TCGA CT-predicted samples as shown by enrichment plots of (c) Proneural versus REST, and (d) Mesenchymal versus REST analyses. No results were statistically significant in Classical or Neural versus REST in both IvyGAP and TCGA analyses. Molecular subtyping was determined after z-score normalizing within only the IvyGAP CT and TCGA CT-predicted samples. ES: Enrichment score; NES: Normalized enrichment score; NOM: Nominal; FDR: False discovery rate.

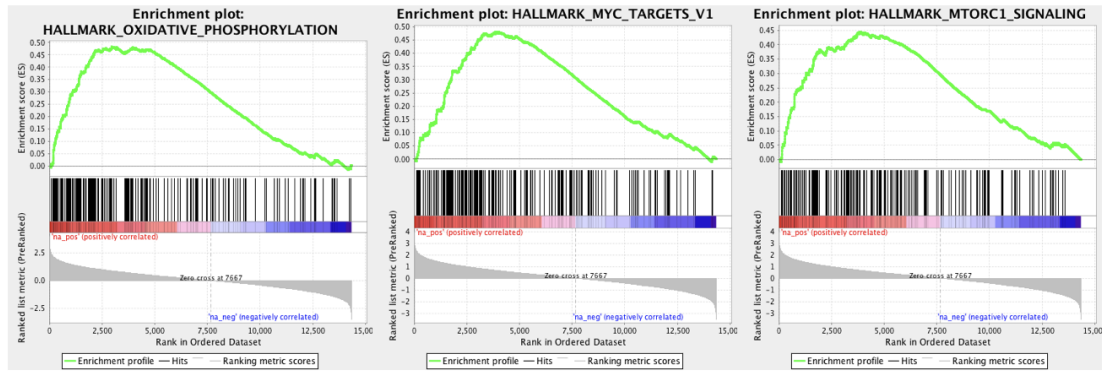


**Supplemental Figure 6. Analysis of established prognostic gene signature expression with all samples.**

(a) A survival prediction gene set, composed of genes associated with poor and good prognosis, shows differential expression based on tumor structure, with opposite expression in IT/LE compared to PAN/PNZ/HBV/MVP. Samples and genes were both organized by unsupervised hierarchical clustering. (b) Survival prediction for each sample, with prognosis determined based on sample metagene score (poor prognosis: metagene score > 0; good prognosis: metagene score < 0).

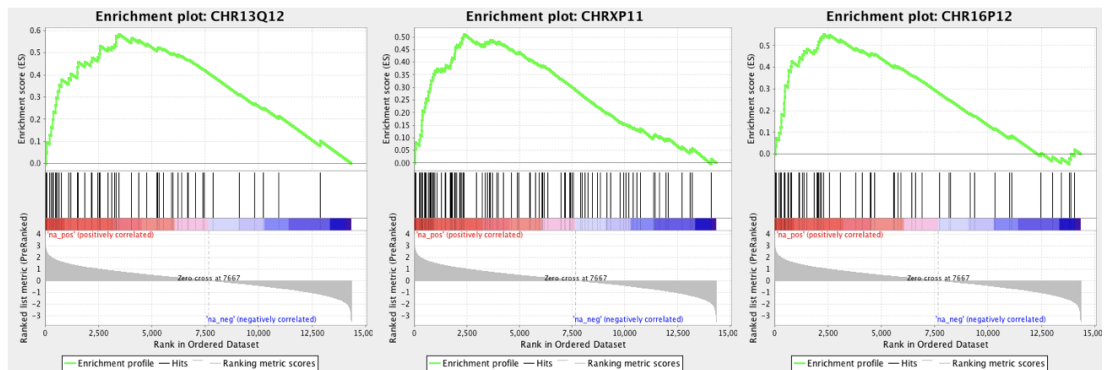
**A** Hallmark gene sets enriched in genes associated with increased risk

NAME	SIZE	ES	NES	NOM p-value	FDR q-value
HALLMARK_OXIDATIVE_PHOSPHORYLATION	200	0.48250204	2.3438652	0	0
HALLMARK_MYC_TARGETS_V1	199	0.4811729	2.3402896	0	0
HALLMARK_MTORC1_SIGNALING	198	0.4453736	2.1591268	0	0
HALLMARK_GLYCOLYSIS	174	0.4292439	2.0522869	0	0
HALLMARK_DNA_REPAIR	143	0.4340285	2.048816	0	0
HALLMARK_ADIPOGENESIS	184	0.3902727	1.8796716	0	7.95E-04
HALLMARK_PROTEIN_SECRETION	95	0.41465107	1.8330313	0	0.001475098
HALLMARK_UNFOLDED_PROTEIN_RESPONSE	111	0.4068424	1.7815337	0	0.003368181
HALLMARK_MYC_TARGETS_V2	56	0.4356806	1.7215402	0	0.005289557
HALLMARK_HYPOXIA	183	0.35446128	1.6935923	0	0.006379128
HALLMARK_E2F_TARGETS	193	0.34097087	1.6559026	0.00152439	0.009363162
HALLMARK_FATTY_ACID_METABOLISM	132	0.3566749	1.6433091	0.001545595	0.009962969
HALLMARK_PEROXISOME	86	0.35787502	1.5513692	0.006688963	0.021522515
HALLMARK_HEME_METABOLISM	166	0.32647696	1.5462751	0.001547988	0.021377744

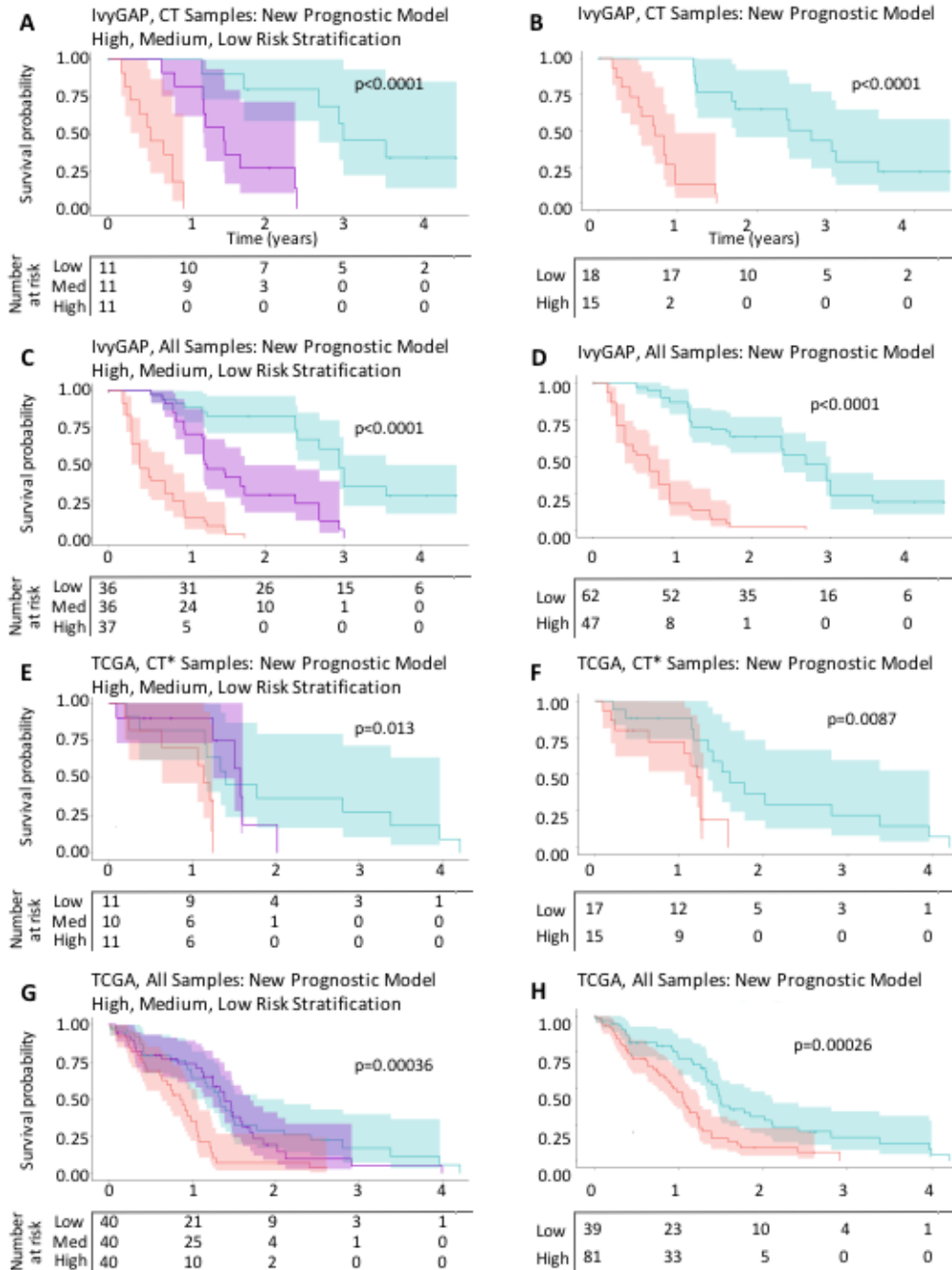


**B** Chromosome location gene sets enriched in genes associated with increased risk

NAME	SIZE	ES	NES	NOM p-value	FDR q-value
CHR13Q12	54	0.58430266	2.3514516	0	0
CHRX11	101	0.5114061	2.2415895	0	0
CHR16P12	56	0.5525256	2.172779	0	3.84E-04
CHR3Q22	26	0.6217498	2.0837045	0	0.001436358
CHR3Q25	39	0.540593	1.9820813	0	0.00526297
CHR17Q12	40	0.53095615	1.9600989	0	0.005811802
CHR11Q14	32	0.5403765	1.8738503	0	0.013258558
CHR15Q23	19	0.5982987	1.837828	0.001795332	0.016123157
CHR8P22	29	0.5085268	1.7315481	0.003571429	0.040951725
CHR16Q23	23	0.5266617	1.7146358	0.008741259	0.041767307
CHR11P14	18	0.5191604	1.5899329	0.02259887	0.08823041
CHRXQ24	19	0.52990526	1.5853989	0.02877698	0.08869763
CHR21Q21	15	0.5295314	1.5300134	0.047368422	0.11551796



**Supplemental Figure 7. Enriched gene sets in IvyGAP CT genes associated with increased risk.** (a) Hallmark and (b) chromosome location gene sets enriched in genes associated with high risk of short overall survival with enrichment plots of the top 3 gene sets for each. ES: Enrichment score; NES: Normalized enrichment score; NOM: Nominal; FDR: False discovery rate.

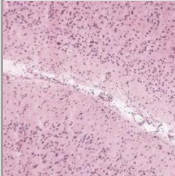
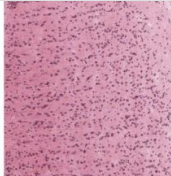
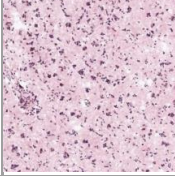
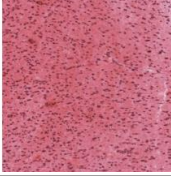
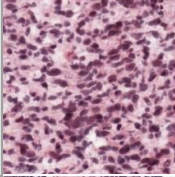
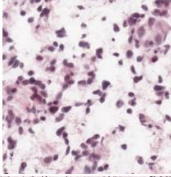
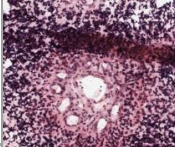
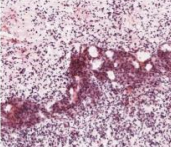
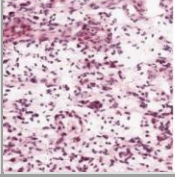
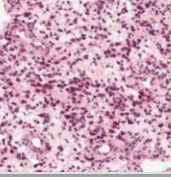
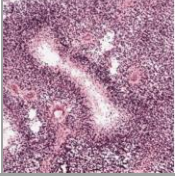
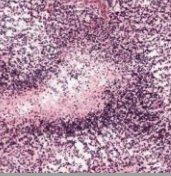
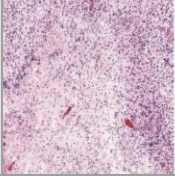
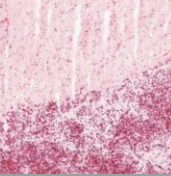
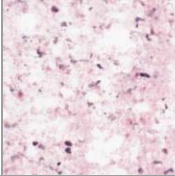
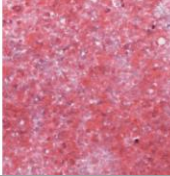


**Supplemental Figure 8. Survival analysis using the new survival prediction gene signature.**

Kaplan-Meier survival analysis of (a,b) IvyGAP CT samples, (c,d) all IvyGAP samples, (e,f) CT-predicted TCGA samples, and (g,h) all TCGA samples. Based on predicted HR, samples were separated into high, medium, and low risk groups (a,c,e,g; high risk:  $HR > \text{quantile}(\frac{2}{3})$ ; medium risk:  $\text{quantile}(\frac{1}{3}) < HR < \text{quantile}(\frac{2}{3})$ ; low risk:  $HR < \text{quantile}(\frac{1}{3})$ ), or high and low risk (b,d,f,h; high risk:  $HR > 1$ ; low risk:  $HR < 1$ ). Differences between survival curves was evaluated using the log-rank test. All tests were two-tailed, and p-values less than 0.05 were considered to be significant. Shading on survival lines correspond to 95% confidence intervals. \*Predicted to be predominantly CT as classified using the structure-based lasso logistic regression classifier.

**Supplemental Table 1. Tumor structure definitions.**

Adapted from IvyGAP Technical White Paper Figures 2-9.

Structure	Example Images		Definition
Leading Edge (LE)			"Leading Edge is the outermost boundary of the tumor, where the ratio of tumor to normal cells is about 1-3/100. Layers of the cortex are often observed."
Infiltrating Tumor (IT)			"Infiltrating tumor is the intermediate zone between the Leading Edge (LE) and Cellular Tumor (CT), where the ratio of tumor cells is about 10-20/100. Neuronal cell bodies as well as glial cell aggregating on neurons, are often observed."
Cellular Tumor (CT)			"Cellular tumor constitutes the major part of core, where the ratio of tumor cells to normal cells is about 100/1 to 500/1. Tumor densities often exceed typical levels of cells (left panel), but can also have low cell mass due to edema or early necrosis (right panel)."
Microvascular Proliferation (MVP)			"...generally found in the core of tumors, and is marked by two or more blood vessels sharing a common vessel wall of endothelial and smooth muscle cells (e.g. 100 μm diameter). They can appear as glomerulus (left panel, 100 μm diameter), or as a "garland" of multiple interconnected blood vessels (right panel, 50 μm diameter x 1-6 mm)."
Hyperplastic Blood Vessels (HBV)			Hyperplastic blood vessels are found throughout tumors, and exhibit many sizes and shapes (left panel). The features are marked by increased density of blood vessels that appear to have thickened walls (endothelial cell proliferation) (right panel).
Pseudo-palisading Cells around Necrosis (PAN)			Pseudopalisading cells around necrosis is generally found in the core of tumors. Tumor cells aggregate or line up in rows 10-30 nuclei wide at higher density than the surrounding CT to form pseudopalisading cells, which may appear to point toward a common center in necrosis. Necrosis is required for PAN."
Perinecrotic Zone (PNZ)			"Perinecrotic zone is generally found in the core of tumors, and refers to a boundary of tumor cells typically 10-30 nuclei wide along the edge of necrosis that lacks a clear demarcation of PAN."
Necrosis (NE)  <i>*No RNAseq data for this structure</i>			"Perinecrotic zone is generally found in the core of tumors, and refers to a boundary of tumor cells typically 10-30 nuclei wide along the edge of necrosis that lacks a clear demarcation of PAN."

**Supplemental Table 2. New prognostic gene signature statistics.**

	Beta	HR	Std error	Wald statistic	Significance p-value	95% confidence interval for $\beta$	
						Lower bound	Upper bound
Methylated MGMT	-5.386419	0.004578	1.29504	-4.159	3.19E-05	0.0003617	0.05795
Age	0.180779	1.198151	0.040497	4.464	8.04E-06	1.106726	1.29713
PGAM4 (441531)	2.378263	10.786156	0.632315	3.761	0.000169	3.1234858	37.24722
ETNK2 (55224)	2.390812	10.92236	0.665472	3.593	0.000327	2.9639155	40.25012
MIA (8190)	1.891907	6.632006	0.536646	3.525	0.000423	2.3165995	18.98623
GMPS (8833)	1.412626	4.106727	0.412839	3.422	0.000622	1.8284657	9.22369
BCL7B (9275)	2.784148	16.186019	0.656765	4.239	2.24E-05	4.4678673	58.63809
IBSP (3381)	-0.910068	0.402497	0.368536	-2.469	0.013534	0.1954627	0.82882

## 2.4 Discussion

Improving outcomes for GBM is hindered by our inability to stratify patients into cohorts that require different clinical care. Patient-to-patient tumor comparisons are difficult in GBM due to intra-tumoral heterogeneity. We demonstrated that histologic structures account for part of this heterogeneity, and propose that assessing gene expression in CT will improve inter-tumoral comparisons. Our results highlight that using mixed-structure samples or samples rich in non-CT regions to determine GBM subtype could produce invalid results, while classifying subtypes using CT identifies distinct cohorts with unique biology. Additionally, utilizing exclusively CT, we created a prognostic model to identify the highest-risk patients. The biological patterns uncovered in the subtypes and risk-stratified groups have important implications for guiding precision medicine and steering future studies investigating malignant pathways in GBM.

The enriched biological processes we identified in GBM subtypes have the potential to guide therapeutic intervention. Proneural tumors showed enrichment of genes expressed during cell cycle checkpoints, stages of cell replication when DNA integrity is assessed. Current standard-of-care treatment for GBM is CRT, which functions through eliciting DNA damage<sup>149</sup>. Having elevated expression of cell cycle checkpoints makes it plausible that proneural tumors have different sensitivity to CRT than other subtypes. Accordingly, purely proneural tumors have been reported to have longer survival than other GBMs, while mesenchymal differentiation has been associated with therapeutic resistance and decreased survival<sup>153,167,230</sup>. In contrast, mesenchymal tumors had enriched immune processes - the target of immunotherapies. This is consistent with previous reports showing that mesenchymal GBM has elevated immune activation and leukocyte infiltration<sup>231-233</sup>. This distinction is essential to consider in the context of immunotherapies, as highly immunogenic tumors are more responsive



to immunotherapy than tumors with a weak endogenous immune response<sup>234</sup>. Thus, mesenchymal GBM may be exceptional candidates for single-agent immunotherapy, whereas proneural tumors may require an immunogenic vaccine prior to immunotherapy<sup>233,235,236</sup>. Future studies should investigate the influence of pretreatment levels of cell cycle checkpoint transcripts and immune phenotype on GBM susceptibility to CRT and immunotherapies. Additionally, stratifying patients based on CT-characterized subtype in analysis of retrospective and prospective treatment efficacy trials may identify cohorts sensitive to specific therapies.

Our analyses of the established prognostic gene signature suggest that structure composition contributes to its prognostic prediction. Colman and colleagues noted that worse prognosis in their gene set was associated with a mesenchymal-angiogenic phenotype<sup>229</sup>. This observation is supported by our findings that vascular and necrotic tissue have a poor prognostic signature and that vascular regions have a strong mesenchymal phenotype. While GBM is differentiated from grade III gliomas by the presence of vascular proliferation and necrosis<sup>121</sup>, much less is known about how the extent of vascular proliferation and necrosis within GBM relate to the rate of tumor progression. It is plausible that the relative amount of these regions within GBM may be prognostic themselves, perhaps secondary to rapid tumor proliferation. Other groups have noted that angiogenic, necrotic and highly proliferative GBMs may be more aggressive<sup>230,237,238</sup>. As immunohistochemistry and magnetic resonance imaging (MRI) can detect these elements<sup>239,240</sup>, investigating the relationship between the level of vascularity and necrosis in GBM with survival merits further evaluation.

Using CT to create a novel prognostic gene signature allowed us to identify the highest-risk patients and probe the underlying biology of this cohort. Among the pathways we identified in the high-risk genes, MYC targets are attractive because MYC has multiple pro-tumorigenic functions in GBM<sup>20,241</sup>. Unfortunately, there are currently no

clinically viable MYC inhibitors<sup>242</sup>. Work developing these inhibitors is critical as they may have utility in treating the most aggressive GBMs. Additionally, multiple metabolic pathways were associated with high risk of rapid progression (Supplemental Figure 7A). Previous work has demonstrated a link between differential metabolic signatures with GBM subtypes and outcomes<sup>243</sup>. Taken together with our findings, this highlights the importance of GBM subtypes as possibly harboring distinct biology, bio-energetics, proliferative capacity, immune interaction, and disease progression, all of which are appreciable when accounting for structural variability in tumor analysis. Expression of genes from specific chromosomal locations were also enriched in the high-risk group. As MGMT promoter methylation is strongly correlated with survival outcomes in GBM<sup>162</sup>, it is probable that unappreciated epigenetic modifications that drive rapid tumor progression exist. Epigenetic modifications are aberrant in many cancers, and are intriguing as they provide modifiable targets<sup>244</sup>. While studies have investigated global methylation in GBM<sup>245</sup>, we propose that specifically analyzing the patterns in CT may expose novel drivers of GBM malignancy.

As CT-based transcriptomics permit inter-patient comparison, work is now needed to translate this stratification method for clinical utility. The next steps include (1) creating predictive signatures for tumor sensitivity and response to treatment, and (2) identifying methods to collect CT without microdissection. To create predictive signatures for treatment sensitivity that can be used for personalized medicine, studies should correlate gene expression in newly diagnosed GBM with outcomes following CRT, targeted therapies, and immunotherapies. Unfortunately, using CT for clinical purposes will be hindered by the labor-intensive microdissection, and work is needed to identify clinically feasible methods to collect CT. Image-guided biopsy is one potential method to obtain predominantly CT tissue. Previous investigations demonstrated that diffusion weighted MRI and amino acid positron tomography can localize GBM regions

with elevated tumor cellularity and mitotic indices<sup>170,246</sup>. These imaging modalities are already being integrated into the operating room via neuronavigational image-guided tissue sampling and could allow for selective CT localization and biopsy<sup>146</sup>. Alternatively, macro-dissection may be sufficient to collect cellular tumor with minimal contamination of other structures, and a study comparing the utility of this method versus microdissection is needed.

We have shown that analysis of transcriptomics in CT can stratify patients into distinct cohorts, and that using mixed structure samples can give misleading information. Ultimately, we believe the present study is the first step in generating a novel set of transcriptomic-based clinical tools utilized to plan and execute optimal care for GBM patients. Limitations of this study include low patient number (n=36), and the current inability to fully externally validate the results reported due to the lack of similar datasets in existence. Furthermore, we cannot extend clinical applicability without first externally validating the results in an independent cohort with histologic structures laser microdissected from patient GBM tissue samples along with RNA sequencing and DNA methylation performed.

## 2.5 Online Methods

### 2.5.1 Data sets.

The analyses described herein were performed on either the IvyGAP or TCGA data set with described processing steps.

#### 2.5.1.4 *IvyGAP.*

We mined RNA-sequencing data from the open-source Ivy Glioblastoma Atlas Project (Allen Brain Institute) and Swedish IvyGAP Database for clinical data. A detailed explanation of the methods used to generate these data are available (<http://glioblastoma.alleninstitute.org>). Briefly, tissue blocks were obtained at tumor resection, subdivided, and rapidly frozen. Tissues were later sectioned and subjected to H&E staining. Histologic structures including infiltrative tumor (IT), leading edge (LE), microvascular proliferation (MVP), hyperplastic blood vessels (HBV), perinecrotic zones (PNZ), pseudopalisading cells (PAN), and cellular tumor (CT) were outlined on one section and then laser microdissected on adjacent sections. Dissected structures then underwent RNA sequencing; results were normalized as Fragments Per Kilobase of transcript per Million (FPKM) mapped reads. The total number of patients enrolled was 42; 36 patients (18 male; 18 female) had usable samples with intact RNA, and of these each subject had variable numbers of samples obtained for each region. Not all patients have data from all structures and recurrent tumors (2) were excluded.

#### 2.5.1.5 *TCGA.*

The gene expression data (174 cases, Workflow Type: HTSeq-FPKM) and corresponding clinical information were downloaded from the Genomic Data Commons Data Portal for the Glioblastoma Multiforme projects (TCGA-GBM; <https://portal.gdc.cancer.gov>). Methylation data was downloaded from <https://tcga->

[data.nci.nih.gov/docs/publications/gbm\\_2013/](http://data.nci.nih.gov/docs/publications/gbm_2013/). Recurrent tumors and normal brain samples were excluded yielding a total of 156 cases.

#### 2.5.1.6 Data pre-processing.

To obtain a log-transformed, normal distributed data set, we excluded genes with very low expression across all samples by applying the following filtering method to IvyGAP and TCGA data sets: 1) Take expression values for all genes and all samples, remove zero's and find quartiles to be used as filtering value. 2) Calculate mean of each gene across samples and exclude genes with a mean less than the lower quartile filtering value. A combination of raw FPKM values, log2-transformed data, and z-score normalized values, where every transcript had mean value of 0 and standard deviation of 1, were used for all analyses.

#### 2.5.2 Variation in gene expression is primarily explained by histologic structure.

To assess the interrelationships between all samples in the IvyGAP data set, we used principal component analysis (PCA) and transcript-to-transcript correlation network analysis. To determine the optimal number of clusters within the dataset, we applied the gap statistic method, followed by k-means clustering and hierarchical clustering to identify the constituents of the optimally numbered clusters.

#### 2.5.2.7 PCA.

We performed PCA using the 1000 most variable genes in the IvyGAP data set to assess the variance among sample transcriptomes on the log2-transformed and z-score normalized data matrix (PCA() function in [FactoMineR R package] and [factoextra package in R]).

#### 2.5.2.8 *Correlation network analysis.*

Regional differences were also assessed in BioLayout Express3D by plotting a sample-to-sample correlation graph with the Pearson correlation threshold,  $r = 0.92$ , for visualization. Nodes represent individual samples, and edge length depicts the degree of correlation between samples with Pearson correlation coefficients above the selected threshold.

#### 2.5.2.9 *Gap statistic analysis.*

To identify the optimal number of clusters for subsequent partitioning methods in the IvyGAP dataset, we determined the gap statistic on the top 1000 most variable genes, which compares the total intra-cluster variation for  $k = 1-10$  with expected values under null distribution of the data. The optimal number of clusters is the value that maximizes the gap statistic, meaning that the clustering structure is far from random uniform distribution (`fviz_nbclust()` function [factoextra R package]).

#### 2.5.2.10 *K-means clustering.*

To identify which of the seven histologic structures collapse together for subsequent analysis, we performed k-means clustering on the 1000 most variable genes in the IvyGAP data set using  $k=4$ , the optimal number of clusters determined by the gap statistic analysis. The clusters were visualized by principal components (`kmeans()` function [stats R package]; `fviz_cluster()` function [factoextra R package]).

#### 2.5.2.11 *Dendrogram.*

To identify which of the seven histologic structures collapse together for subsequent analysis, we also computed a distance matrix on the 1000 most variable genes in the IvyGAP dataset using Euclidean distance measure and performed

hierarchical cluster analysis using Ward's method. The dendrogram was constructed using  $k=4$  groups, as determined by gap statistic analysis (distance matrix and clustering was computed using `dist()` and `hclust()` functions in [stats *R* package]; `fviz_dend()` function in [factoextra *R* package]).

### 2.5.3 Structure-based lasso logistic regression classifier.

We aimed to create a method for discriminating between GBM histologic structures using transcriptomic features with the goal of applying this method to mixed GBM samples to identify the predominant CT region for further analysis.

The IvyGAP data set was first balanced between structures and evenly split into train and test sets based on structure using Stratified K-Folds cross-validator (`n_splits=5`). Next, using train sets, a lasso regularized multinomial logistic regression classifier was built to predict GBM structure in independent data sets (`penalty='L1'`; `solver='saga'`; `C='1/8'`, `multi-class='multinomial'`, `fit_intercept=True`, ). The 5-fold cross validation average accuracy for the logistic regression classifier on test sets is 98.45%. Lastly, the classifier was used to predict the structure classification of all GBM-TCGA samples (class `sklearn.linear_model.StratifiedKFolds` and `.LogisticRegression`; Python3.6).

### 2.5.4 Gene Set Enrichment Analysis (GSEA) to assess for enriched biological processes and perform GBM subtype analysis.

Gene set enrichment analysis was performed using GSEA software (ref = Subramanian et al, PNAS, 2005) (Broad Institute) with FPKM gene expression data. Defaults were used for GSEA analysis, including Signal2Noise ranking metrics. Gene sets were excluded that were smaller than 15 genes and greater than 500 genes, and enrichment p-values were estimated by 1,000 permutations and corrected for multiple

testing using the Benjamini-Hochberg method. Analyzed gene sets were from the molecular signature database (MsigDB), Gene Ontology (C5), Hallmark (H), or Positional (C1) collections, at [www.broadinstitute.org/gsea/msigdb/collections.jsp](http://www.broadinstitute.org/gsea/msigdb/collections.jsp).

For structurally enriched biological processes, GSEA results were visualized using the Enrichment Map (ref= Merico, Bader et al, PLoS one, 2010) plugin for Cytoscape (V2.8, [www.cytoscape.org](http://www.cytoscape.org)). For visualization purposes, clusters of functionally related enriched GO terms were manually circled and labeled, and significance thresholds were set to be highly conservative for the LE/IT and HBV/MVP structures (p-value cutoff 0.005; FDR q-value cutoff 0.001), conservative for PNZ/PAN (p-value cutoff 0.005; FDR q-value cutoff 0.1), and loose for CT (p-value cutoff 0.1; FDR q-value cutoff 0.4).

#### 2.5.5 Survival prediction using an established prognostic gene signature and metagene score.

To determine if expression of an established multigene predictor of GBM outcome has structural specificity, we calculated a metagene score for each sample in the IvyGAP dataset (z-scored using all samples) following methods from Colman and colleagues. Kaplan-Meier survival analysis was performed using the metagene score to separate all IvyGAP samples into high (metagene score > 0) and low risk (metagene score < 0) groups.

To test if assessing the gene signature within a specific structure could accurately stratify subjects in terms of overall survival, we z-scored samples within each structure independently, and re-calculated a metagene score for each sample followed by Kaplan-Meier analysis as before.



## 2.5.6 Cox proportional hazards model for survival analysis.

We aimed to create a method for discriminating between high risk (short overall survival) versus low risk (long overall survival) patients using transcriptomic features in the CT and clinical characteristics to calculate an individual's risk score. This risk score method was then applied to CT predicted GBM samples for validation.

### 2.5.6.12 *Univariate Analysis.*

To determine whether the clinical covariates age, gender, MGMT methylation status, IDH1 mutation status, 1p19q deletion status and KPS score were significantly associated with overall survival in the IvyGAP CT samples, univariate Cox proportional hazards regression was performed (coxph() function in [survival package in R]).

### 2.5.6.13 *Multivariate Analysis.*

To determine whether genes were significantly associated with overall survival and independent of clinical covariates, multivariate Cox proportional hazards regression using the clinical covariates MGMT methylation status, IDH1 mutation status and age was performed. Each gene was assigned a hazard ratio (HR), Wald statistic, and a corresponding p-value using Cox regression analysis. Genes were selected as candidates significantly associated with survival if the p-value was  $< 0.05$ , which also coincides with the confidence interval for the combined HR for a given gene not crossing the baseline risk (HR = 1). The HR for a given gene  $>1$ , was defined as a potential risk gene,  $<1$ , it was defined as a potential protective gene (coxph() function in [survival package in R]).

#### 2.5.6.14 *Stepwise selection.*

The gene candidates from multivariate analysis were applied to the process of forward stepwise selection, which is designed to add genes to the base model with clinical covariates that increase the model's ability to discriminate between long versus short-term survivors. First, 10 random seeds were generated and for each seed the IvyGAP CT samples were split into train and test sets using 5-fold cross validation. Next, using train sets, HR's, log-rank test scores and associated p-values are computed for the base model, iteratively fit with each candidate gene. An updated model is created adding only the candidate gene with the highest log-rank test score (and the lowest log-rank test p-value) to the base model. Then, the process is repeated to determine which of the remaining candidate genes will lead to the greatest improvement if added to the model. This process is continued until the concordance for the model reaches 1, signifying that the discriminatory power of the model is perfect, or 10 genes have been added, whichever occurs first (`createFolds()` function in [caret R package]; `coxph()` function in [survival package in R]).

#### 2.5.6.15 *Internal validation.*

The model for each training set that underwent stepwise selection was used to predict the HR of the corresponding test set and the concordance and log-rank test p-value was computed. Models were excluded that, upon prediction on the test set, had concordance  $< 0.5$  or log-rank test p-value  $> 0.05$ . To avoid overfitting, the model that was selected for subsequent analyses was the model with concordance nearest the mean (0.75) of all remaining models (`predict()` function in [stats package in R]).

#### 2.5.6.16 *Finalized survival model.*

Since we want to ensure generalizability and that each feature of the model is an independent predictor, to finalize the model, it was applied to the entire IvyGAP CT data set and features were excluded that had a Wald statistic p-value  $>0.05$ . The resulting finalized model was trained on the IvyGAP CT data and used to predict the HR's for each sample in the IvyGAP CT set alone as well as the entire IvyGAP data set (coxph() function in [survival R package]; predict() function in [stats R package]).

#### 2.5.6.17 *External validation.*

The GBM-TCGA samples that were predicted to be predominantly CT by the structure-based lasso logistic regression classifier were used for external validation of the finalized survival model. The model was trained on the IvyGAP CT data and used to predict the HR's for the GBM-TCGA CT samples alone as well as the entire GBM-TCGA data set (predict() function in [stats package in R]).

#### 2.5.6.18 *Survival analysis.*

Under different circumstances, an HR of 1 (high risk:  $HR > 1$ ; low risk:  $HR < 1$ ) was taken as the cut-off point for group classification, or tertiles of HR values were used to classify into two (high risk:  $HR > \text{quantile}^{(2/3)}$ ; low risk:  $HR < \text{quantile}^{(2/3)}$ ) or three groups (high risk:  $HR > \text{quantile}^{(2/3)}$ ; medium-risk:  $\text{quantile}^{(1/3)} < HR < \text{quantile}^{(2/3)}$ ; low risk:  $HR < \text{quantile}^{(1/3)}$ ). The Kaplan-Meier method was used to generate survival curves based on the different cut-offs and the difference between survival curves was evaluated using the log-rank test. All tests were two-tailed, and p-values less than 0.05 were considered to be significant (survfit() function in [survival package in R]; ggsurvplot() function in [survminer R package]).

### 2.5.7 Heatmaps.

For all heatmap visualizations, if clustering was performed, transcripts and samples were organized by unsupervised hierarchical clustering using Ward's method with the Euclidean distance metric. Heatmap visualization and hierarchical clustering were performed on log2-transformed and z-score-normalized data (pheatmap() function [pheatmap R package]).

### 2.5.8 Data availability.

All computer code used in this work is free and open-source software available at <https://github.com/gbm-dx>. IvyGAP data were acquired from <http://glioblastoma.alleninstitute.org>. TCGA data were acquired from <https://portal.gdc.cancer.gov> and [https://tcga-data.nci.nih.gov/docs/publications/gbm\\_2013/](https://tcga-data.nci.nih.gov/docs/publications/gbm_2013/)

## CHAPTER 3. MICROENVIRONMENT FACTORS INFLUENCE CELL COUNT AND DIFFERENTIATION STATE CHANGES IN HUMAN BLADDER CANCER CELL LINES

The contents of this chapter are in preparation for a submission to PLOS ONE for publication.

### 3.1 Abstract

Bladder cancer is the sixth most prevalent cancer in the United States and is a major contributor to patient morbidity and mortality. The tumor microenvironment (TME) may play a role in cell growth and differentiation that may be associated with disease recurrence and metastasis. TME signals cooperate with tumor cell genotype (mutations, translocations, copy number), and phenotype (differentiation state) to select for the cell type most fit to survive the conditions of the environment. This interplay is important to understand to identify signals that stimulate a pro-proliferative phenotype, and determine whether cells exhibit differentiation state plasticity to highlight potential targets for cancer interventions and predict outcome. We hypothesize that distinct TME signals stimulate proliferation and differentiation state plasticity in human bladder cancer cell lines in the presence and absence of drug treatment. To test our hypothesis, we utilized microenvironment microarray (MEMA) technology and identified lymphatic vessel endothelial hyaluronan receptor 1 (LYVE1) and cluster of differentiation 44 (CD44) as potential protein combinations that increased 5-ethynyl-2'-deoxyuridine (EdU) incorporation, a surrogate marker for proliferation. Validation results showed that LYVE1 and CD44 can independently increase cell count, but have a greater ability to do so in combination in the presence or absence of cisplatin. Cell cycle analysis indicated that LYVE1 had a trend in reducing apoptosis, and either increases proliferation or enhances DNA repair in cells treated with cisplatin. Additionally, neuregulin (NRG) isoforms

differentially affected bladder cancer cell count, EdU incorporation, and differentiation. Regardless of the specific TME signals, a switch to a more differentiated, intermediate or luminal state promoted an increase in cell number. The identified microenvironment factors that promote cell growth and differentiation will lay the foundation for improved strategies to predict recurrence and metastasis, and provide insight into potential therapeutic targets.

### **3.2 Introduction**

Bladder cancer is the sixth most prevalent cancer in the United States with 81,190 new cases and 17,240 deaths estimated in 2018<sup>1</sup>. The majority of these deaths are due to muscle-invasive bladder cancer, the more aggressive form of the disease (34% 5-year survival)<sup>191,247</sup>. Progression to metastasis will result in even poorer survival (5% 5-year survival)<sup>248,249</sup>. Standard care for invasive disease is aggressive treatment with cisplatin, and surgical intervention (cystectomy and an extended lymphadenectomy)<sup>194,250,251</sup>. Bladder carcinomas have a high propensity to recur despite aggressive treatment<sup>113</sup>. Many patients who initially respond to standard of care treatment exhibit refractory disease within a few years. The high rate of recurrence presents a challenge for the clinical management of this disease requiring frequent and often life-long surveillance of patients<sup>194</sup>. Many intrinsic factors that promote tumor progression and recurrence have been elucidated<sup>252</sup>. For example, bladder tumors frequently exhibit enhanced fibroblast growth factor receptor 3 (FGFR3) signaling through FGFR3 overexpression or FGFR3-transforming acid coiled-coil containing protein 3 (FGFR-TACC3) fusions, and also display aberrant human epidermal growth factor receptor 2 (HER2) activity<sup>112,113</sup>. However, the contribution of extrinsic factors to tumor progression has been understudied.

Extrinsic components of the TME have recently been implicated in promoting tumor growth and differentiation in many cancers, and has been shown to influence resistance to targeted therapy in bladder cancer cell lines<sup>35–38,253</sup>. The TME consists of the collection of neighboring stromal cells, immune cells, blood and lymphatic vessels, and their secretions<sup>36</sup>. TME factors provide multiple inputs into cells to control survival, proliferation and differentiation of cells via transducing signals into cells through a variety of cell surface receptors<sup>35</sup>.

Bladder tumors are heterogeneous, with individual cells within a tumor displaying unique differentiation states representing early, mid, and later differentiation states (basal, intermediate, and luminal umbrella cells, respectively)<sup>254</sup>. Basal, intermediate, and umbrella cells are distinguished by unique expression of cytokeratins (KRT) 5/14, 5, and 20, respectively<sup>196–198</sup>. Patient bladder tumors with high expression of KRT-14 have a poorer prognosis, suggesting cellular differentiation state affects disease progression, treatment efficacy, or both. Moreover, any of these cell types can undergo malignant transformation and give rise to tumors with diverse phenotypes and propensities for growth and metastasis<sup>196</sup>. The cancer genome atlas (TCGA) has recently defined molecular subtypes for muscle-invasive bladder cancer that use expression of distinct genes that comprise KRT differentiation state markers<sup>112,113</sup>. However, the clinical use of molecular subtypes for bladder cancer has not been realized.

It is critical to understand the communication between bladder cancer and its microenvironment to begin to target signals that promote growth. Currently, the extent to which extrinsic signals within the TME influence bladder cancer growth and differentiation is unknown, including whether response is subtype dependent. With this work, we aim to identify microenvironment factors that affect cell number, proliferation,

and differentiation state changes, and determine if a relationship exists between these endpoints. Identifying microenvironment factors that promote cell growth and differentiation will lay the foundation for improved strategies to predict recurrence and metastasis, and provide insight into potential therapeutic targets.

### **3.3 Results**

#### **3.3.1 Molecular subtyping of bladder cancer cell lines revealed 5 subtypes.**

Cell lines were utilized in the current studies for their relative ease of use along with high reproducibility, and because cell lines model the genomic diversity of primary bladder cancer as shown by hierarchical clustering of patient samples with cell lines (Supplemental Figure 9). Thirty-two bladder cancer cell lines were organized by unsupervised hierarchical clustering to identify molecular subtypes using z-scored expression of genes defined by TCGA (Supplemental Figure 10). Gene sets are grouped as luminal, extracellular matrix (ECM) and smooth muscle (SM), epithelial to mesenchymal transition (EMT) and claudin, basal, squamous, immune, neuronal, carcinoma in situ (CIS), and sonic hedgehog sets. Clustering revealed poor organization of a portion of the gene set groups into clusters (ECM and SM, immune, neuronal, CIS, and sonic hedgehog). This seemed to suggest that the gene sets associated with components of the microenvironment did not cluster well due to their lack of representation in cell lines. Hierarchical clustering was then repeated without the gene sets representative of the microenvironment while still containing the gene set groups luminal, EMT and claudin, basal, and squamous to better define molecular subtypes that were representative of the cancer cells themselves (Figure 10). Five main clusters were identified corresponding to a mesenchymal subtype rich in EMT genes (Cluster I), a basal-squamous subtype (Cluster II), a luminal/TP63-high subtype (Cluster III), a luminal/TP63-low/FGFR3-low subtype (Cluster IV), and a luminal claudin-high KRT20-



high subtype (Cluster V). Additional information about bladder cancer cell lines including known gene mutations of major oncogenes and tumor suppressors, as well as stage, and grade of tumors the cell lines were derived from can be found in Supplemental Table 3.

### 3.3.2 Expression of differentiation state markers showed phenotypic heterogeneity in bladder cancer patient tissue and cell lines.

Heterogeneity between patients (inter-tumoral heterogeneity) and between cell lines exists, according to molecular subtyping performed by TCGA on bladder cancer patient tissues, and our subtyping on bladder cancer cell lines, respectively. We performed immunofluorescence staining for expression of bladder differentiation state markers KRT5, KRT14, and KRT20 to determine if heterogeneity exists within tumors (intra-tumoral heterogeneity) or within cell lines. Expression patterns in a fresh frozen paraffin embedded patient bladder cancer tissue sample showed the presence of intra-tumoral heterogeneity with nests of KRT14 positive cells in some regions and other regions KRT14 negative and positive in KRT5 and KRT20. (Figure 11A). Cell lines also demonstrated heterogeneity in the expression patterns of KRT5, KRT14, and KRT20 (Figure 11C). The basal-squamous cell line SCaBER displayed extensive heterogeneity when stained for KRT14 and the squamous marker TP63 with all possible combinations present: double negative, double positive, KRT14 positive and TP63 negative, and KRT14 negative and TP63 positive (Figure 11B). These results suggest that when subtyping is performed on a tumor or a cell line, the predominant subtype or expression pattern is what drives classification, but subtype heterogeneity likely exists at lower levels.

### 3.3.3 MEMAs identified factors that promote EdU incorporation and induce differentiation state changes.

Microenvironment Microarrays (Figure 12) were used to identify pairwise combinations of soluble and insoluble microenvironment factors that promote proliferation and differentiation changes in luminal/TP63-high FGFR3-TACC3 fusion cell lines RT112 (Figure 13) and RT4 (Supplemental Figure 11)<sup>255,256</sup>. FGFR3-TACC3 fusion resulting in FGFR3 overexpression is a resounding feature in bladder tumors and modeling this characteristic in the context of microenvironmental influences is of clinical relevance. MEMAs were manufactured on-site and were comprised of 2688 different combinations of 56 soluble and 48 insoluble microenvironment components. These proteins were selected as a standard set of proteins that are representative of different types of local and metastatic tumor environments, including, but not limited to the bladder microenvironment. These proteins are constituents of extracellular matrix molecules, lymphocytic infiltrates, stroma, macrophages, as well as blood and lymphatic system secretions and endothelium. Collagen I was mixed with each insoluble protein to ensure robust printing and promote cell attachment. An array consists of insoluble proteins robotically printed in a well of an 8-well plate as ~300  $\mu$ m diameter spots, which served as growth substrates for cells. Fifteen replicate spots of each insoluble substrate were printed in random locations to attain good statistical power within an array.

RT112 cells or RT4 cells were seeded onto each MEMA set, and the cells were allowed to attach to the spots for 1 hour. After ensuring cell adhesion to the spots via bright field microscopy, excess cells were then removed, incubated overnight, and then a single soluble ligand or PBS was added to each well along with either 25  $\mu$ M cisplatin or DMSO as a control in the case of RT112, or 200 nM PD173074 (an FGFR inhibitor) in the case of RT4. The concentration of each drug was selected based on the 50% growth

inhibition of the respective cells after 72 hours. Following 47 hours of drug treatment, cells were pulsed for one hour with EdU, fixed in 2% paraformaldehyde, and stained with markers for DNA content (DAPI), EdU incorporation as a surrogate for proliferation, and differentiation state markers (KRT5 and KRT20 (RT112) or KRT5 and KRT14 (RT4)). The stained arrays were imaged using a GE IN Cell Analyzer 6000 high-content, laser-based imaging platform and the IN Cell Analyzer image analysis software suite was used for image segmentation and extraction of quantitative image features. Resulting image features were normalized by RUV3 and LOESS regression to reduce variation in cell counts and staining intensity. The fraction of cells incorporating EdU, and expression of basal (KRT14/5), intermediate (KRT5), and luminal (KRT20) differentiation state markers due to combinatorial microenvironment factors in the presence or absence of drug treatment were assessed.

With regard to RT112 cells, there was a high dynamic range of EdU incorporation in both settings of DMSO and cisplatin treatment. In the DMSO treatment group, the proportion of cells that incorporated EdU ranged from approximately 6% to 40% with a median at about 18% (Figure 13A). Similarly, after cisplatin treatment, RT112 cells incorporated EdU at a rate of about 5% to 40% (Figure 14A). However, the median was higher in the cisplatin treated group (~ 22.5%), with the majority of combinations eliciting a mean incorporation of EdU between 18.25% and 27%. The top factors that promoted EdU incorporation in the DMSO treated set included fibroblast growth factor-2 (FGF2), hepatocyte growth factor (HGF), fms-related tyrosine kinase 3 ligand (FLT3) ligand, and connective tissue growth factor (CTGF). Alternatively, pleiotrophin (PTN), lymphatic vessel endothelial hyaluronan receptor 1 (LYVE1), delta-like protein 1 (DLL1), and neuregulin1- $\alpha$  (NRG1- $\alpha$  or NRG1|1) promoted EdU incorporation in the cisplatin treated set. Interestingly, NRG isoforms differentially affected the ability of RT112 cells to

incorporate EdU when exposed to cisplatin. Of the NRG isoforms, NRG1- $\alpha$  had the greatest ability to promote EdU incorporation, while sensory and motor neuron-derived factor (NRG1-SMDF or NRG1|10) had affects similar to the DMSO treated group, and neuregulin1- $\beta$ 1 (NRG1- $\beta$  or NRG1|6) diminished EdU incorporation (approximately 26%, 22%, and 15%, respectively). Microenvironment factors also influenced basal/intermediate and luminal differentiation (Figure 13B, 14B). The ratio of KRT20 to KRT5 was assessed after exposure to microenvironment factors with the presence or absence of cisplatin. Without drug treatment, the ratio of KRT20/KRT5 (Figure 13B), extended from approximately 1/3 to 1/56 as opposed to cisplatin treatment (Figure 14B), which influenced a narrower range of differentiation change of about 1/9 to 1/35.

Regarding RT4 cells, microenvironment conditions induced a wide range of EdU incorporation after treatment with the tyrosine kinase inhibitor (TKI) inhibitor PD173074 (Supplemental Figure 11A). TNF was the most prominent of all soluble factors that promoted EdU incorporation, which is consistent with TNF-mediated resistance reported in bladder cancer after administration of BCG. The Settleman group showed that NRG1- $\beta$ 1 had the ability to rescue cells from PD173071 induced effects, and that HGF, FGF basic, and PDGF could not rescue cells<sup>257</sup>. Analogously, our MEMA studies with RT4 and PD173074 treatment showed a similar trend with NRG1- $\beta$  capable of promoting EdU incorporation to a greater extent than HGF, FGF2, and PDGF. Differentiation state was also broadly affected (Supplemental Figure 11B).

#### 3.3.4 LYVE1 promotes EdU incorporation in the presence of cisplatin

Increased EdU incorporation upon cisplatin treatment in RT112 cells is likely due to enhanced DNA repair, not DNA synthesis. Cisplatin is the front-line therapy in bladder

cancer and therefore, clinically relevant to identify combinatorial microenvironments that enhance DNA repair upon treatment. For this reason, we decided to pursue validation of LYVE1 as a potentially important mediator of enhanced DNA repair upon cisplatin treatment. LYVE1 is a secreted receptor primarily expressed on the luminal and abluminal surface of lymphatic endothelial cells, is used as a lymphatic marker, and plays a role in lymphangiogenesis, invasion and metastasis of certain cancers<sup>258–263</sup>. As bladder cancer cells invade past the basement membrane, they are exposed to blood and lymphatic vessels and their secretions. Additionally, bladder cancer frequently invades the lymphatics and metastasizes to distant sites primarily via this route<sup>264</sup>. Therefore, it is logical that bladder cancer cells are exposed to LYVE1, and it is important to understand this interaction especially in the context of cisplatin treatment.

Further examination of the effects of insoluble microenvironment factors in combination with LYVE1 in the RT112 MEMA cisplatin treated set showed differential EdU incorporation ranging from approximately 18.25% to 35% (Figure 14C). Interestingly, the combination of LYVE1 with its homolog CD44 resulted in the greatest EdU incorporation, suggesting that their region of sequence homology elicits this response. On the other hand, LYVE1 in combination with the basement membrane protein nidogen-1 resulted in the least EdU incorporation. Nidogen-1 in combination with other soluble factors in the DMSO or cisplatin treated set (not shown) resulted in a similar response, indicating that nidogen-1 universally inhibits bladder cancer proliferation.

For validation of the LYVE1 response, cell count was assessed in RT112 cells plated in multi-well tissue-culture treated plates and treated with DMSO or 25  $\mu$ M cisplatin and PBS or 7 two-fold dilutions of LYVE1 ranging from 6.25 ng/ml to 400 ng/ml

(Figure 15). Results showed that cell count steadily increased with increasing concentrations of LYVE1 in both the DMSO and cisplatin treated groups. Response peaked at 200 ng/ml LYVE1 and resulted in a 1.7-fold increase over PBS for the DMSO treated cells and a 4.6-fold increase over PBS for the cisplatin treated cells. At the highest concentration of LYVE1 at 400 ng/ml, there was a dip in response that was slightly less than that observed at 100 ng/ml LYVE1.

Next, effects of LYVE1 in combination with insoluble collagen I or CD44 mixed with collagen I were tested to fully validate the MEMA results and model the spots from the MEMA, which were comprised of collagen I or collagen I mixed with other proteins (Figure 16). RT112 cells were plated in multi-well plates pre-coated with collagen I or CD44 and collagen I and treated with PBS or 50 ng/ml LYVE1 and DMSO or 7 two-fold dilutions of cisplatin ranging from 3.125  $\mu$ M to 200  $\mu$ M. In the DMSO treated group, there was a trend of increased cell count in collagen I/LYVE1 treated versus collagen I/PBS treated cells. A significant increase in cell count was observed in CD44/PBS in comparison to collagen I/PBS, indicating that CD44 alone has the ability to increase cell count. A significant increase in cell count was also seen with CD44/LYVE exposure in comparison to collagen I/LYVE1. The greatest affect was detected in the CD44/LYVE1 treatment compared to collagen I/PBS with a 2.3-fold increase, suggesting that together CD44 and LYVE1 have the potential to dramatically increase cell count. Similar affects were seen in the 3.125  $\mu$ M cisplatin treated cells with significant increases in cell count seen in CD44/LYVE1 exposure versus all other treatments, thereby negating cisplatin treatment. In 6.25, 12.5 and 25  $\mu$ M cisplatin treated concentrations, there was a trend of increased cell count with CD44/PBS and CD44/LYVE1 over collagen I/PBS and collagen

I/LYVE1. A diminished response is seen at 50  $\mu$ M cisplatin and a rebound in response is observed at 200  $\mu$ M.

The effects of LYVE1 and CD44 were further investigated at 3.125  $\mu$ M cisplatin, the concentration with the most significant response. RT112 cells were plated in multi-well plates pre-coated with collagen I (Supplemental Figure 12) or CD44 and collagen I (Figure 17A) and treated with DMSO or 3.125  $\mu$ M cisplatin and PBS or 7 two-fold dilutions of LYVE1 ranging from 6.25 ng/ml to 400 ng/ml. The cisplatin effect at this concentration was not as pronounced as previously observed, which could be due to cisplatin batch effects or degradation of cisplatin making it less effective. Despite this, there was a steady increase in cell count in collagen I coated plates in both DMSO and cisplatin treated cells in response to increasing concentrations of LYVE1 peaking at 50 ng/ml and a subsequent decrease up to 400 ng/ml, which were near PBS/DMSO control levels. There was also an increase in cell count in coated plates containing CD44 mixed with collagen I, which peaked at 12.5 and 50 ng/ml and decreased at 400 ng/ml.

Cell cycle analysis revealed there was a significant, but modest increase in the proportion of LYVE1 and cisplatin treated cells in S-phase in comparison to PBS and cisplatin treated cells in both CD44 (27% versus 22%) and collagen I (29% versus 25%) coated plates (Figure 17B). A significant difference was also observed between LYVE1 and cisplatin treated cells in S-phase in comparison to LYVE and DMSO, as well as PBS and DMSO. In CD44 coated plates, a trend in S-phase is appreciated with an increasing proportion of cells from PBS/DMSO, through LYVE1/DMSO, PBS/Cisplatin up to LYVE1/Cisplatin. A concomitant decrease trended in G0/G1 phase. Sub-G0/G1 phase is indicative of cells undergoing apoptosis. There was a trend in increased apoptotic cells

with PBS/cisplatin treatment, as well as a trend in LYVE1/DMSO and LYVE1/cisplatin treatment reducing levels of apoptotic cells. Collectively, cell cycle analysis suggests that LYVE1 reduces apoptosis, and either increases proliferation or enhances DNA repair in cells treated with cisplatin.

### 3.3.5 Effect of ligand treatment on cell count, proliferation, and differentiation in bladder cancer cell lines.

To determine whether the responses of cells to microenvironmental ligands is subtype dependent, experiments were conducted in cell lines representative of distinct subtypes. The luminal/claudin-high/KRT20-high cell line UMUC9, luminal/TP63-high subtype RT112, basal-squamous cell line HT1376, and mesenchymal cell lines JMSU1, TCCSUP were plated into collagen I coated or tissue culture treated plates, incubated overnight and treated with a single soluble ligand or PBS. After 23 or 47 hours of ligand treatment, cells were pulsed for one hour with EdU, fixed in 2% paraformaldehyde, and stained with immunofluorescent markers for DNA content (DAPI), EdU incorporation as a surrogate for proliferation, and differentiation state markers. The ratio of KRT14 to KRT20 was assessed in RT112 and UMUC9 on collagen I coated plates and RT112 on tissue culture treated plates treated with ligands for 24 hours, and the ratio of KRT14 to KRT5 on collagen I coated and tissue culture treated plates treated with ligands for 48 hours. Hierarchical clustering and a heatmap representation of cell count, EdU incorporation, KRT14 to 5 ratio, and KRT14 to 20 ratio were performed to assess the effects of ligand treatment across cell lines and plating conditions.

NRG1- $\alpha$  was stimulatory and promoted an increase in cell count across all cell lines and conditions, with the exception of RT112 plated in a tissue culture treated plate, which had a cell count similar to PBS (Figure 18A). NRG1- $\beta$  stimulated an increase in

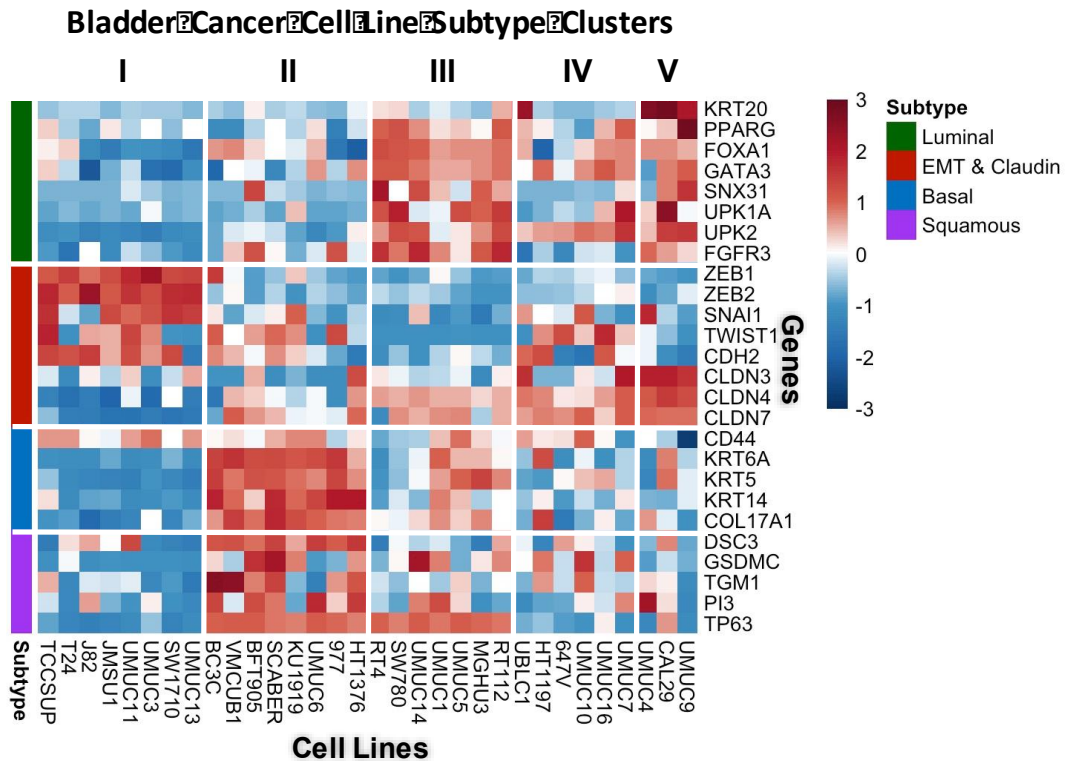


cell count in collagen I conditions, but inhibited cell count in tissue culture treated conditions leading to a differential response between NRG1- $\alpha$  and NRG1- $\beta$  in tissue culture treated plates. NRG1-SMDF mostly decreased cell count except for UMUC9 plated in collagen I, which was slightly stimulatory. Additionally, proteins that promote angiogenesis or lymphangiogenesis such as angiopoietin-1, VEGFA, CXCL12-  $\beta$  and LYVE1 clustered together due to having similar effects on cell count.

The most profound effects in EdU incorporation were observed in the cell lines TCCSUP and UMUC9 (Figure 18B). NRG1- $\alpha$  induced differential EdU incorporation by decreasing incorporation in TCCSUP and dramatically increasing in UMUC9. NRG1- $\beta$  and NRG1-SMDF both stimulated EdU incorporation in TCCSUP and UMUC9 demonstrating a differential response between NRG1- $\beta$  and NRG1- $\alpha$  in TCCSUP.

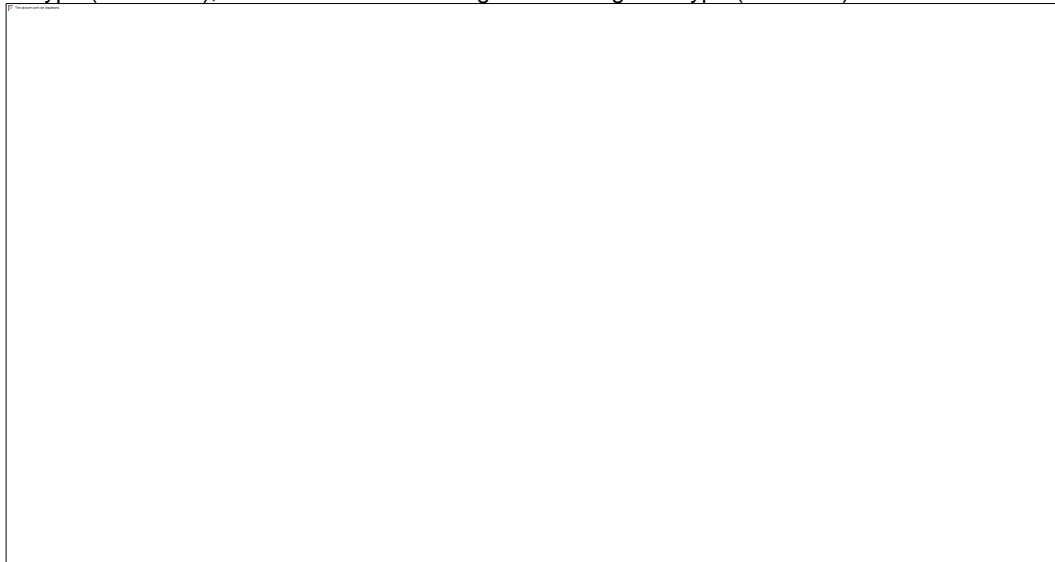
The most dramatic effects of ligands on KRT14 to KRT5 ratio were observed in the mesenchymal cell lines TCCSUP and JMSU1 (Figure 18C). NRG1- $\alpha$  promoted a decrease in KRT14 to 5 ratio indicating a shift to a more intermediate differentiation state, while NRG1- $\beta$  promoted an increase in KRT14 to 5 ratio indicating a shift to a more stem like state. NRG1-SMDF slightly increased KRT14 to 5 ratio in mesenchymal cell lines TCCSUP and JMSU1. NRG1-SMDF also clustered with other proteins such as LYVE1 that similarly promoted a decrease in KRT14 to 5 ratio in non-mesenchymal cell lines, excluding RT112 under tissue culture treated conditions. The ratio of KRT14 to 5 correlate with cell count in the mesenchymal cell lines JMSU1 and TCCSUP (Figure 18E). In general, the lower ratios correspond with higher cell count and vice versa. This indicates that ligands that promote an increase in cell number change their differentiation to a more intermediate state.

KRT14 to KRT20 ratio was assessed in only the luminal/claudin-high/KRT20-high cell line UMUC9, and the luminal/TP63-high subtype RT112 (Figure 18D). NRG1- $\alpha$ , NRG1- $\beta$ , and NRG1-SMDF all decreased the KRT14 to KRT20 ratio in UMUC9 cells, which also corresponded with an increase in EdU incorporation and cell count. Angiogenic and lymphangiogenic factors promoted a decrease in KRT14 to KRT20 ratio in UMUC9, with VEGFA inducing the most potent affect, which also stimulated the highest cell count. In RT112 cells, NRG1- $\beta$  and NRG1-SMDF promoted an increase in KRT14 to KRT20, which corresponded with a decrease in cell count. NRG1- $\alpha$  showed a decrease in KRT14 to KRT20 ratio and corresponded with an increase in cell count. The ratio of KRT20 to 14 correlate with cell count in the luminal cell lines RT112 and UMUC9 (Figure 18E). In general, the higher ratios correspond with higher cell count and vice versa. This collectively suggests that a greater shift to a fully differentiated state promotes an increase in proliferation and cell.



**Figure 10. Heatmap of bladder cancer cell lines hierarchically clustered to identify molecular subtypes.**

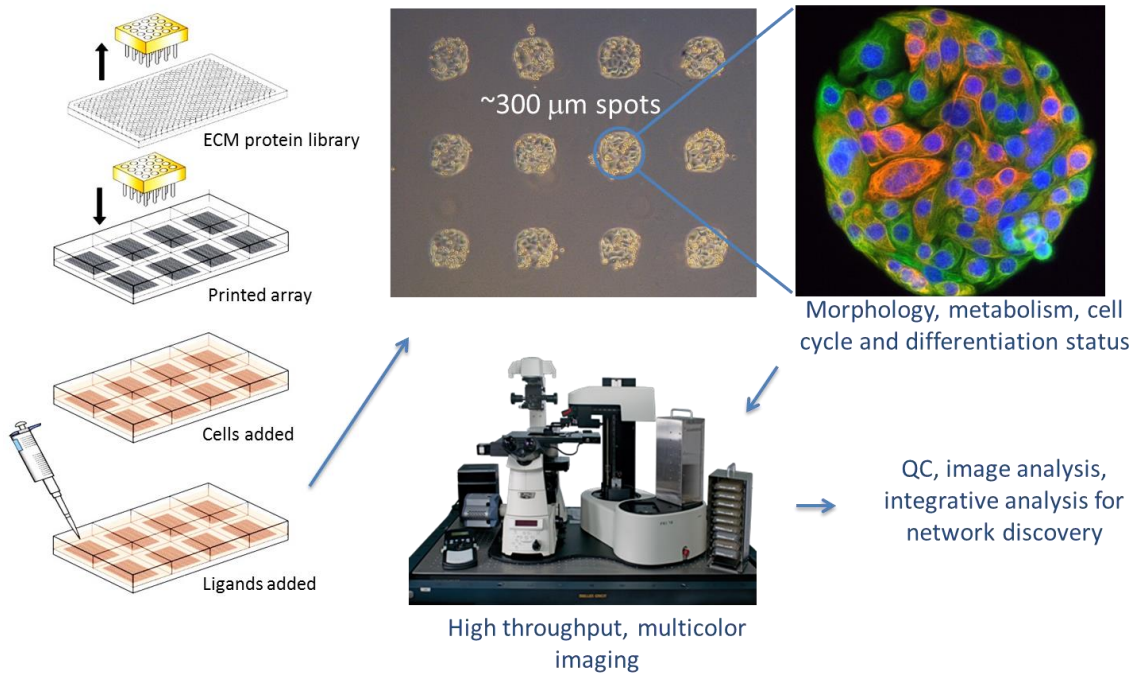
Thirty-two bladder cancer cell lines (x-axis) were organized by unsupervised hierarchically clustering using z-scored expression of a subset of genes defined by TCGA (y-axis) to identify molecular subtypes. Five main clusters were identified corresponding to a mesenchymal subtype rich in EMT genes (Cluster I), a basal-squamous subtype (Cluster II), a luminal/TP63-high subtype (Cluster III), a luminal/TP63-low/FGFR3-low subtype (Cluster IV), and a luminal/claudin-high/KRT20-high subtype (Cluster V).



**Figure 11. Expression of differentiation state markers reveals phenotypic heterogeneity in bladder cancer cell lines.**

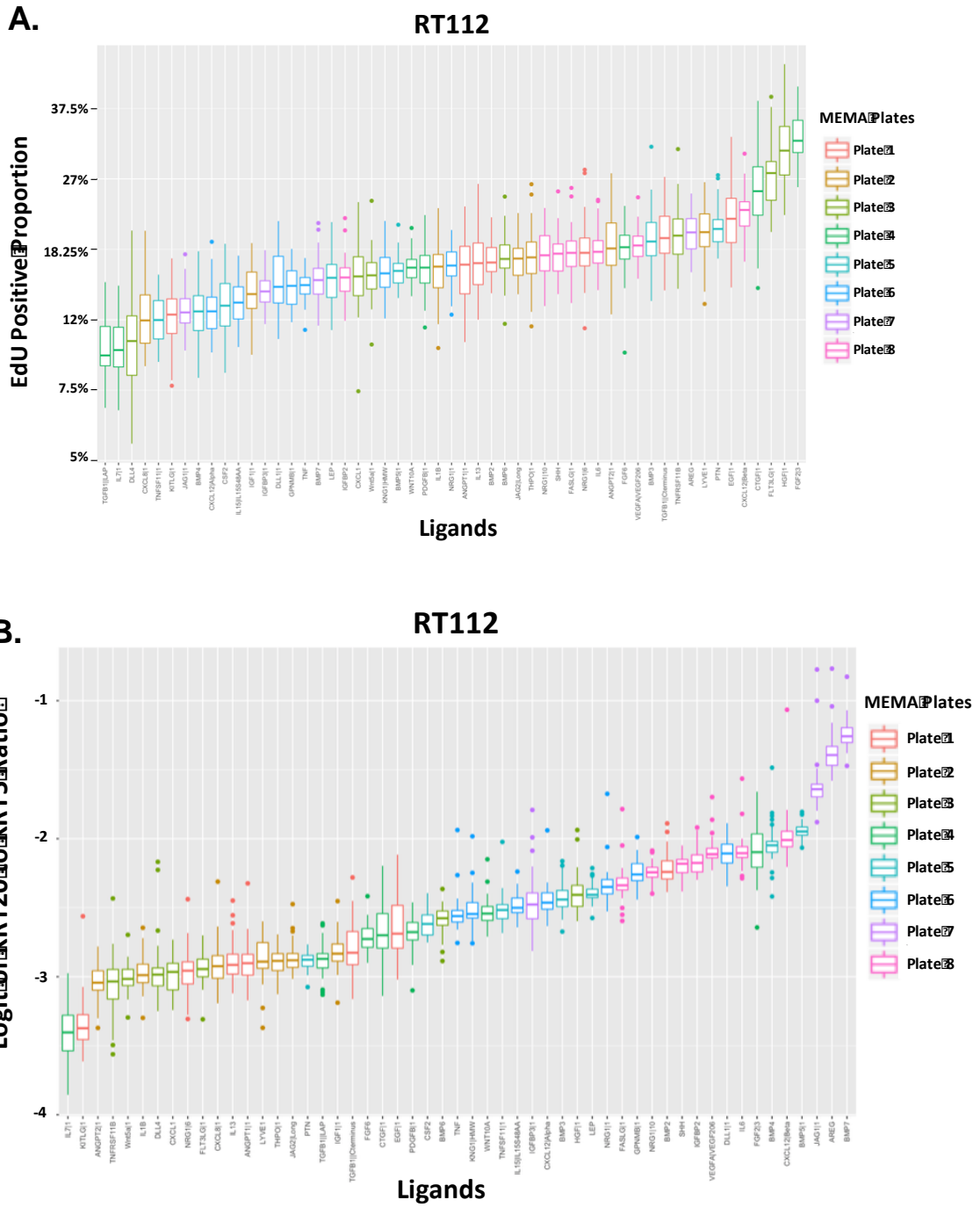
(A) Expression patterns in a fresh frozen paraffin embedded patient bladder cancer tissue sample stained with DAPI and for expression of KRT5, KRT14, and KRT20. (B) The basal-squamous cell line SCaBER stained with DAPI and for KRT14 and the squamous marker TP63. (C) Bladder cancer cell lines CAL29,

HT1376, JMSU1, RT112, SCaBER, TCCSUP, UMUC9, UMUC10, and VMCUB1 stained for the expression patterns of KRT5, KRT14, and KRT20.

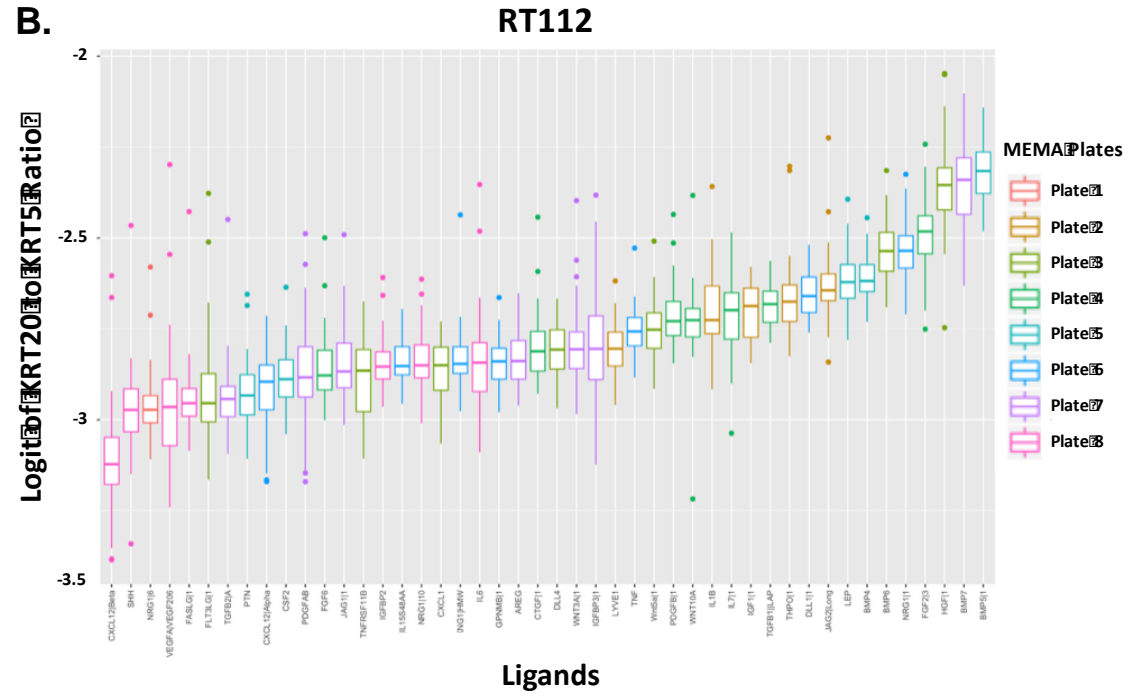
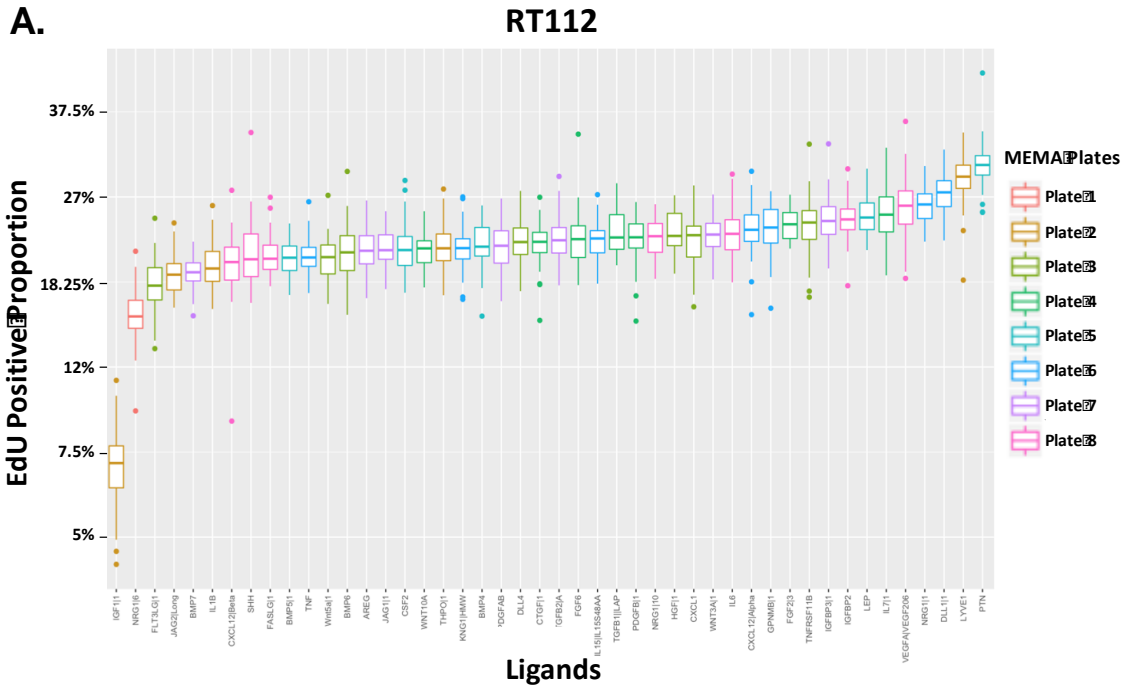


**Figure 12. The MicroEnvironment MicroArray (MEMA) platform.**

A library of 48 insoluble extracellular matrix (ECM) proteins is spotted (300 μm) onto the bottom of 8-well polystyrene microplates and desiccated for 48 hours. Suspended cells are added to each well and allowed to adhere to the ECM spots for 1 hour. Non-adherent cells are washed off and fresh culture media is added. Cells are cultured overnight and a single soluble ligand is added to each well or PBS as a control. Cells are fixed and stained after 48 hours after ligand treatment and stained for endpoints of interest. A high-throughput system captures images of each spot with stained cells followed by quality control and other analyses for extraction of features. Adapted from "Microenvironment-Mediated Mechanisms of Resistance to HER2 Inhibitors Differ between HER2+ Breast Cancer Subtypes" by S. Watson, *et.al.*, 2018, *Cell Systems*, Volume 6 (Issue 3), p.329-342. Copyright [2018] by the Elsevier Inc<sup>255</sup>.



**Figure 13. Microenvironment factors influence EdU incorporation and differentiation state.**  
 (A) Box plots of percent EdU proportion ( $n = 15$ , mean, upper & lower quartile, min & max, with outliers) of RT112 cells following 48 hours of soluble ligand (x-axis) and DMSO treatment on MEMAs. (B) Box plots of normalized KRT20 to KRT5 ratio ( $n = 15$ , mean, upper & lower quartile, min & max, with outliers) of RT112 cells following 48 hours of ligand (x-axis) and DMSO treatment on MEMAs. Plates are colored to identify potential batch effects.



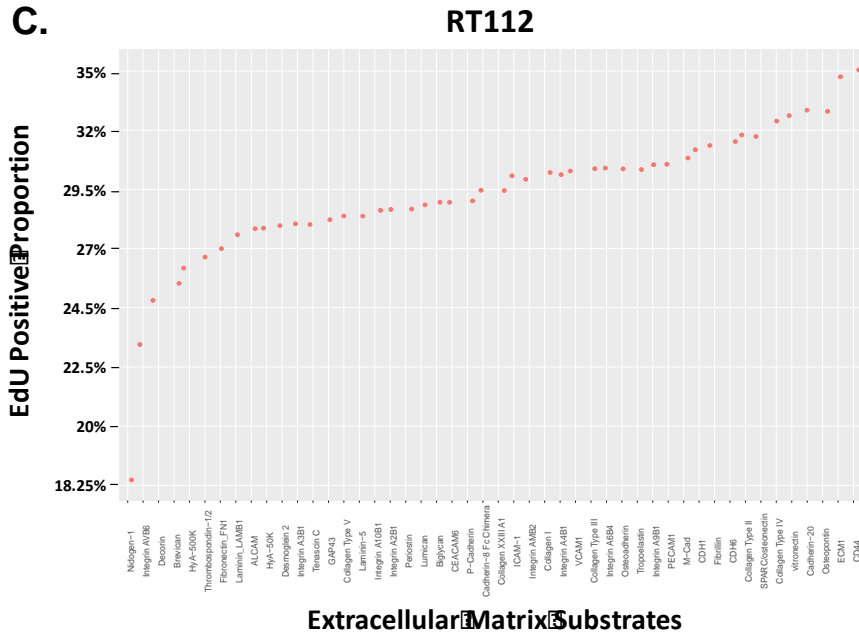


**Figure 14. Microenvironment factors influence EdU incorporation and differentiation state after cisplatin treatment.**

(A) Box plots of percent EdU proportion ( $n = 15$ , mean, upper & lower quartile, min & max, with outliers) of RT112 cells following 48 hours of ligand (x-axis) and  $25 \mu\text{M}$  cisplatin treatment on MEMAs. (B) Box plots of normalized KRT20 to KRT5 ratio ( $n = 15$ , mean, upper & lower quartile, min & max, with outliers) of RT112 cells following 48 hours of ligand (x-axis) and  $25 \mu\text{M}$  cisplatin treatment on MEMAs. (C) Mean values of percent EdU incorporation of RT112 taken from (A) of the soluble ligand LYVE1 in combination with insoluble ECM substrates. Plates are colored to identify potential batch effects.

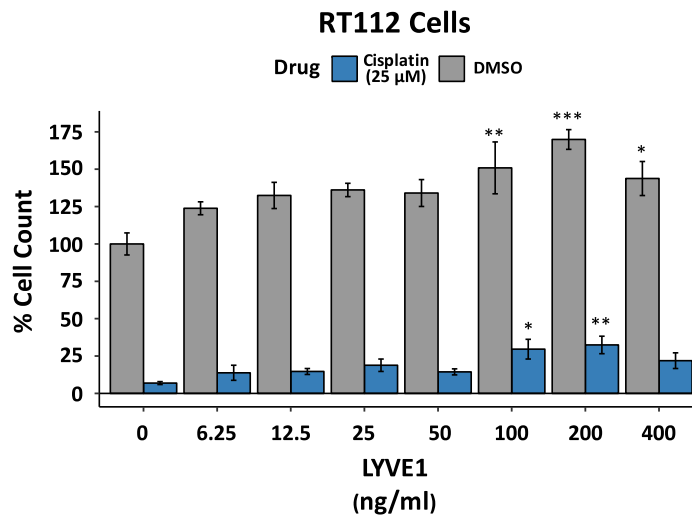


**Figure 15. LYVE-1 increases bladder cancer cell number in a dose response manner and does so in the presence of cisplatin in tissue-culture treated plates.**

Percentage of mean cell count and SEM ( $n = 3$ ) of RT112 cells following 48 hours of  $25 \mu\text{M}$  cisplatin or DMSO treatment, and PBS or 7 two-fold dilutions of LYVE1 ranging from  $6.25 \text{ ng/ml}$  to  $400 \text{ ng/ml}$ . Cell count was normalized to DMSO/PBS treatment.

## RT112 Cells

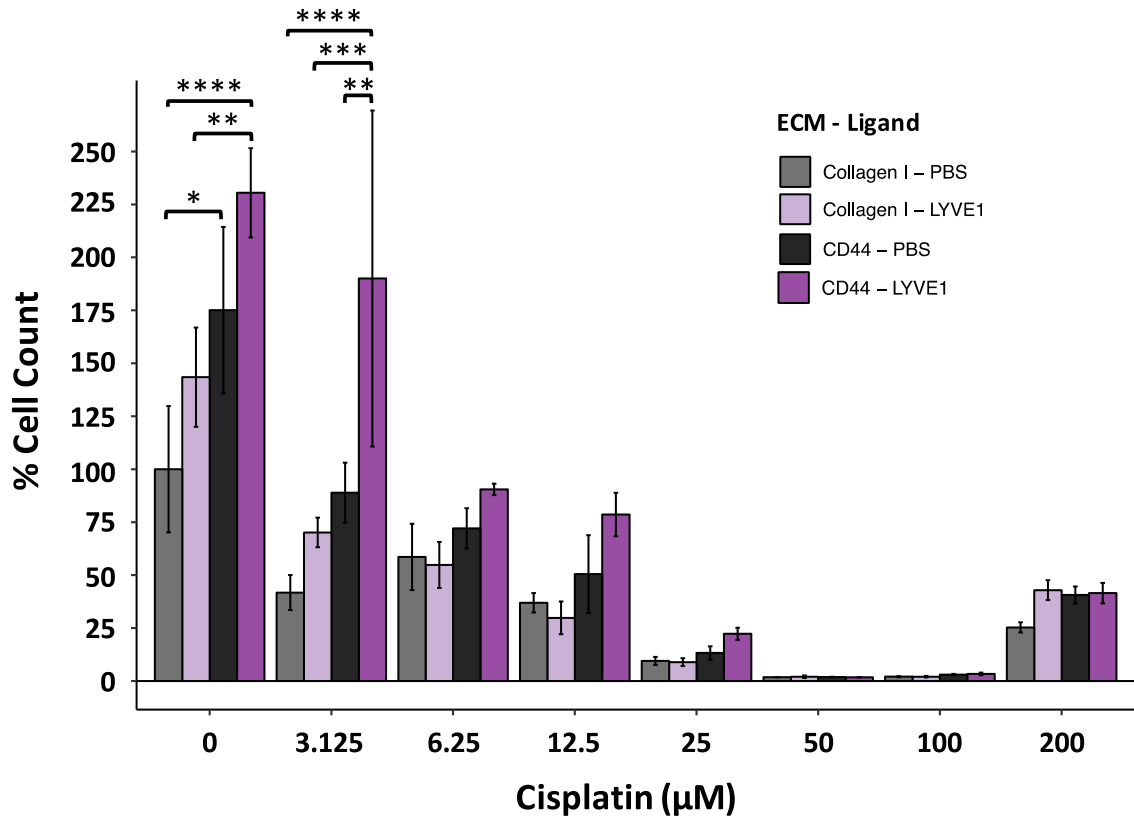
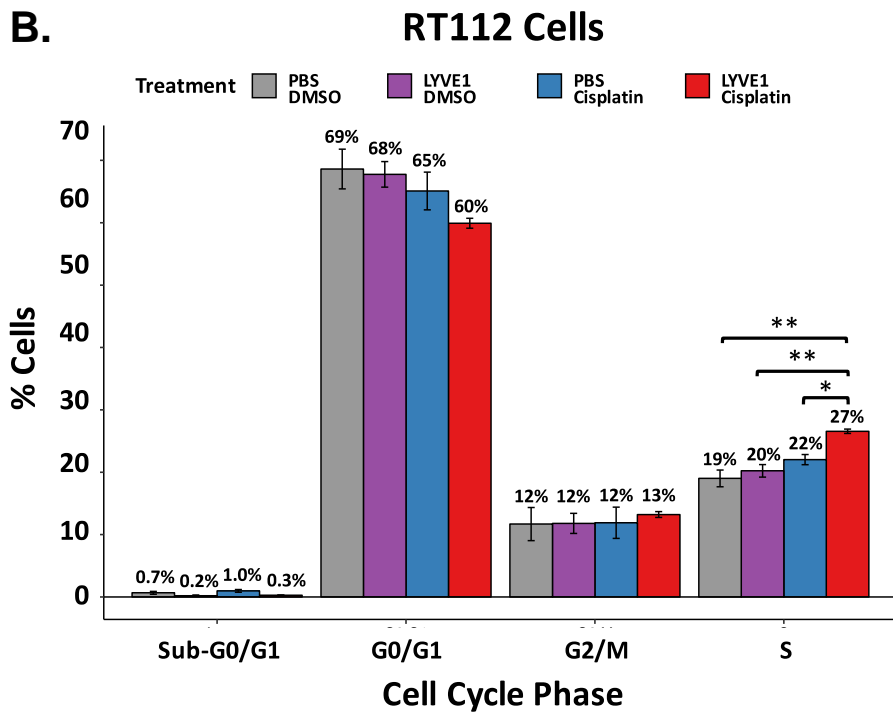
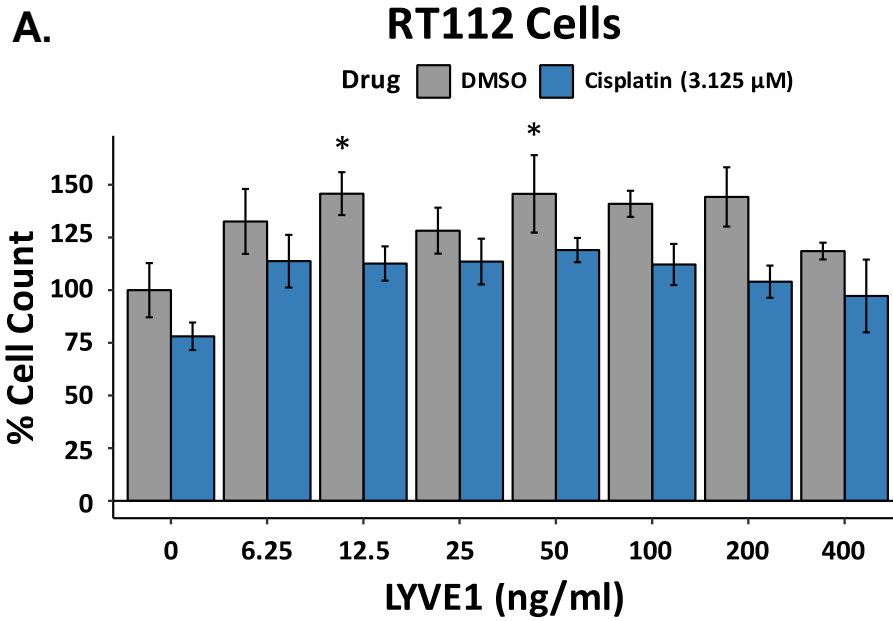


**Figure 16. LYVE-1 increases bladder cancer cell number in plates pre-coated with collagen I or CD44 and collagen I.**

Percentage of mean cell count and SEM ( $n = 3$ ) of RT112 cells seeded into plates pre-coated with collagen I or CD44 and collagen I and exposed for 48 hours to 50 ng/ml LYVE1 or PBS treatment, and DMSO or 7 two-fold dilutions of cisplatin ranging from 3.125  $\mu\text{M}$  to 200  $\mu\text{M}$ . Cell count was normalized to collagen I/DMSO/PBS treatment.





C.

## CD44

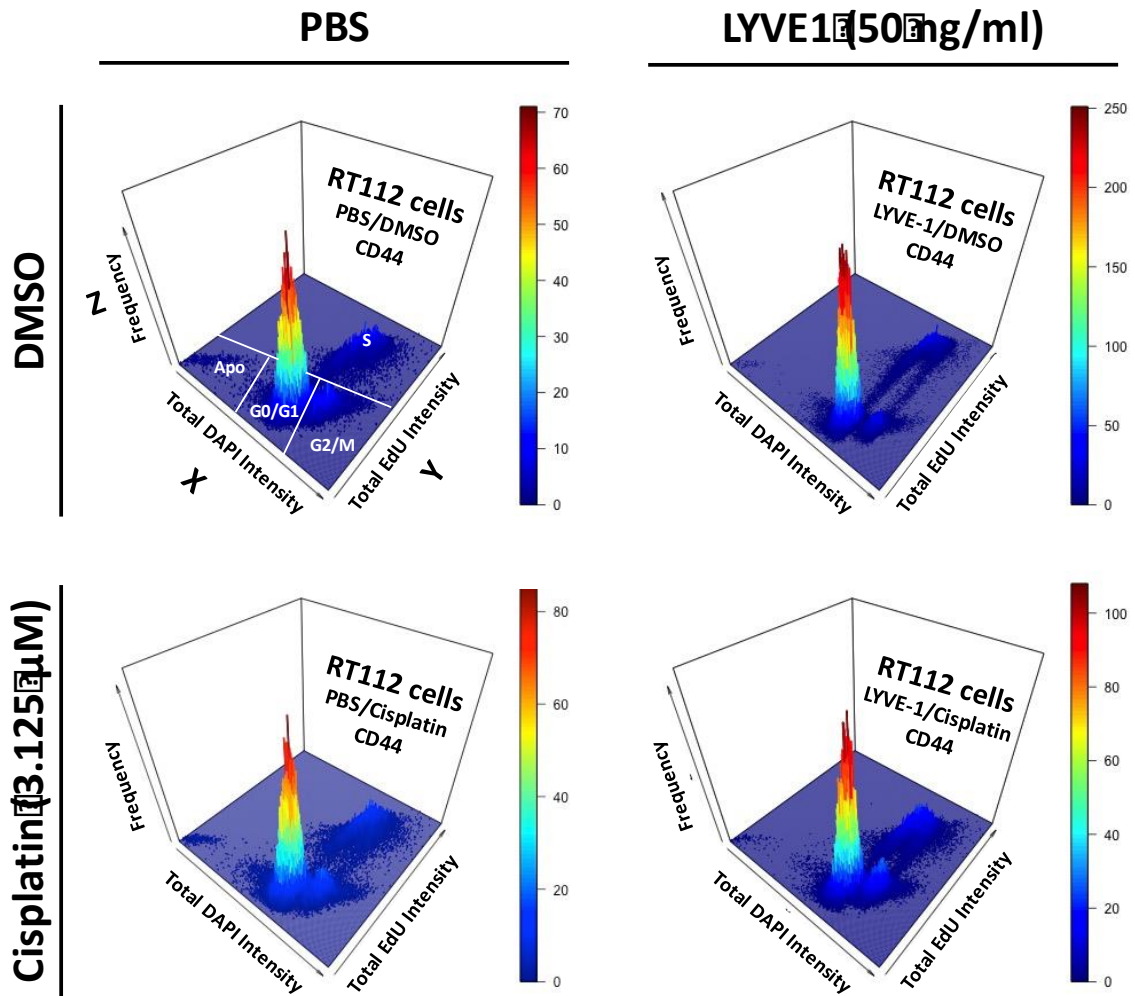
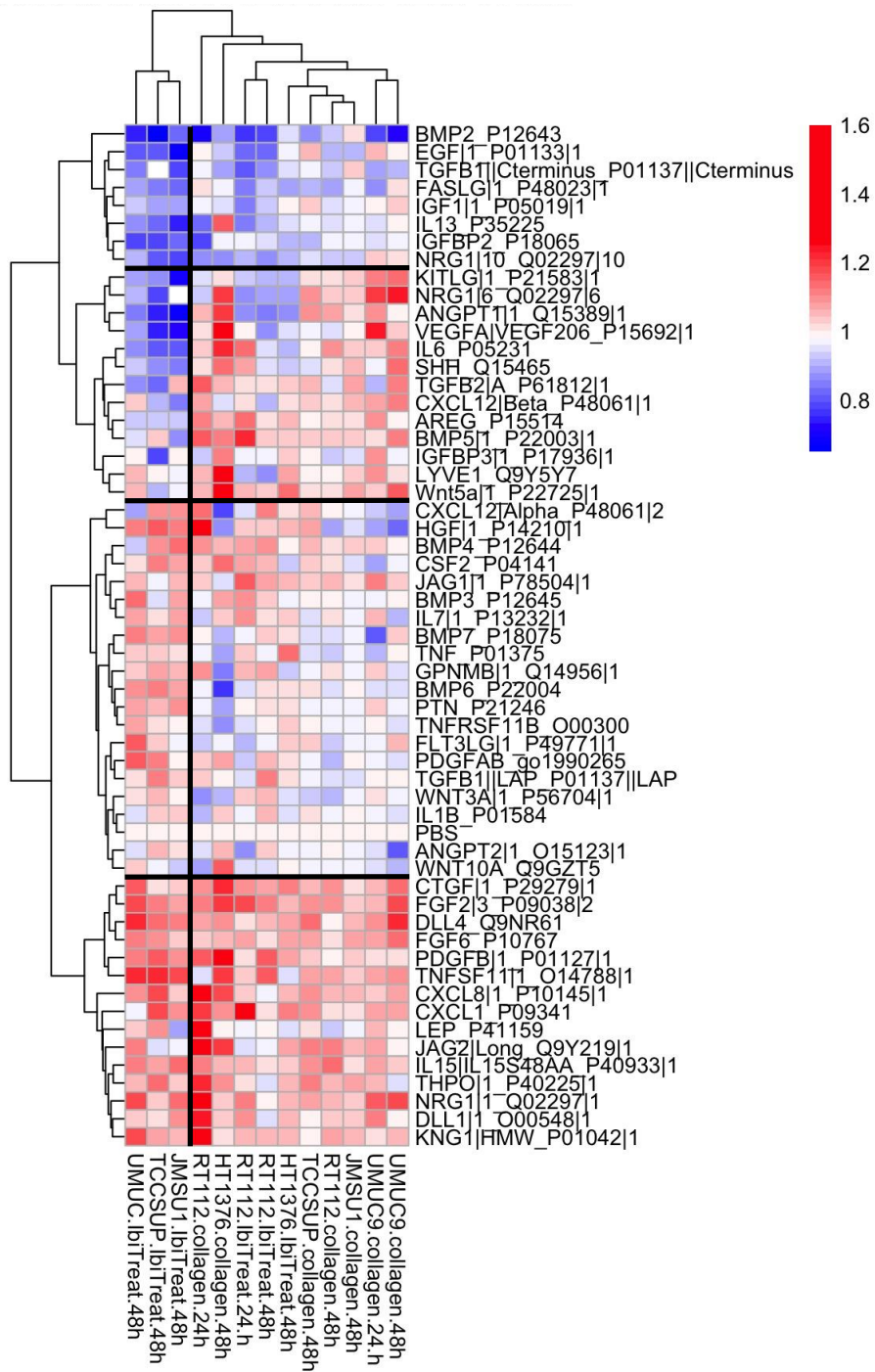


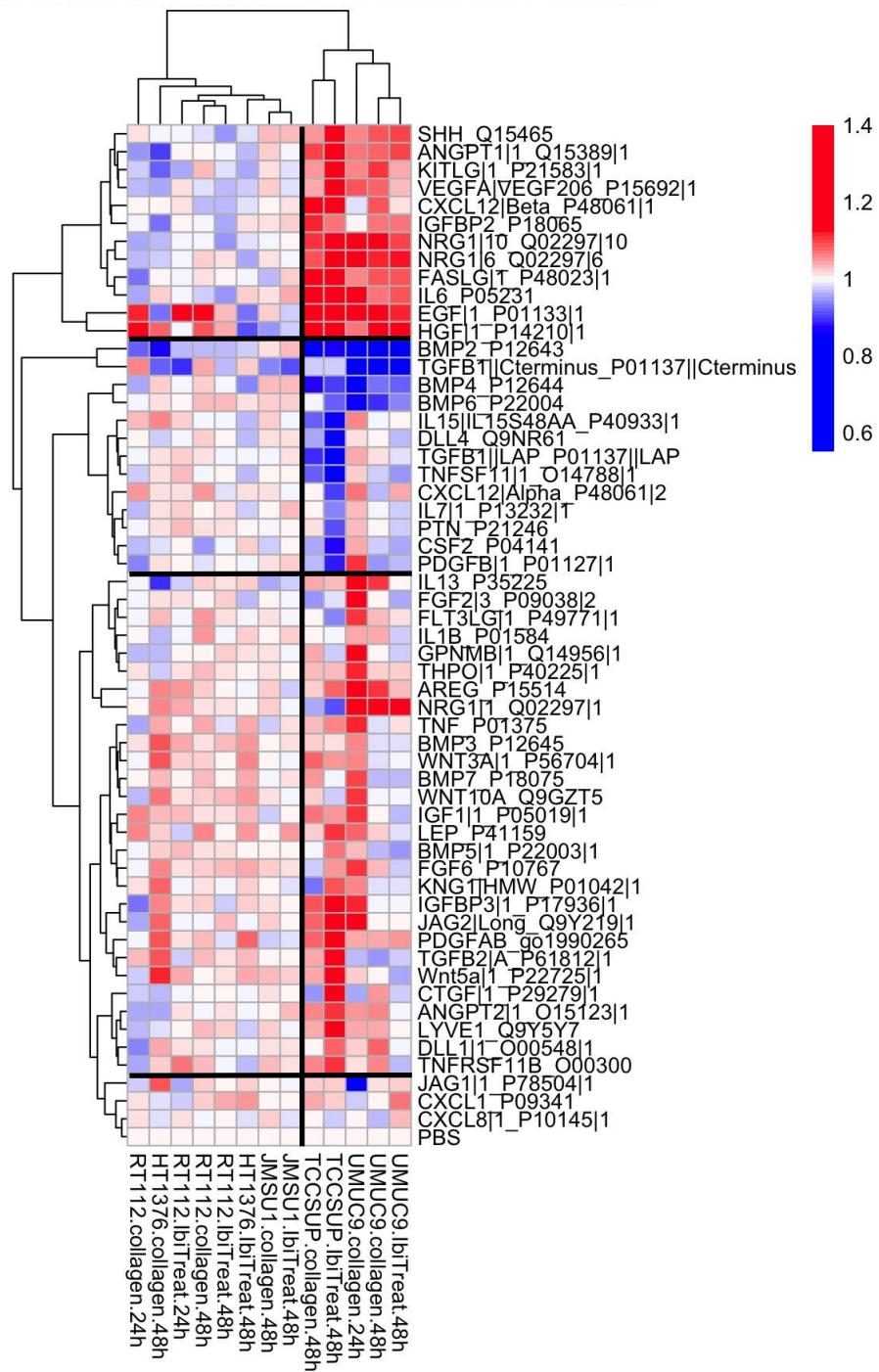
**Figure 17. LYVE-1 increases bladder cancer cell number and percentage of cells in S phase in plates pre-coated with CD44 and collagen I.**

(A) Percentage of mean cell count and SEM ( $n = 3$ ) of RT112 cells seeded into plates pre-coated with CD44 and collagen I and exposed for 48 hours to 3.125  $\mu\text{M}$  cisplatin or DMSO, and PBS or 7 two-fold dilutions of LYVE1 ranging from 6.25 ng/ml to 400 ng/ml. Cell count was normalized to DMSO/PBS treatment. (B) Cell cycle analysis of data from (A) of specific treatments including PBS or 50 ng/ml LYVE1, and DMSO or 3.125  $\mu\text{M}$  cisplatin. Percentage of S phase cells was calculated by identifying a local minimum in the histogram of total EdU intensity and gating cells into EdU positive or negative that were above or below the local minimum, and calculating total EdU positive over total cells. Percentage of sub-G0/G1, G0/G1, and G2/M cells was calculated by identifying two local minimums in the histogram of total DAPI intensity. EdU negative cells were then taken and sub-G0 cells were gated into the lowest DAPI intensity group, G0/G1 were gated into the medium DAPI intensity group, and G2/M cells were gated into the highest DAPI intensity group, and percentages were calculated by quantifying cells in each gate over total cells. (C) 3-dimensional histogram of single cell total intensity of DAPI (x-axis), total intensity of EdU (y-axis), and frequency of cells in each bin (z-axis; 62,500 bins) spatially showing distinct phases of the cell cycle as indicated in the DMSO/PBS treatment. Apo: sub-G0/G1 apoptotic cells; G0/G1: G0/G1 phase of the cell cycle; G2/M: G2/M phase of the cell cycle; S: S phase of the cell cycle.

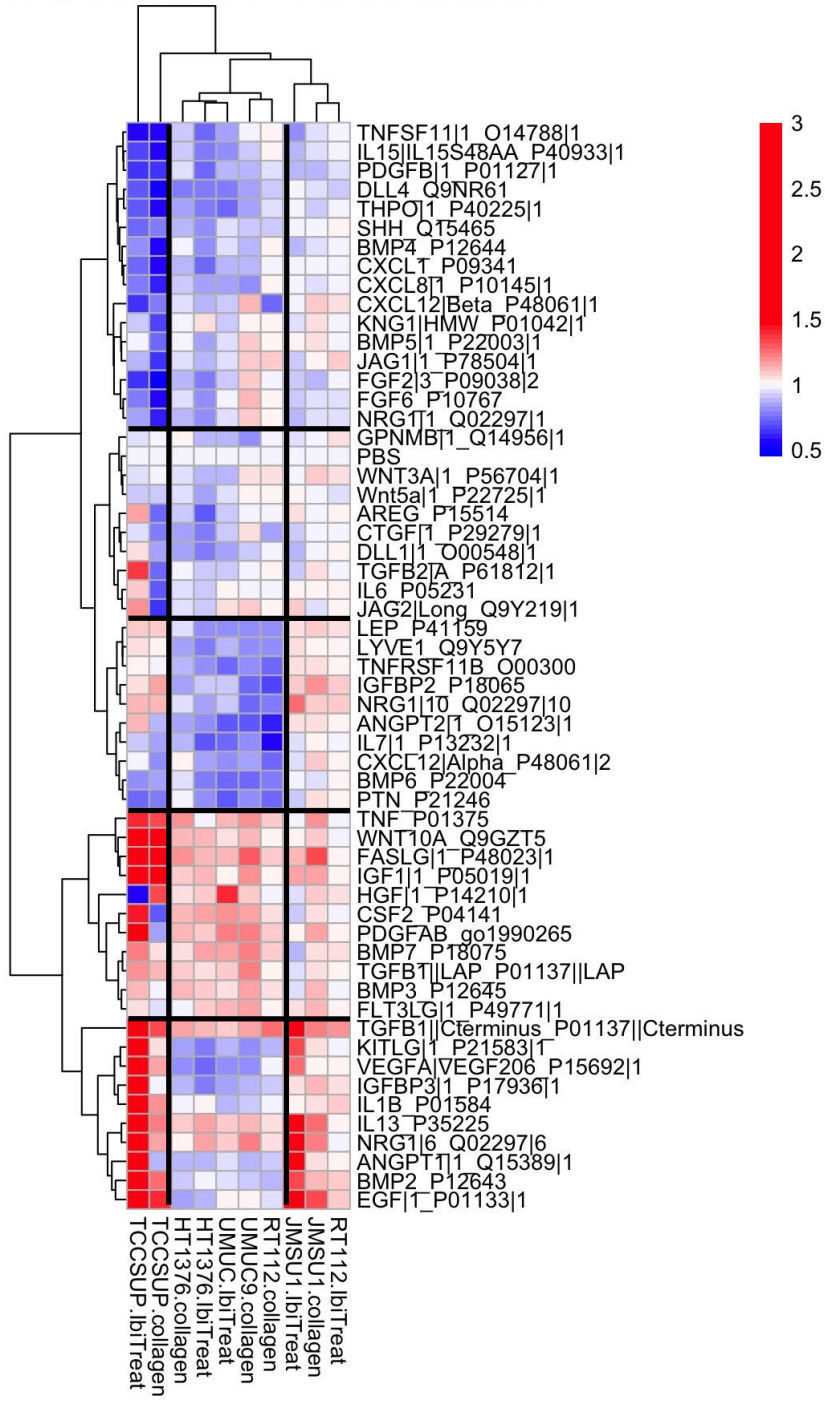
# A. Effect of Ligands on Cell Count



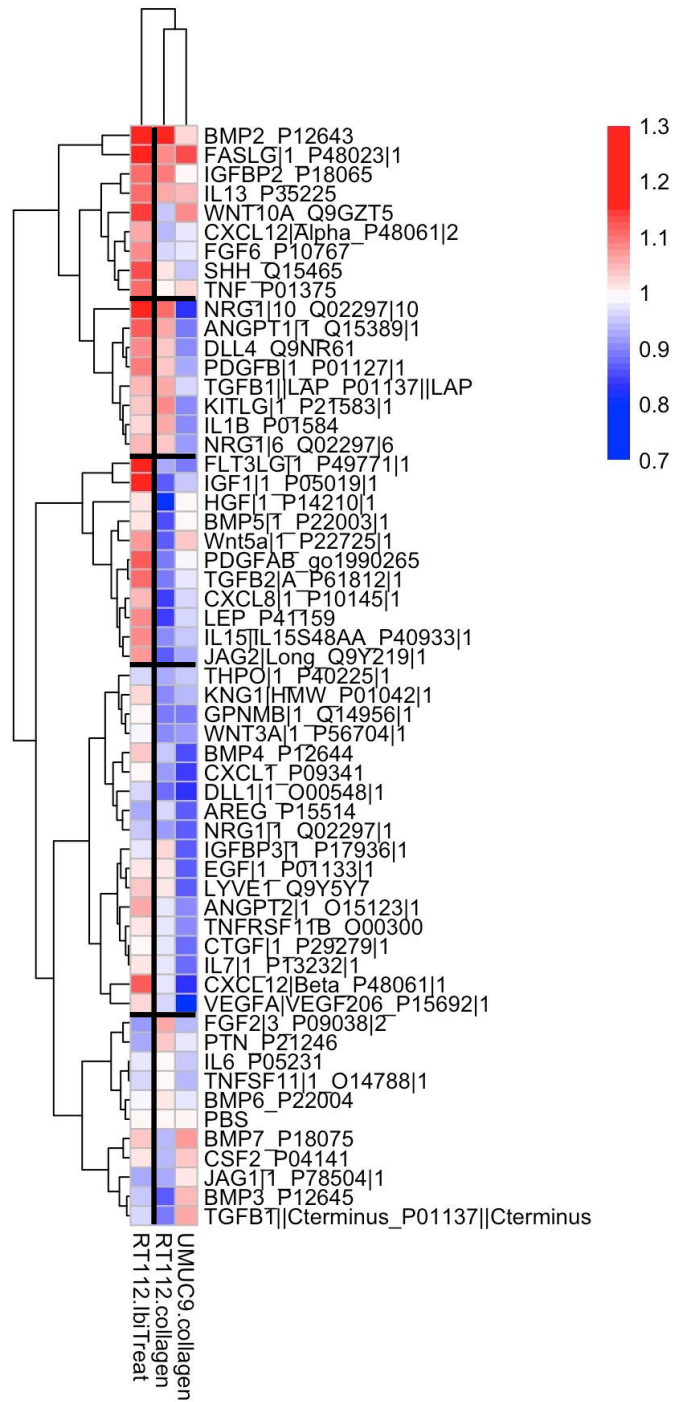
## B. Effect of Ligands on EdU Positive Proportion



### C. Effect of Ligands on KRT14 to KRT5 Ratio



## D. Effect of Ligands on KRT14 to KRT20 Ratio



**E.**

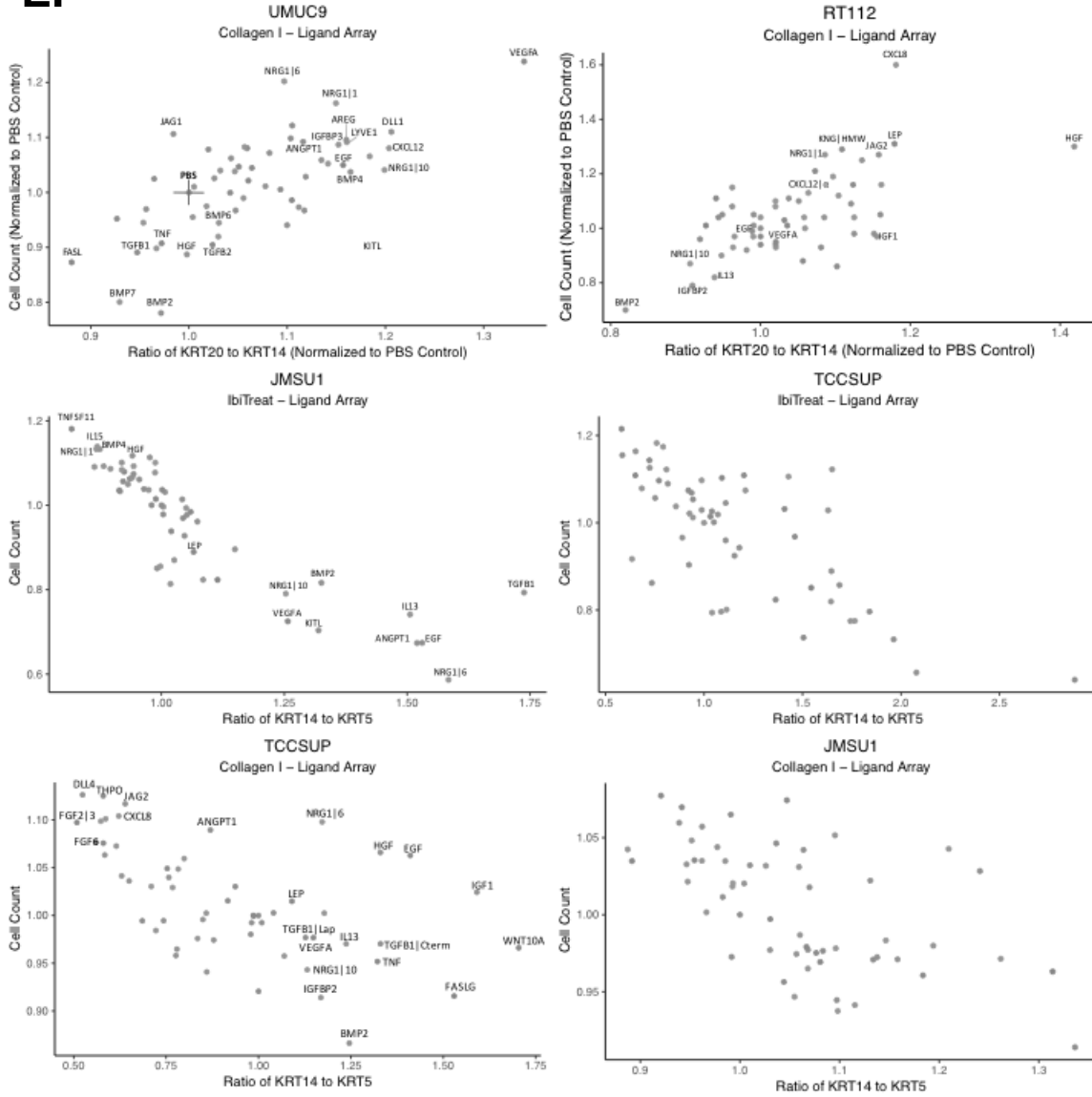
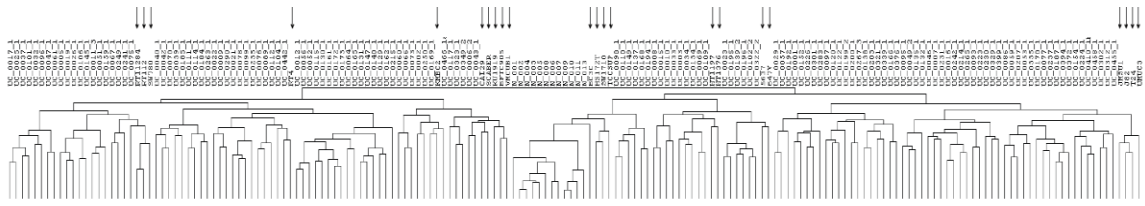


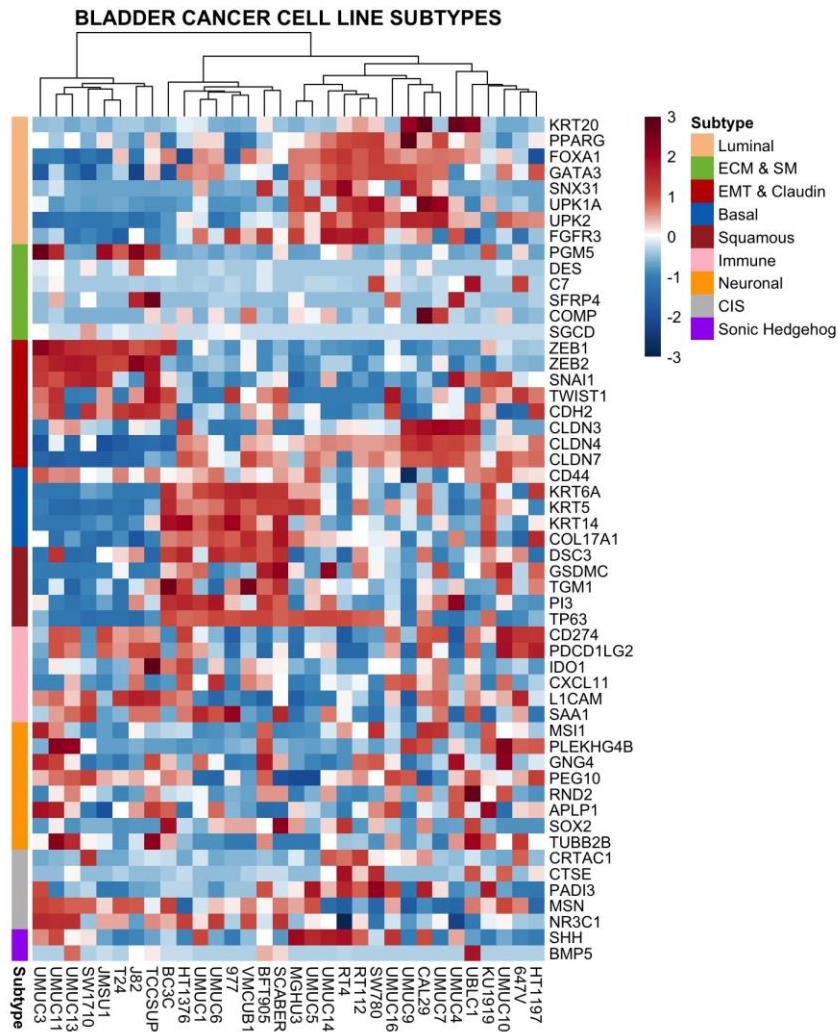
**Figure 18. Effect of soluble ligand treatment on cell count, proliferation, and differentiation in bladder cancer cell lines.**

HT1376, JMSU1, RT112, UMUC9, and TCCSUP1 were seeded onto tissue culture treated plates (IbiTreat) or collagen I pre-coated plates, incubated overnight and treated with soluble ligands for 24 or 48 hours. Heatmaps of the effect of ligands on (A) cell count, (B) EdU incorporation, (C) KRT14 to KRT5 ratio, and (D) KRT14 to KRT20 ratio were plotted. (E) Scatter plot showing the relationship between cell count (y-axis) and the ratio of KRT20 to KRT14 (UMUC9 and RT112 cells after 24 hour ligand treatment) or KRT14 to KRT5 (JMSU1 and TCCSUP cells after 48 hour ligand treatment). All values were normalized to PBS control for each cell line in their respective treatments.



**Supplemental Figure 9. A panel of bladder cancer cell lines models the genomic diversity of primary bladder cancer tumors.**

Gene expression data from the Cancer Cell Line Encyclopedia<sup>265</sup> was integrated with gene expression data from a patient data set<sup>266</sup> and hierarchically clustered. Cell lines (marked with arrows) disperse evenly throughout the cluster dendrogram of patient samples. Adapted from unpublished data from a previous post-doctoral fellow in the Gray lab, Trevor Levin.



**Supplemental Figure 10. Heatmap of bladder cancer cell lines hierarchically clustered to identify molecular subtypes.**

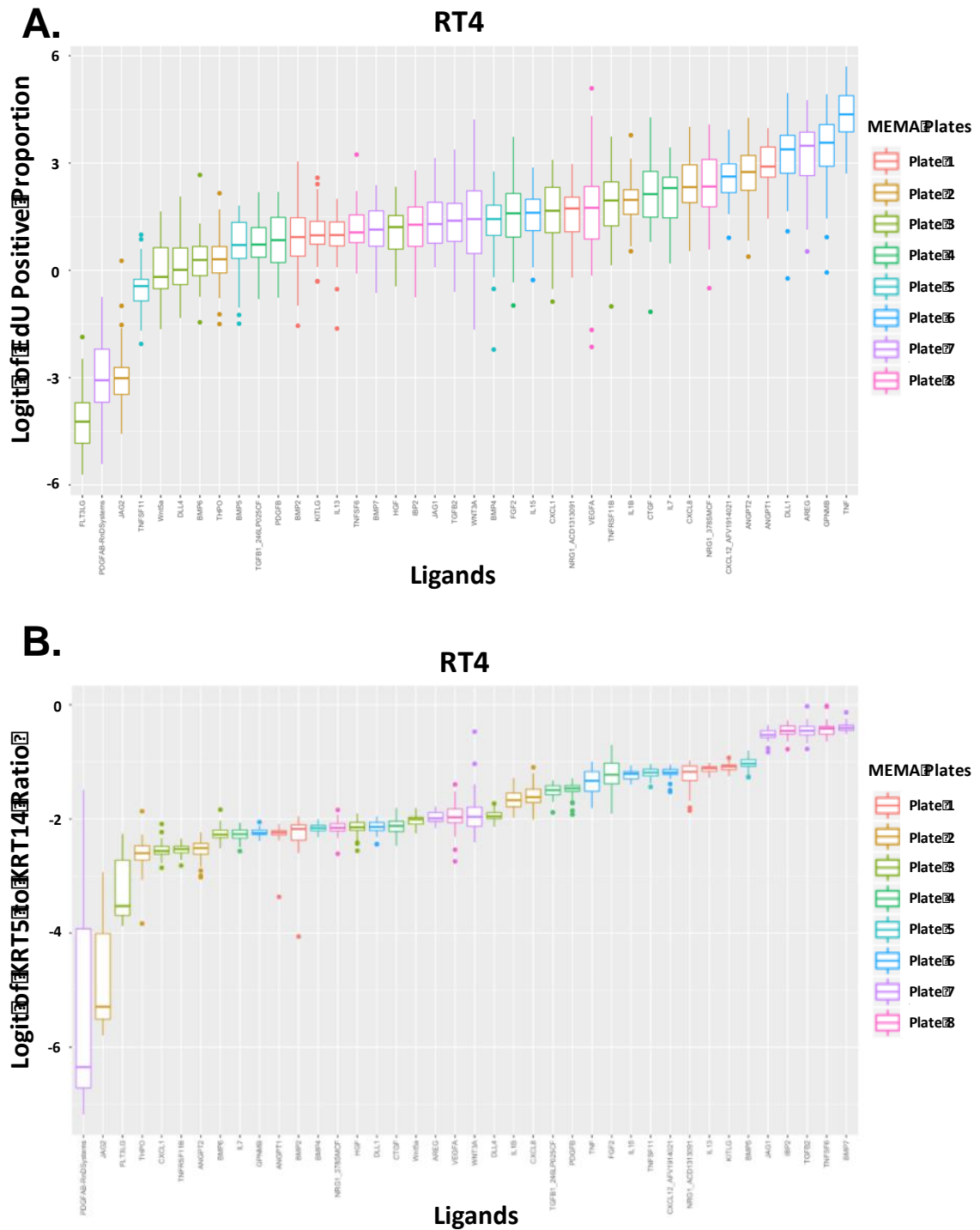
Thirty-two bladder cancer cell lines (x-axis) were organized by unsupervised hierarchically clustering using z-scored expression of genes defined by TCGA (y-axis) to identify molecular subtypes.



**Supplemental Table 3. Genetic characterization of major oncogenes and tumor suppressor genes in urinary bladder cancer cell lines.**

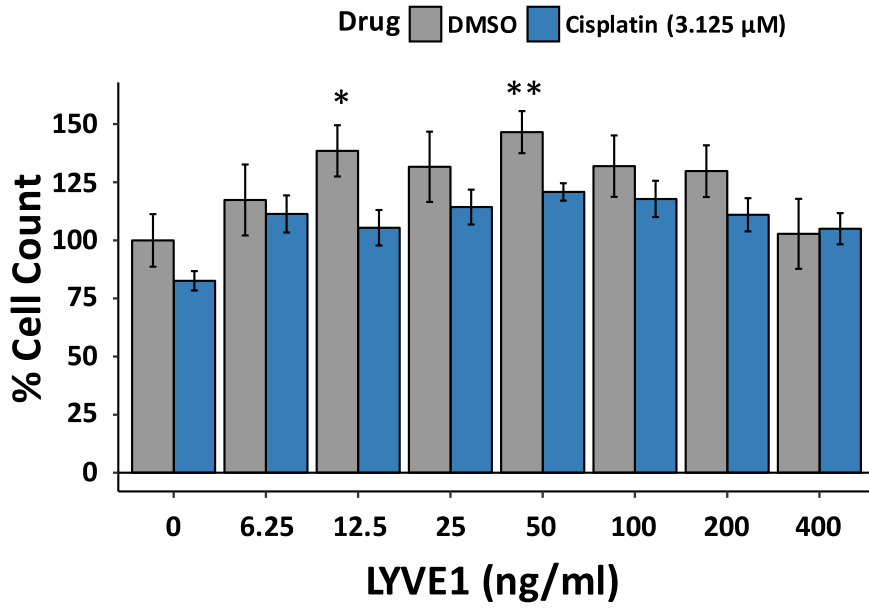
Amp, amplification; WT, wild type; Mut, mutant; LOH, loss of heterozygosity; HD, homozygous deletion; N, copy number neutral; Y, Y chromosome detected. Adapted from "The UBC-40 Urothelial Bladder Cancer cell line index: a genomic resource for functional studies" by J. Earl, *et. al.*, BMC Genomics, 2015, Volume 16 (Issue 1), p.403<sup>267</sup>.

Name	Stage	Grade	Sex	FGFR3	PIK3CA	H-RAS	N-RAS	TERT	INK4A	TP53
97-7	T1	G2/3	Y	S249C	WT	WT	WT	Mut	WT	cd28/N
HT1197	T2	G4	M	S249C	E545K	WT	WT/Q64R	Mut	WT	WT/c.1094A>G
HT1376	T2	G3	F	WT	WT	WT	WT	Mut	WT	c.749C>T/LOH
J82	T3	G3	M	WT/K652E	P124L	WT	WT	Mut	WT	c.960G->C&c.820G->T&c.811G-
MGH-U3	Ta	G1	M	Y375C/Y373C	WT	WT	WT	Mut	HD	WT/N
RT112		G2	F	WT/Amp/FGFR3-TACC3 fusion	WT	WT	WT	Mut	HD	c.743G>A&c.548C>G/LOH
RT4	T2	G1	M	WT/Amp/FGFR3-TACC3 fusion	WT	WT	WT	Mut	HD	WT/LOH
SCaBER	T3		M	WT	WT	WT	WT	Mut	LOH	c.329G>T/LOH
SW-1710			F	WT	WT	WT	WT	Mut	HD	c.817C>T/LOH
SW-780		G1	F	WT/S773F2/FGFR3-BAIAP2L1	WT	WT	WT	Mut	HD	WT/N
T24		G3	F	WT	WT	G12V	WT	Mut	WT/LOH	c.378C>G/N
TCCSUP	T4	G4	F	WT	E545K	WT	WT	Mut	WT	c.1045G>T/LOH
UM-UC-1		G2	M	WT	WT	WT	WT		HD	c.454C->T/LOH
UM-UC-3			M	WT	WT	WT	WT	Mut	HD/WT	c.338T>G/N
UM-UC-4			F	WT	WT				WT	LOH
UM-UC-5			F	WT	E545K	WT	WT	Mut	HD	LOH
UM-UC-6			M	WT/R248C	E545K	WT			HD	WT/LOH
UM-UC-7			M	WT	WT	WT		Mut	WT	LOH
UM-UC-9				WT	WT	WT		Mut	LOH	Mut/LOH
UM-UC-10				WT	WT	WT	WT	Mut		Mut
UM-UC-11				WT	WT	WT	WT	Mut	HD	WT/N
UM-UC-13			Y	WT	WT	WT	WT	Mut	LOH	Mut/N
UM-UC-14			Y	S249C	WT			Mut	HD	Mut/LOH
VM-CUB-1		G2	M	WT	WT/E542K+E67	WT	WT	Mut	c.322G>C/LOH	c.524G>A&c.378C>G/LOH

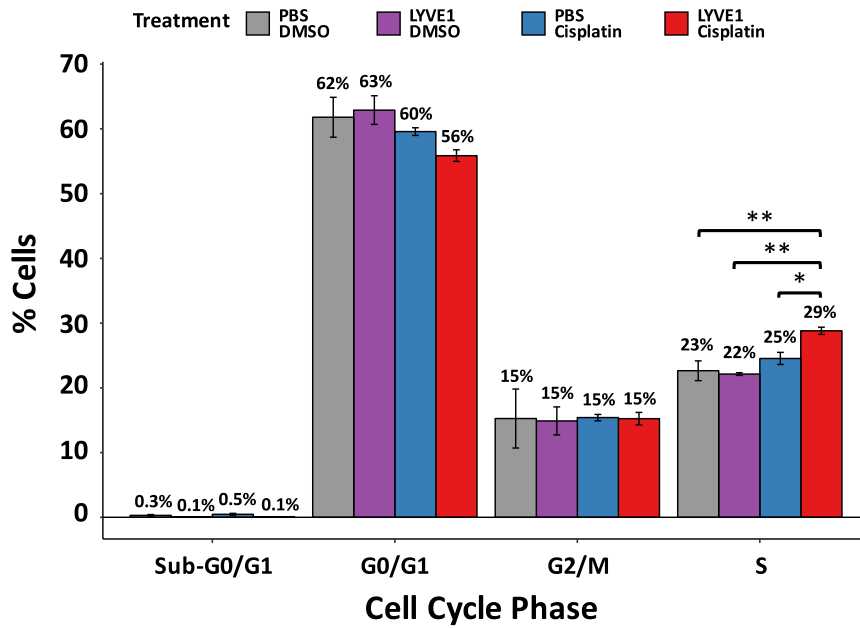


**Supplemental Figure 11. Microenvironment factors influence EdU incorporation and differentiation.** (A) Box plots of percent EdU proportion ( $n = 15$ , mean, upper & lower quartile, min & max, with outliers) of RT4 cells following 48 hours of soluble ligand (x-axis) and 200 nM PD173071 treatment on MEMAs. (B) Box plots of normalized KRT5 to KRT14 ratio ( $n = 15$ , mean, upper & lower quartile, min & max, with outliers) of RT4 cells following 48 hours of ligand (x-axis) and 200 nM PD173071 treatment on MEMAs. Plates are colored to identify potential batch effects.

### A. RT112 Cells

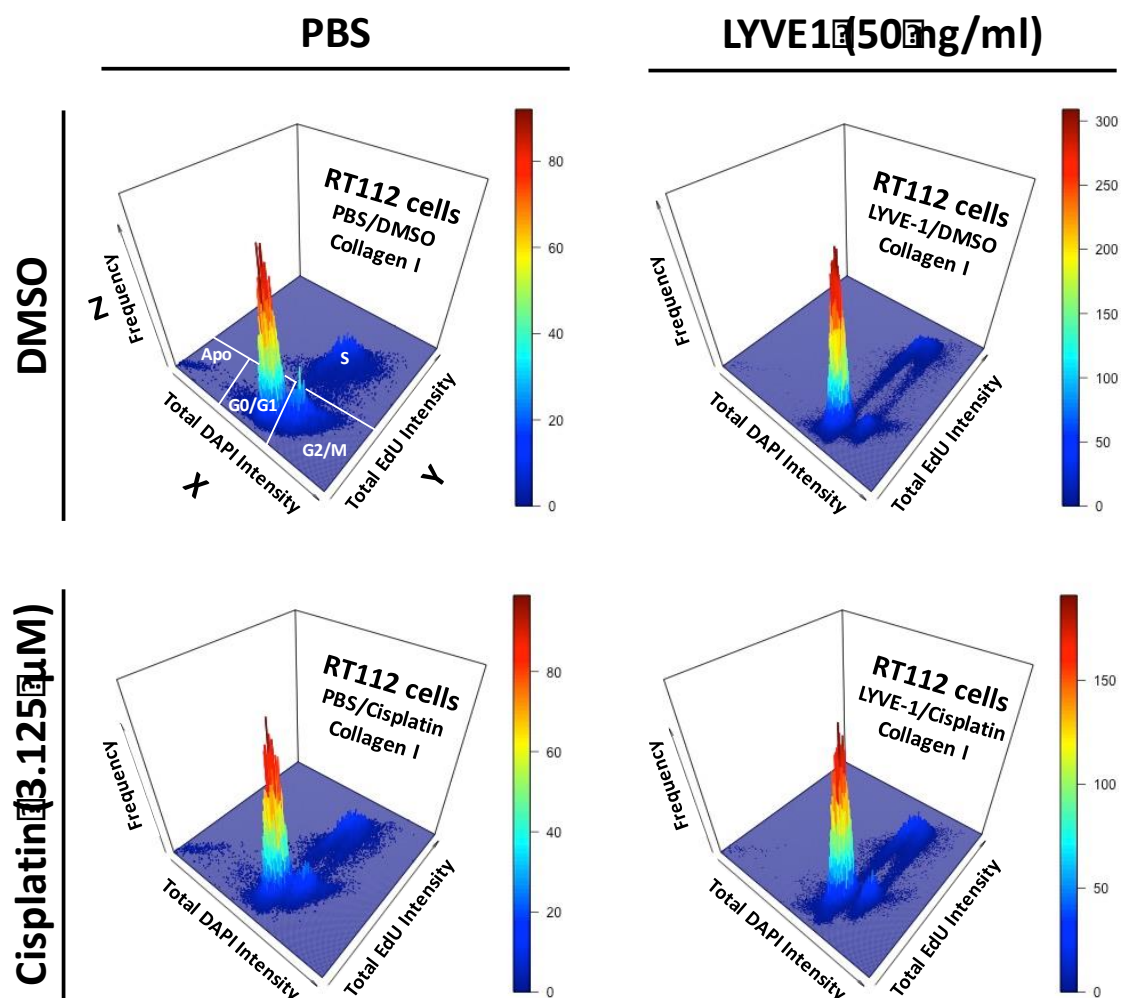


### B. RT112 Cells



C.

## Collagen I



**Supplemental Figure 12. LYVE-1 increases bladder cancer cell number and percentage of cells in S phase in plates pre-coated with collagen I.**

(A) Percentage of mean cell count and SEM ( $n = 3$ ) of RT112 cells seeded into plates pre-coated with CD44 and collagen I and exposed for 48 hours to 3.125  $\mu\text{M}$  cisplatin or DMSO, and PBS or 7 two-fold dilutions of LYVE1 ranging from 6.25 ng/ml to 400 ng/ml. Cell count was normalized to DMSO/PBS treatment. (B) Cell cycle analysis of data from (A) of specific treatments including PBS or 50 ng/ml LYVE1, and DMSO or 3.125  $\mu\text{M}$  cisplatin. Percentage of S phase cells was calculated by identifying a local minimum in the histogram of total EdU intensity and gating cells into EdU positive or negative that were above or below the local minimum, and calculating total EdU positive over total cells. Percentage of sub-G0/G1, G0/G1, and G2/M cells was calculated by identifying two local minimums in the histogram of total DAPI intensity. EdU negative cells were then taken and sub-G0 cells were gated into the lowest DAPI intensity group, G0/G1 were gated into the medium DAPI intensity group, and G2/M cells were gated into the highest DAPI intensity group, and percentages were calculated by quantifying cells in each gate over total cells. (C) 3-dimensional histogram of single cell total intensity of DAPI (x-axis), total intensity of EdU (y-axis), and frequency of cells in each bin (z-axis; 62,500 bins) spatially showing distinct phases of the cell cycle as indicated in the DMSO/PBS treatment. Apo: sub-G0/G1 apoptotic cells; G0/G1: G0/G1 phase.

### 3.4 Discussion

The TME in bladder cancer may play a role in stimulating a pro-proliferative phenotype and induce differentiation state plasticity. Understanding responses to TME signals in the context of molecular subtype characterization of bladder cancer cells will ultimately highlight potential targets for cancer interventions and allow predictions of outcome. The current study interrogates the response of bladder cancer cells lines, with refined molecular subtype characterization, to TME signals and uncovers relationships between cell count, EdU incorporation, and differentiation state.

Five molecular subtypes for bladder cancer cell lines were identified based on a subset of gene expression markers defined by TCGA (Figure 10)<sup>112</sup>. Bladder cancer cell lines were used as a tool to refine molecular subtyping that may be broadly applicable due to the focus on the cancer cells themselves, devoid of the TME, as opposed to patient tissue that is potentially TME-rich. While it is important to consider the TME, signals derived from each need to be better understood to fully understand cancer cell-TME communication so that we can identify targeted therapies to disrupt pro-proliferative communication. Subtyping patients based on this new classification may help identify therapeutic vulnerabilities. Patients subtyped as mesenchymal or luminal/TP63-low may be good candidates for recently approved PD-L1 inhibitors as cell lines classified as such were enriched in PD-L1(CD274) (Supplemental Figure 10 and Figure 10)<sup>79</sup>. Patients subtyped as luminal/TP63-high subtype, or a luminal claudin-high KRT20-high subtype may respond well to tyrosine kinase inhibitors targeting FGFR3 as these cell line clusters overexpressed FGFR3. (Supplemental Figure 10 and Figure 10).

MEMA technology was utilized as a discovery tool to identify TME factors that increase cell count and promote EdU incorporation. Limitations of this technology include the lack of replicate ligand wells and the requirement of multiple plates (8 plates) to assess the effects of the entire MEMA ligand set (56 ligands), which necessitates additional statistical methods for normalization. Other limitations include not being able to discern the difference between cellular responses due to the added soluble ligands versus cellular responses due nearby cells secreting soluble factors.

MEMA technology helped identify TNF as a pro-proliferative TME signal in a FGFR3-TACC3 fusion cell line upon exposure to the TKI inhibitor PD173074 (Supplemental Figure 11). In bladder cancer, the TME was first implicated in conferring resistance to treatment in studies aimed at elucidating the mechanisms of resistance to BCG therapy, the gold standard immunotherapy. Upon administration of BCG, neutrophils are recruited to the TME where they secrete TNF, which causes upregulation of anti-apoptotic pathway genes to cause resistance<sup>268</sup>. This is important to consider during design of clinical trials as recently approved immunotherapies begin combination therapy with targeted TKI inhibitors.

LYVE1 and CD44 were identified as a potential protein combinations that enhanced DNA repair upon cisplatin treatment with the aid of MEMAs (Figure 14). Cisplatin is the standard of care chemotherapy in bladder cancer, making it important to better understand the interaction between bladder cancer cells, LYVE1, and/or CD44. Validation of the MEMA results in a non-array format showed that LYVE1 increased cell count regardless of cisplatin being present at concentrations that are physiologically relevant (Figure 15). Additionally, CD44 alone had the ability to increase cell count in the presence and absence of cisplatin at physiological concentrations, but the greatest

affect, albeit modest, was detected when CD44 and LYVE1 were in combination (Figure 16). Furthermore, cell cycle analysis indicated that LYVE1 reduces apoptosis, and either increases proliferation or enhances DNA repair in cells treated with cisplatin (Figure 17). It is possible that LYVE1 and CD44 stimulate the secretion of another unknown protein that initiates a positive-feedback loop in bladder cancer cells to elicit the responses observed. CD44 and LYVE1 have 43% sequence homology and are hyaluronan receptors on blood endothelial cells and lymphatic endothelial cells, respectively<sup>261</sup>. Bladder cancer frequently invades the lymphatics and metastasizes to lymph nodes and distant sites via this route<sup>269</sup>. As bladder cancer cells invade past the urothelium, they are exposed to blood and lymphatic vessels and their secretions. Just below the urothelium, LYVE1 positive lymphatic vessels are normally present in the lamina propria of the bladder, as well as in the detrusor muscle, and in the bladder adventitia<sup>270</sup>. Studies in neuroblastoma have shown that LYVE1 upregulation correlates with unfavorable prognosis and lymph node metastasis<sup>262</sup>. CD44 has been shown to mediate growth, migration, and cisplatin resistance in head and neck cancer<sup>271,272</sup>. In gastric cancer, LYVE1 and CD44 gene expression was significantly higher in comparison to normal tissue and correlated with lymph node metastasis<sup>263</sup>. Collectively, these studies suggest a potential role for LYVE1 and CD44 in progression of bladder cancer. Future studies should examine the mechanism of interaction of LYVE1 and CD44 with bladder cancer, their role in progression of bladder cancer and whether they contribute to lymph node metastasis.

NRG isoforms differentially affected the ability of bladder cancer cells to incorporate EdU when exposed to cisplatin (Figure 14A). In the absence of drug, NRG isoforms also differentially affected bladder cancer cell count (Figure 18A), EdU incorporation (Figure 18B), and differentiation state changes (Figures 18C, 18D).

Previous studies of bladder tumors showed that NRG1- $\alpha$  and NRG1- $\beta$  were expressed with increased NRG1- $\alpha$  in higher stage and grade<sup>273</sup>. NRG1 is an epidermal growth factor (EGF) family member and has at least 10 *NRG1* soluble or transmembrane isoforms through alternative splicing or the use of alternative promoters.

Transmembrane isoforms can be cleaved by proteases and become solubilized. All isoforms possess an EGF-like domain, which is necessary for binding to the receptor tyrosine kinases HER3 and HER4. Subsequent recruitment and heterodimerization with HER2 leads to tyrosine phosphorylation and downstream signaling. NRG1 isoforms are classified into types I, II, and III with distinct domains. Types I and II have an Ig-like domain, whereas type III has a cysteine-rich domain. Types I and II differ by a glycosylation-rich domain in type II. Alternative splicing of the EGF-like domain results in  $\alpha$  and  $\beta$  variants. NRG1- $\alpha$  and NRG1- $\beta$  are type I and NRG1-SMDF is type III<sup>274–276</sup>.

Using targeted HER2 therapy such as trastuzumab on subsets of patients that overexpress HER2 and HER3 and have NRG1 isoforms present may overcome the shift in differentiation state and growth promotion. Further studies need to be done to fully understand the differential response of the NRG isoforms in terms of cell number and differentiation state to identify patients that would most benefit from therapy aimed at blocking the interaction of NRG with its receptors.

Regardless of the specific TME signals, a switch to a more differentiated, intermediate or luminal state promoted an increase in cell number (Figure 18E). Identifying therapies that disrupt this transition could help improve survival in bladder cancer. Furthermore, predicting which tumors have a higher propensity for a differentiation shift to occur could help predict outcomes.



These results have the potential to provide new information that will enable researchers to devise novel targeted approaches aimed at anticipating or overcoming pro-proliferative TME signaling. Thus, this work has the potential to greatly impact bladder cancer patients' quality of life and overall survival.

### **3.5 Materials and Methods**

#### **3.5.1 Cell Lines and Cell Culture**

All cell lines were cultured according to the protocols recommended for each cell line (ATCC, Manassos, VA, USA).

#### **3.5.2 Heatmap**

For heatmap visualization, samples were organized by unsupervised hierarchical clustering using Ward's method with the Euclidean distance metric. Heatmap visualization and hierarchical clustering were performed on log<sub>2</sub>-transformed and z-score-normalized data (pheatmap() function [pheatmap R package]).

#### **3.5.3 MicroEnvironment MicroArrays**

MEMAs in this study were manufactured on-site and all are spotted in separate wells that have the same design of 300 µm diameter spots of 48 ECM proteins spotted in 35 rows and 20 columns on the well bottom of polystyrene microplates (8 wells per plate, Nunc Brand, Roskilde, Denmark) using an Aushon2470 microarray printing platform. For each assay, there are 2688 microenvironment perturbations (MEPs) that are pairwise combinations of 48 printed ECM proteins (15 replicates) and 56 ligands or growth factors. One full MEMA set consists of eight 8-well plates, each consisting of one control well, equating to a total of 56 ligand treatment wells and 8 control wells. Cells were dispersed with non-trypsin cell detachment reagent HyQtase (HyClone, South Logan,

UT, USA) and  $\sim 5 \times 10^6$  cells in 4 mL of growth medium were added to each well and allowed to adhere at 37 °C for 1 hour. Non-adherent cells were washed off and 4 ml of fresh media was added. Cells incubated overnight, and then a single soluble ligand or PBS was added to each well along with either drug treatment or vehicle as control.

#### 3.5.4 Cell Line Assays and Image Cytometry

Immunofluorescence staining was performed on cells according to the following protocol 24 or 48 hours after culturing depending on the assay. First, EdU was added to wells for 1 h at 37°C in 5% CO<sub>2</sub>. The culture medium was aspirated and the cells were fixed with 2% paraformaldehyde (Sigma-Aldrich, St. Louis, MO, USA) in PBS for 15 min at room temperature (RT). Cells were washed for 5 min with PBS and permeabilized with 0.1% Triton-X100 in PBS for 15 min at RT. The Click-IT reaction for proliferation was performed, then the arrays were washed 3 × 5 min with PBS, rinsed with 0.05% PBS-Tween 20 and stained with primary antibody in 2% BSA-PBS overnight at 4 °C. Primary antibodies are against KRTs 5, 14 and 20 to assess for differentiation state (Abcam). Wells were washed 2 × 5 min with PBS and for 5 min with 0.05% PBS-Tween 20 and then stained with diluted Alexa fluorochrome-conjugated (Life Technologies) secondary antibodies along with DAPI counterstaining for 1 hour at RT. Cells were then washed as described above.

Imaging was performed using an IN Cell Analyzer 6000 Cell Imaging System (GE Healthcare Bio-Sciences, USA) equipped with sCMOS 5.5 Mp digital camera. Each printed spot was imaged individually with a 20× 0.45 objective using four LED lasers (405, 488, 561, and 642 nm) for DAPI, Alexa488, Alexa555 and Alexa647 dyes. The IN Cell Analyzer image analysis software suite was used for extraction of quantitative image features. Image features were quantified for cell populations using the IN Cell

software and further analyzed using *R* software. The effects of each drug on each specific response endpoint in each cell line was assessed by comparing image parameters (e.g., total fluorescence intensity per cell) with comparable image parameters measured for untreated cells.

### 3.5.5 Statistics

For MEMAs, 15 replicate spots of each ECM was analyzed to attain good statistical power within an array. The dataset is organized into the four imaging categories, which include raw data, normalized data, normalized data aggregated to the spot level and normalized data aggregated to the replicate level. The data merging and analysis was done in *R* using open source software that allows comparison of activity in one ME relative to another, as well as compare activity in a control environment with the drug treated microenvironments. Each well is scored for even cell seeding according to the count of the DAPI-stained nuclei. Quality analysis scores range from 0 to 1 and represent the proportion of the spots that have at least one cell and are not in low cell count neighborhoods. The data was normalized with the RUV3 and LOESS regression methods to determine within and between MEMA well comparisons. In brief, this is done by normalizing the mean of replicate spots in non-control wells to the collective mean of replicate spots of all PBS control wells. The proliferation analysis method is as follows: First, the cells within each well are gated into EdU+. The proportion of EdU+ cells at each spot was calculated. The proportions are logit transformed then normalized. The normalized proportions are then summarized by the medians of their replicates. A highly-filtered dataset is created as follows: spots with less than 20 cells, wells with quality analysis scores below 0.7, wells with low quality DAPI, MEPs with less than 3 replicates and the FBS control wells are removed from the dataset<sup>255,277,278</sup>.

For 96-well assays, significance was computed by performing ANOVA tests followed by Tukey's HSD or Dunnett's tests in  $R$ <sup>279,280</sup>.

## CHAPTER 4. CONCLUSIONS AND FUTURE DIRECTIONS

### 4.1 Conclusions

Histologic and differentiation state intra-tumoral heterogeneity and TME signals represent a problem in the ability to accurately subtype cancers to be able to predict response to therapy and outcome. TCGA has molecularly defined distinct subtypes in GBM and MIBC, but these subtypes have failed to translate clinically. This is likely due to heterogeneity and the influence of TME signals confounding the signature. We hypothesized that more accurate molecular subtyping and patient stratification can be achieved by taking into account intra-tumoral heterogeneity and microenvironment signals. We were able to support our hypothesis in GBM and MIBC by refining patient stratification and molecular subtyping through distinct approaches.

We hypothesized that stratification into subtypes and prognostic groups can be achieved by taking GBM intra-tumoral heterogeneity into account. We supported this hypothesis by demonstrating that intra-tumoral heterogeneity in GBM is accounted for in part by histologic structures, and that by assessing gene expression in CT inter-tumoral comparisons are able to be made. We show that GBM subtypes, characterized based on gene expression in CT, identify cohorts with distinct biology, while subtypes can be misclassified if samples contain mixed structures or are rich in non-CT architecture. Furthermore, the role of the TME in GBM should be contemplated and whether the histologic structures identified within a single tumor should be considered TME features. It seems fitting that these histologic structures would be TME components as they are seemingly normal cells that co-mingle with tumor cells. However, there is a clear definition for each histologic structure in GBM and it seems more helpful to define these

regions in this way as opposed to identifying them more generally as components of the TME. There is no definitive answer at this time, but this concept should be revisited.

Additionally, we hypothesize that distinct TME signals stimulate proliferation and differentiation state plasticity in human bladder cancer cell lines in the presence and absence of drug treatment. This hypothesis was supported through the utilization of MEMAs and soluble ligand libraries and by refining molecular subtyping based on gene expression of bladder cancer cells themselves. We showed that TME signals in bladder cancer can influence cell count and differentiation state, and that cell count and differentiation state changes correlate. Increases in cell count can be a function of increased proliferation or decreased cell death. While cell cycle analysis was explored to identify proliferation and cell death, this only captures one moment in time at the end of the experiment. It is possible and likely that responses to the TME regarding proliferation and cell death are time dependent. Kinetic experiments should be performed to further elucidate the response of bladder cancer to the TME over time. Moreover, results suggest that differentiation state changes may be a good potential therapeutic intervention point. If drugs are identified that inhibit the differentiation state shift, it is plausible that cell count will not be increased. Furthering this logic, drugs may be able to reverse differentiation state shifts upon stimulation with certain TME components and render cancer cells vulnerable to cell death. Studies should investigate the potential of altering differentiation state to render cells vulnerable to treatment.

The concept of molecular subtyping is plagued by controversy due to the lack of clear clinical translation in some cancers. Here, we demonstrate a refinement of molecular subtypes that identify potential targets for therapeutic intervention. However, there is no guarantee that this refinement of molecular subtypes would be any better

than targeting a few genetic drivers of tumorigenesis. The best compromise between the two concepts would be to identify molecular subtypes based on clear drivers.

Additionally, the design of clinical trials and the delivery of therapies would benefit the most out of molecular subtypes truly identifying subsets of patients with therapeutic vulnerabilities. If this is realized, rapid diagnostic tools can be developed to identify the subtype patients belong to, and definitive treatment regimens can be prescribed that benefit patients the best with accurate predictions in outcome.

This represents contributions to our understanding of how histologic structures and the TME influence GBM and bladder cancer cell interpretation, respectively. Identifying signatures from cancer cells themselves and devising methods of integrating them with signals from the TME may hold the key to advancing GBM and MIBC into the realm of precision medicine.

#### **4.2 Future Directions Validation**

Future work includes validating the current study. Once validated, the repertoire of CT-specific gene signatures will be expanded, as well as creating a workflow to obtain CT-rich clinical samples should be explored to advance the clinical management of GBM.

- Validate CT as the best histological structure to assess for diagnostics and prognostics.
  - This is currently underway in an independent cohort of banked GBM tissue samples at Oregon Health & Science University. Steps involved include:
    1. A neuropathologist identifying CT regions.
    2. A trained technician performing laser capture microdissection of CT.

3. RNA and DNA extraction for RNA sequencing and DNA methylation profiling.
  4. Data normalization and processing and running the pipelines established for the current study should be carried out.
  5. Comparing these findings to bulk dissected CT regions in GBM should be performed to determine if similar findings can be obtained, as bulk dissection has more clinical utility due to the relative ease of use in comparison to laser capture.
- Further validating the prognostic gene signature in the aforementioned independent cohort of GBM samples as well as other databases.
    - Subsequent development of a prognostic gene chip that probes for gene expression of the genes identified here as prognostic to determine risk in patients.
  - Improving methods to obtain predominantly CT in GBM should be explored through the use of image-guided biopsy.
  - Further refining molecular subtyping using CT gene expression in GBM may also help in realizing clinical utility of molecular subtypes by identifying targetable pathways distinct to subtypes.
  - Ultimately, we believe that CT gene expression signatures can become clinical tools utilized to plan and execute optimal care for GBM patients, which could function as follows:
    - 1) A patient receives an image-guided biopsy, targeting CT devoid of vasculature and necrotic regions.
    - 2) This sample is subsequently probed for omic signatures to rapidly risk stratify the patient and predict their individual therapeutic sensitivity.



- 3) The patient then receives personalized treatment.
- 4) When radiographic progression is observed, this is categorized as tumor growth or treatment-related immune response based on an initial gene signature.

Our results coupled with continued efforts to develop CT signatures have the potential to enhance methods for GBM patient stratification to guide clinical care.

Future directions for MIBC include improving molecular subtyping to better predict therapeutic response and outcome. Macrodissection or microdissection of tumor cells from MIBC may help in better distinguishing subtypes of MIBC that differ in intrinsic biology, therapeutic response, and survival. Plans should follow similarly to what has been proposed for future work in GBM. Once more accurate subtypes have been defined, characterizing the response of the TME in each subtype could help further elucidate drug targets and refine predictions of response and outcome. Co-culture and 3D cell culture systems can help further investigate the influence of the TME on cell response. Future work should also explore cues that influence differentiation state change and identify therapeutic inhibitors of differentiation to inhibit adaption to the environment.

## BIBLIOGRAPHY

1. American Cancer Society. Cancer Facts & Figures 2018. *Am. Cancer Soc.* (2018). doi:10.1182/blood-2015-12-687814
2. Sudhakar, a. History of Cancer, Ancient and Modern Treatment Methods Akulapalli. *J Cancer Sci Ther.* (2010). doi:10.4172/1948-5956.100000e2.History
3. Saber, A. Ancient Egyptian surgical heritage. *J. Investig. Surg.* (2010). doi:10.3109/08941939.2010.515289
4. Feldman, R. P. & Goodrich, J. T. The Edwin Smith Surgical Papyrus. *Child's Nerv. Syst.* (1999). doi:10.1007/s003810050395
5. Vargas, A., López, M., Lillo, C. & Vargas, M. J. [The Edwin Smith papyrus in the history of medicine]. *Rev. médica Chile* (2012). doi:10.4067/S0034-98872012001000020
6. Jouanna, J. Greek Medicine from Hippocrates to Galen. *Stud. Anc. Med.* (2012). doi:10.1017/CBO9781107415324.004
7. Mayhew, R. :Hippocrates on Ancient Medicine. *Isis* (2006). doi:10.1086/507360
8. DeVita, V. T. & Rosenberg, S. A. Two Hundred Years of Cancer Research. *N. Engl. J. Med.* (2012). doi:10.1056/NEJMra1204479
9. Hajdu, S. I., Vadmal, M. & Tang, P. A note from history: Landmarks in history of cancer, part 7. *Cancer* (2015). doi:10.1002/cncr.29365
10. Ribatti, D. An historical note on the cell theory. *Experimental Cell Research* (2018). doi:10.1016/j.yexcr.2018.01.038
11. Talmadge, J. E. & Fidler, I. J. AACR centennial series: The biology of cancer metastasis: Historical perspective. *Cancer Research* (2010). doi:10.1158/0008-5472.CAN-10-1040
12. Fidler, I. J. & Poste, G. The 'seed and soil' hypothesis revisited. *The Lancet*

- Oncology* (2008). doi:10.1016/S1470-2045(08)70201-8
13. Boveri, T. Concerning the Origin of Malignant Tumours by Theodor Boveri. Translated and annotated by Henry Harris. *J. Cell Sci.* (2008). doi:10.1242/jcs.025742
  14. Hansford, S. & Huntsman, D. G. Boveri at 100: Theodor Boveri and genetic predisposition to cancer. *Journal of Pathology* (2014). doi:10.1002/path.4414
  15. Weiss, R. A. & Vogt, P. K. 100 years of Rous sarcoma virus. *J. Exp. Med.* (2011). doi:10.1084/jem.20112160
  16. Vogt, P. K. Retroviral oncogenes: A historical primer. *Nature Reviews Cancer* (2012). doi:10.1038/nrc3320
  17. Martin, G. S. The road to Src. *Oncogene* (2004). doi:10.1038/sj.onc.1208077
  18. Rubin, H. The early history of tumor virology: Rous, RIF, and RAV. *Proc. Natl. Acad. Sci.* (2011). doi:10.1073/pnas.1108655108
  19. Malumbres, M. & Barbacid, M. RAS oncogenes: The first 30 years. *Nature Reviews Cancer* (2003). doi:10.1038/nrc1097
  20. Wang, J. *et al.* c-Myc is required for maintenance of glioma cancer stem cells. *PLoS One* (2008). doi:10.1371/journal.pone.0003769
  21. Dang, C. V. MYC on the path to cancer. *Cell* (2012). doi:10.1016/j.cell.2012.03.003
  22. Lee, C. M. & Reddy, E. P. The v-myc oncogene. *Oncogene* (1999). doi:10.1038/sj.onc.1202786
  23. Dalla-Favera, R. *et al.* Human c-myc onc Gene is Located on the Region of Chromosome 8 that is Translocated in Burkitt Lymphoma Cells. *Proc. Natl. Acad. Sci.* (1982). doi:10.1073/pnas.79.24.7824
  24. Chang, E. H., Gonda, M. A., Ellis, R. W., Scolnick, E. M. & Lowy, D. R. Human genome contains four genes homologous to transforming genes of Harvey and

- Kirsten murine sarcoma viruses. *Proc. Natl. Acad. Sci.* (1982).  
doi:10.1073/pnas.79.16.4848
25. Pipas, J. M. SV40: Cell transformation and tumorigenesis. *Virology* (2009).  
doi:10.1016/j.virol.2008.11.024
26. Lodish, H. *et al.* Proto-Oncogenes and Tumor-Suppressor Genes. in *Molecular Cell Biology. 4th edition* (2000).
27. Narita, M. *et al.* Rb-mediated heterochromatin formation and silencing of E2F target genes during cellular senescence. *Cell* (2003). doi:10.1016/S0092-8674(03)00401-X
28. Burkhart, D. L. & Sage, J. Cellular mechanisms of tumour suppression by the retinoblastoma gene. *Nature Reviews Cancer* (2008). doi:10.1038/nrc2399
29. Sherr, C. J. & McCormick, F. The RB and p53 pathways in cancer. *Cancer Cell* (2002). doi:10.1016/S1535-6108(02)00102-2
30. Levine, A. J. & Oren, M. The first 30 years of p53: Growing ever more complex. *Nature Reviews Cancer* (2009). doi:10.1038/nrc2723
31. Soussi, T. & Wiman, K. G. TP53: An oncogene in disguise. *Cell Death and Differentiation* (2015). doi:10.1038/cdd.2015.53
32. Marutani, M. *et al.* Dominant-negative mutations of the tumor suppressor p53 relating to early onset of glioblastoma multiforme. *Cancer Res.* **59**, 4765–4769 (1999).
33. BLAGOSKLONNY, M. V. p53 from complexity to simplicity: mutant p53 stabilization, gain-of-function, and dominant-negative effect. *FASEB J.* (2000).  
doi:10.1096/fj.99-1078rev
34. Muller, P. A. J. & Vousden, K. H. p53 mutations in cancer. *Nat. Cell Biol.* (2013).  
doi:10.1038/ncb2641
35. Hanahan, D. & Weinberg, R. A. Hallmarks of cancer: The next generation. *Cell*

- 144**, 646–674 (2011).
36. Grimm, S. *et al.* Malignancy of bladder cancer cells is enhanced by tumor-associated fibroblasts through a multifaceted cytokine-chemokine loop. *Exp. Cell Res.* 1–11 (2015). doi:10.1016/j.yexcr.2015.04.001
  37. Klemm, F. & Joyce, J. a. Microenvironmental regulation of therapeutic response in cancer. *Trends Cell Biol.* **25**, 198–213 (2015).
  38. van der Horst, G., Bos, L. & van der Pluijm, G. Epithelial Plasticity, Cancer Stem Cells, and the Tumor-Supportive Stroma in Bladder Carcinoma. *Mol. Cancer Res.* **10**, 995–1009 (2012).
  39. Mathiasen, H. Mastectomy without anesthesia: The cases of Abigail Adams Smith and Fanny Burney. *American Journal of Medicine* (2011). doi:10.1016/j.amjmed.2011.01.004
  40. Robinson, D. H. & Toledo, A. H. Historical development of modern anesthesia. *Journal of Investigative Surgery* (2012). doi:10.3109/08941939.2012.690328
  41. Greene, N. M. Anesthesia and the development of surgery (1846-1896). *Middle East J. Anaesthesiol.* (1979). doi:10.1213/00000539-197901000-00003
  42. Ghossain, A. & Ghossain, M. A. History of mastectomy before and after Halsted. *Journal Medical Libanais* (2009).
  43. Plesca, M., Bordea, C., El Houcheimi, B., Ichim, E. & Blidaru, A. Evolution of radical mastectomy for breast cancer. *J. Med. Life* (2016).
  44. Cotlar, A. M., Dubose, J. J. & Rose, D. M. History of surgery for breast cancer: Radical to the sublime. *Curr. Surg.* (2003). doi:10.1016/S0149-7944(02)00777-8
  45. Veronesi, U. *et al.* Twenty-year follow-up of a randomized study comparing breast-conserving surgery with radical mastectomy for early breast cancer. *N. Engl. J. Med.* (2002). doi:10.1056/NEJMoa020989
  46. Early Breast Cancer Trialists' Collaborative Group (EBCTCG), E. B. C. T. C. G. *et*

- al.* Effect of radiotherapy after breast-conserving surgery on 10-year recurrence and 15-year breast cancer death: meta-analysis of individual patient data for 10,801 women in 17 randomised trials. *Lancet (London, England)* (2011).  
doi:10.1016/S0140-6736(11)61629-2
47. Sakorafas, G. H. & Safioleas, M. Breast cancer surgery: An historical narrative. Part II. 18th and 19th centuries. *European Journal of Cancer Care* (2010).  
doi:10.1111/j.1365-2354.2008.01060.x
48. M., S.-T. Clinical features and imaging. *Cardiovasc. Intervent. Radiol.* (2009).
49. Spana, G., Rane, A. & Kaouk, J. H. Is robotics the future of laparoendoscopic single-site surgery (LESS)? *BJU International* (2011). doi:10.1111/j.1464-410X.2011.10513.x
50. Zimmerman, E. E. & Crawford, P. Cutaneous cryosurgery. *Am. Fam. Physician* (2012).
51. Cooper, S. M. & Dawber, R. P. The history of cryosurgery. *J. R. Soc. Med.* (2001).  
doi:10.1177/014107680109400416
52. Chen, W. Y. Exogenous and endogenous hormones and breast cancer. *Best Pract. Res. Clin. Endocrinol. Metab.* (2008). doi:10.1016/j.beem.2008.08.001
53. Kumar, R. J., Barqawi, A. & Crawford, E. D. Preventing and treating the complications of hormone therapy. *Current urology reports* (2005).  
doi:10.1007/s11934-005-0010-9
54. Webb, S. The physics of radiation treatment. *Phys. World* (1998).  
doi:10.1118/1.3319185
55. Bortfeld, T. IMRT: A review and preview. *Physics in Medicine and Biology* (2006).  
doi:10.1088/0031-9155/51/13/R21
56. Benedict, S. H. *et al.* Stereotactic body radiation therapy: The report of AAPM Task Group 101. *Medical Physics* (2010). doi:10.1118/1.3438081

57. Calvo, F. A., Meirino, R. M. & Orecchia, R. Intraoperative radiation therapy. Part 2. Clinical results. *Critical Reviews in Oncology/Hematology* (2006). doi:10.1016/j.critrevonc.2006.04.004
58. Willett, C. G., Czito, B. G. & Tyler, D. S. Intraoperative radiation therapy. *J. Clin. Oncol.* (2007). doi:10.1200/JCO.2006.10.0255
59. DeVita, V. T. & Chu, E. A history of cancer chemotherapy. *Cancer Research* (2008). doi:10.1158/0008-5472.CAN-07-6611
60. Morrison, W. B. Cancer Chemotherapy: An Annotated History. *Journal of Veterinary Internal Medicine* (2010). doi:10.1111/j.1939-1676.2010.0590.x
61. Moudi, M., Go, R., Yien, C. Y. S. & Nazre, M. Vinca alkaloids. *International Journal of Preventive Medicine* (2013). doi:10.1007/BF00569574
62. Fester, K. Plant Alkaloids. in *Encyclopedia of Life Sciences* (2010). doi:10.1002/9780470015902.a0001914.pub2
63. Farber, S., Diamond, L. K., Mercer, R. D., Sylvester, R. F. & Wolff, J. A. Temporary Remissions in Acute Leukemia in Children Produced by Folic Acid Antagonist, 4-Aminopteroyl-Glutamic Acid (Aminopterin). *N. Engl. J. Med.* (1948). doi:10.1056/NEJM194806032382301
64. Ribatti, D. Sidney farber and the treatment of childhood acute lymphoblastic leukemia with a chemotherapeutic agent. *Pediatric Hematology and Oncology* (2012). doi:10.3109/08880018.2012.678969
65. Amarouch, A. & Mazonon, J. J. Radiotherapy plus concomitant and adjuvant Temozolomide for glioblastoma. *Cancer/Radiotherapie* (2005). doi:10.1016/j.canrad.2005.05.001
66. Alderden, R. A., Hall, M. D. & Hambley, T. W. The Discovery and Development of Cisplatin. *J. Chem. Educ.* (2006). doi:10.1021/ed083p728
67. Einhorn, L. H. Curing metastatic testicular cancer. *Proc. Natl. Acad. Sci.* (2002).

doi:10.1073/pnas.072067999

68. Cancer, W. I., States, U. & Papyrus, E. S. The History of Cancer. *Cancer* (2011).
69. Society, A. C. Cancer Treatment. *Cancer Treat. Surviv. Facts Fig.* (2013).
70. McCarthy, E. F. The toxins of William B. Coley and the treatment of bone and soft-tissue sarcomas. *Iowa Orthop. J.* (2006). doi:2006;26:154-8
71. Hopton Cann, S. A., van Netten, J. P. & van Netten, C. Dr William Coley and tumour regression: a place in history or in the future. *Postgrad. Med. J.* (2003). doi:"We have listened to nature..."
72. Richardson, M. A., Ramirez, T., Russell, N. C. & Moye, L. A. Coley toxins immunotherapy: A retrospective review. *Altern. Ther. Health Med.* (1999).
73. Kawai, K., Miyazaki, J., Joraku, A., Nishiyama, H. & Akaza, H. Bacillus Calmette-Guerin (BCG) immunotherapy for bladder cancer: Current understanding and perspectives on engineered BCG vaccine. *Cancer Science* (2013). doi:10.1111/cas.12075
74. Morales, A. BCG: A throwback from the stone age of vaccines opened the path for bladder cancer immunotherapy. *Canadian Journal of Urology* (2017).
75. Gkialas, I., Kalantzis, A. & Lykourinas, M. The response of urological tumours to immunotherapy. *Journal of B.U.ON.* (2005).
76. Topalian, S. L., Weiner, G. J. & Pardoll, D. M. Cancer immunotherapy comes of age. *J. Clin. Oncol.* (2011). doi:10.1200/JCO.2011.38.0899
77. Farkona, S., Diamandis, E. P. & Blasutig, I. M. Cancer immunotherapy: The beginning of the end of cancer? *BMC Medicine* (2016). doi:10.1186/s12916-016-0623-5
78. Thallinger, C. *et al.* Review of cancer treatment with immune checkpoint inhibitors: Current concepts, expectations, limitations and pitfalls. *Wiener Klinische Wochenschrift* (2018). doi:10.1007/s00508-017-1285-9



79. Bellmunt, J., Powles, T. & Vogelzang, N. J. A review on the evolution of PD-1/PD-L1 immunotherapy for bladder cancer: The future is now. *Cancer Treat. Rev.* **54**, 58–67 (2017).
80. Sunshine, J. & Taube, J. M. PD-1/PD-L1 inhibitors. *Current Opinion in Pharmacology* (2015). doi:10.1016/j.coph.2015.05.011
81. Cross, R. CAR-T therapy. *C&EN Glob. Enterp.* (2018). doi:10.1021/cen-09619-cover
82. Yip, A. & Webster, R. M. The market for chimeric antigen receptor T cell therapies. *Nat. Rev. Drug Discov.* (2018). doi:10.1038/nrd.2017.266
83. Zheng, P. P., Kros, J. M. & Li, J. Approved CAR T cell therapies: ice bucket challenges on glaring safety risks and long-term impacts. *Drug Discovery Today* (2018). doi:10.1016/j.drudis.2018.02.012
84. Wang, R. F. & Wang, H. Y. Immune targets and neoantigens for cancer immunotherapy and precision medicine. *Cell Research* (2017). doi:10.1038/cr.2016.155
85. Gattinoni, L. *et al.* Removal of homeostatic cytokine sinks by lymphodepletion enhances the efficacy of adoptively transferred tumor-specific CD8<sup>+</sup> T cells. *J. Exp. Med.* (2005). doi:10.1084/jem.20050732
86. Coulson, A., Levy, A. & Gossell-Williams, M. Monoclonal antibodies in cancer therapy: Mechanisms, successes and limitations. *West Indian Med. J.* (2014). doi:10.7727/wimj.2013.241
87. Dranoff, G. Cytokines in cancer pathogenesis and cancer therapy. *Nature Reviews Cancer* (2004). doi:10.1038/nrc1252
88. Lippitz, B. E. Cytokine patterns in patients with cancer: A systematic review. *The Lancet Oncology* (2013). doi:10.1016/S1470-2045(12)70582-X
89. Xu, X. J. & Tang, Y. M. Cytokine release syndrome in cancer immunotherapy with

- chimeric antigen receptor engineered T cells. *Cancer Letters* (2014).  
doi:10.1016/j.canlet.2013.10.004
90. American Cancer Society. Targeted Therapy. *Am. Cancer Soc.* (2013).  
doi:10.1007/978-3-540-47648-1\_5677
91. Sawyers, C. Targeted cancer therapy. *Nature* (2004). doi:10.1038/nature03095
92. Arteaga, C. L. Inhibiting tyrosine kinases: successes and limitations. *Cancer biology & therapy* (2003).
93. Arora, a & Scholar, E. M. Role of tyrosine kinase inhibitors in cancer therapy. *J Pharmacol Exp Ther* (2005). doi:10.1124/jpet.105.084145.have
94. Sund, M. & Kalluri, R. Endogenous inhibitors of angiogenesis. in *Tumor Angiogenesis: Basic Mechanisms and Cancer Therapy* (2008). doi:10.1007/978-3-540-33177-3\_12
95. Papadopoulos, N. *et al.* Binding and neutralization of vascular endothelial growth factor (VEGF) and related ligands by VEGF Trap, ranibizumab and bevacizumab. *Angiogenesis* (2012). doi:10.1007/s10456-011-9249-6
96. Pàez-Ribes, M. *et al.* Antiangiogenic Therapy Elicits Malignant Progression of Tumors to Increased Local Invasion and Distant Metastasis. *Cancer Cell* (2009).  
doi:10.1016/j.ccr.2009.01.027
97. Chung, C. Restoring the switch for cancer cell death: Targeting the apoptosis signaling pathway. *Am. J. Heal. Pharm.* **75**, 942–952 (2018).
98. Baig, S. *et al.* Potential of apoptotic pathway-targeted cancer therapeutic research: Where do we stand. *Cell Death and Disease* (2016).  
doi:10.1038/cddis.2015.275
99. Garay, J. P. & Gray, J. W. Omics and therapy - A basis for precision medicine. *Mol. Oncol.* **6**, 128–139 (2012).
100. Kandpal, R. P., Saviola, B. & Felton, J. The era of 'omics unlimited.

*BioTechniques* (2009). doi:10.2144/000113137

101. Gomez-Cabrero, D. *et al.* Data integration in the era of omics: current and future challenges. *BMC systems biology* (2014). doi:10.1186/1752-0509-8-S2-11
102. Kitano, H. Computational systems biology. *Nature* (2002). doi:10.1038/nature01254
103. Westerhoff, H. V. & Palsson, B. O. The evolution of molecular biology into systems biology. *Nature Biotechnology* (2004). doi:10.1038/nbt1020
104. Ashley, E. A. Towards precision medicine. *Nature Reviews Genetics* (2016). doi:10.1038/nrg.2016.86
105. Collins, F. S. & Varmus, H. A New Initiative on Precision Medicine. *N. Engl. J. Med.* (2015). doi:10.1056/NEJMp1500523
106. Hodson, R. Precision medicine. *Nature* (2016). doi:10.1038/537S49a
107. Westphal, M., Maire, C. L. & Lamszus, K. EGFR as a Target for Glioblastoma Treatment: An Unfulfilled Promise. *CNS Drugs* (2017). doi:10.1007/s40263-017-0456-6
108. Xu, H. *et al.* Epidermal growth factor receptor in glioblastoma. *Oncology Letters* **14**, 512–516 (2017).
109. Blum, A., Wang, P. & Zenklusen, J. C. SnapShot: TCGA-Analyzed Tumors. *Cell* (2018). doi:10.1016/j.cell.2018.03.059
110. Tomczak, K., Czerwińska, P. & Wiznerowicz, M. The Cancer Genome Atlas (TCGA): An immeasurable source of knowledge. *Wspolczesna Onkologia* (2015). doi:10.5114/wo.2014.47136
111. Senft, D., Leiserson, M. D. M., Ruppin, E. & Ronai, Z. A. Precision Oncology: The Road Ahead. *Trends in Molecular Medicine* (2017). doi:10.1016/j.molmed.2017.08.003
112. Robertson, A. G. *et al.* Comprehensive Molecular Characterization of Muscle-

- Invasive Bladder Cancer. *Cell* **171**, 540–556.e25 (2017).
113. Weinstein, J. N. *et al.* Comprehensive molecular characterization of urothelial bladder carcinoma. *Nature* **507**, 315–322 (2014).
  114. McLendon, R, Friedman, A, Bigner, D, Van Meir, EG, Brat, DJ, Mastrogianakis, GM, Olson, JJ, *et al.* Comprehensive genomic characterization defines human glioblastoma genes and core pathways. *Nature* (2008). doi:10.1038/nature07385
  115. Verhaak, R. G. W. *et al.* Integrated Genomic Analysis Identifies Clinically Relevant Subtypes of Glioblastoma Characterized by Abnormalities in PDGFRA, IDH1, EGFR, and NF1. *Cancer Cell* (2010). doi:10.1016/j.ccr.2009.12.020
  116. Brennan, C. W. *et al.* The somatic genomic landscape of glioblastoma. *Cell* (2013). doi:10.1016/j.cell.2013.09.034
  117. Ostrom, Q. T. *et al.* CBTRUS Statistical Report: Primary Brain and Central Nervous System Tumors Diagnosed in the United States in 2008-2012. *Neuro-Oncology* **17**, iv1-iv62 (2015).
  118. Norden, A. D., Drappatz, J. & Wen, P. Y. Malignant gliomas in adults. *Blue Books Neurol.* (2010). doi:10.1016/B978-0-7506-7516-1.00005-0
  119. Ohgaki, H. & Kleihues, P. Epidemiology and etiology of gliomas. *Acta Neuropathologica* (2005). doi:10.1007/s00401-005-0991-y
  120. Ostrom, Q. T. *et al.* The epidemiology of glioma in adults: A state of the science review. *Neuro-Oncology* (2014). doi:10.1093/neuonc/nou087
  121. Louis, D. N. *et al.* The 2016 World Health Organization Classification of Tumors of the Central Nervous System: a summary. *Acta Neuropathol.* **131**, 803–820 (2016).
  122. Ellingson, B. M. *et al.* Anatomic localization of O6-methylguanine DNA methyltransferase (MGMT) promoter methylated and unmethylated tumors: A radiographic study in 358 de novo human glioblastomas. *Neuroimage* (2012).

doi:10.1016/j.neuroimage.2011.09.076

123. Parsons, D. W. *et al.* An integrated genomic analysis of human glioblastoma multiforme. *Sci. (New York, NY)* (2008). doi:10.1126/science.1164382
124. Liu, M. *et al.* National cancer database analysis of outcomes in pediatric glioblastoma. *Cancer Med.* (2018). doi:10.1002/cam4.1404
125. Guillamo, J. S. *et al.* Brainstem gliomas in adults: prognostic factors and classification. *Brain* (2001). doi:10.1093/brain/124.12.2528
126. Hanif, F., Muzaffar, K., Perveen, K., Malhi, S. M. & Simjee, S. U. Glioblastoma Multiforme: A Review of its Epidemiology and Pathogenesis through Clinical Presentation and Treatment. *Asian Pacific Journal of Cancer Prevention : APJCP* **18**, 3–9 (2017).
127. Tamimi, A. F. & Juweid, M. Epidemiology and Outcome of Glioblastoma. *Glioblastoma* (2017). doi:10.4065/mcp.2009.0410
128. Thakkar, J. P. *et al.* Epidemiologic and molecular prognostic review of glioblastoma. *Cancer Epidemiology Biomarkers and Prevention* (2014). doi:10.1158/1055-9965.EPI-14-0275
129. Czapski, B., Baluszek, S., Herold-Mende, C. & Kaminska, B. Clinical and immunological correlates of long term survival in glioblastoma. *Contemporary Oncology* **22**, 81–85 (2018).
130. Cohen, A. L., Holmen, S. L. & Colman, H. IDH1 and IDH2 mutations in gliomas. *Curr. Neurol. Neurosci. Rep.* (2013). doi:10.1007/s11910-013-0345-4
131. Eckel-Passow, J. E. *et al.* Glioma groups based on 1p/19q, IDH, and TERT promoter mutations in tumors. *N. Engl. J. Med.* (2015). doi:10.1056/NEJMoa1407279
132. Martínez-García, M. *et al.* SEOM clinical guidelines for diagnosis and treatment of glioblastoma (2017). *Clin. Transl. Oncol.* (2017). doi:10.1007/s12094-017-1763-6

133. Golla, H. *et al.* Glioblastoma multiforme from diagnosis to death: a prospective, hospital-based, cohort, pilot feasibility study of patient reported symptoms and needs. *Support. Care Cancer* (2014). doi:10.1007/s00520-014-2384-z
134. Ohgaki, H. & Kleihues, P. The definition of primary and secondary glioblastoma. *Clin. Cancer Res.* **19**, 764–772 (2013).
135. Urbanska, K., Sokolowska, J., Szmidt, M. & Sysa, P. Glioblastoma multiforme - An overview. *Wspolczesna Onkologia* (2014). doi:10.5114/wo.2014.40559
136. Aldape, K., Zadeh, G., Mansouri, S., Reifenberger, G. & von Deimling, A. Glioblastoma: pathology, molecular mechanisms and markers. *Acta Neuropathol.* **129**, 829–848 (2015).
137. Noushmehr, H. *et al.* Identification of a CpG Island Methylator Phenotype that Defines a Distinct Subgroup of Glioma. *Cancer Cell* (2010). doi:10.1016/j.ccr.2010.03.017
138. Turcan, S. *et al.* IDH1 mutation is sufficient to establish the glioma hypermethylator phenotype. *Nature* (2012). doi:10.1038/nature10866
139. Schwartzbaum, J. A., Fisher, J. L., Aldape, K. D. & Wrensch, M. Epidemiology and molecular pathology of glioma. *Nature Clinical Practice Neurology* (2006). doi:10.1038/ncpneuro0289
140. Goodenberger, M. L. & Jenkins, R. B. Genetics of adult glioma. *Cancer Genetics* (2012). doi:10.1016/j.cancergen.2012.10.009
141. Hottinger, A. F., Abdullah, K. G. & Stupp, R. Current Standards of Care in Glioblastoma Therapy. in *Glioblastoma* (2016). doi:10.1016/B978-0-323-47660-7.00006-9
142. Kreth, F. W. *et al.* Gross total but not incomplete resection of glioblastoma prolongs survival in the era of radiochemotherapy. *Ann. Oncol.* (2013). doi:10.1093/annonc/mdt388

143. Rainer Wirtz, W. S. *et al.* The benefit of neuronavigation for neurosurgery analyzed by its impact on glioblastoma surgery. *Neurol. Res.* (2000). doi:10.1080/01616412.2000.11740684
144. Kubben, P. L. *et al.* Intraoperative MRI-guided resection of glioblastoma multiforme: A systematic review. *The Lancet Oncology* (2011). doi:10.1016/S1470-2045(11)70130-9
145. Ken, S. *et al.* Integration method of 3D MR spectroscopy into treatment planning system for glioblastoma IMRT dose painting with integrated simultaneous boost. *Radiat. Oncol.* (2013). doi:10.1186/1748-717X-8-1
146. Sherman, J. H. *et al.* Neurosurgery for brain tumors: Update on recent technical advances. *Current Neurology and Neuroscience Reports* (2011). doi:10.1007/s11910-011-0188-9
147. Silbergeld, D. L. & Chicoine, M. R. Isolation and characterization of human malignant glioma cells from histologically normal brain. *J. Neurosurg.* (1997). doi:10.3171/jns.1997.86.3.0525
148. Bao, S. *et al.* Glioma stem cells promote radioresistance by preferential activation of the DNA damage response. *Nature* (2006). doi:10.1038/nature05236
149. Stupp, R. *et al.* Effects of radiotherapy with concomitant and adjuvant temozolomide versus radiotherapy alone on survival in glioblastoma in a randomised phase III study: 5-year analysis of the EORTC-NCIC trial. *Lancet Oncol.* (2009). doi:10.1016/S1470-2045(09)70025-7
150. Stupp, R. *et al.* Radiotherapy plus Concomitant and Adjuvant Temozolomide for Glioblastoma. *N. Engl. J. Med.* (2005). doi:10.1056/NEJMoa043330
151. Arvold, N. D. & Reardon, D. A. Treatment options and outcomes for glioblastoma in the elderly patient. *Clin. Interv. Aging* (2014). doi:10.2147/CIA.S44259
152. Noroxxe, D. S., Poulsen, H. S. & Lassen, U. Hallmarks of glioblastoma: a

- systematic review. *ESMO open* **1**, e000144 (2016).
153. Patel, A. P. *et al.* Single-cell RNA-seq highlights intratumoral heterogeneity in primary glioblastoma. *Science* (80-. ). (2014). doi:10.1126/science.1254257
  154. Meyer, M. *et al.* Single cell-derived clonal analysis of human glioblastoma links functional and genomic heterogeneity. *Proc. Natl. Acad. Sci. U. S. A.* **112**, 851–856 (2015).
  155. Sottoriva, A. *et al.* Intratumor heterogeneity in human glioblastoma reflects cancer evolutionary dynamics. *Proc Natl Acad Sci U S A* (2013).  
doi:10.1073/pnas.1219747110
  156. Kalpathy-Cramer, J., Gerstner, E. R., Emblem, K. E., Andronesi, O. C. & Rosen, B. Advanced magnetic resonance imaging of the physical processes in human Glioblastoma. *Cancer Research* (2014). doi:10.1158/0008-5472.CAN-14-0383
  157. Hrabalek, L. *et al.* Resection versus biopsy of glioblastomas in eloquent brain areas. *Biomed. Pap.* (2015). doi:10.5507/bp.2013.052
  158. Wesolowski, J. R., Rajdev, P. & Mukherji, S. K. Temozolomide (Temodar). *Am. J. Neuroradiol.* (2010). doi:10.3174/ajnr.A2170
  159. Agarwala, S. S. & Kirkwood, J. M. Temozolomide, a novel alkylating agent with activity in the central nervous system, may improve the treatment of advanced metastatic melanoma. *Oncologist* (2000). doi:10.1634/THEONCOLOGIST.5-2-144
  160. Zhang, J., F.G. Stevens, M. & D. Bradshaw, T. Temozolomide: Mechanisms of Action, Repair and Resistance. *Curr. Mol. Pharmacol.* (2012).  
doi:10.2174/1874467211205010102
  161. Esteller, M. *et al.* Inactivation of the DNA-Repair Gene *MGMT* and the Clinical Response of Gliomas to Alkylating Agents. *N. Engl. J. Med.* (2000).  
doi:10.1056/NEJM200011093431901



162. Hegi, M. E. *et al.* MGMT Gene Silencing and Benefit from Temozolomide in Glioblastoma. *N. Engl. J. Med.* (2005). doi:10.1056/NEJMoa043331
163. Vlachostergios, P. J., Hatzidaki, E. & Papandreou, C. N. MGMT repletion after treatment of glioblastoma cells with temozolomide and O6-benzylguanine implicates NFkappaB and mutant p53. *Neurol Res* (2013). doi:10.1179/1743132813Y.0000000191
164. Quinn, J. A. *et al.* Phase II Trial of Temozolomide Plus O6-Benzylguanine in Adults with Recurrent, Temozolomide-Resistant Malignant Glioma. *J. Clin. Oncol.* (2009). doi:10.1200/JCO.2008.18.8417
165. Choi, S. *et al.* Temozolomide-associated Hypermutation in Gliomas. *Neuro. Oncol.* (2018). doi:10.1093/neuonc/noy016
166. Muscat, A. M. *et al.* The evolutionary pattern of mutations in glioblastoma reveals therapy-mediated selection. *Oncotarget* **9**, 7844–7858 (2018).
167. Bhat, K. P. L. *et al.* Mesenchymal Differentiation Mediated by NF-κB Promotes Radiation Resistance in Glioblastoma. *Cancer Cell* (2013). doi:10.1016/j.ccr.2013.08.001
168. Parker, N. R., Khong, P., Parkinson, J. F., Howell, V. M. & Wheeler, H. R. Molecular Heterogeneity in Glioblastoma: Potential Clinical Implications. *Front. Oncol.* (2015). doi:10.3389/fonc.2015.00055
169. Inda, M.-M., Bonavia, R. & Seoane, J. Glioblastoma Multiforme: A Look Inside Its Heterogeneous Nature. *Cancers (Basel)*. (2014). doi:10.3390/cancers6010226
170. Barajas, R. F. *et al.* Regional variation in histopathologic features of tumor specimens from treatment-naive glioblastoma correlates with anatomic and physiologic MR Imaging. *Neuro. Oncol.* (2012). doi:10.1093/neuonc/nos128
171. Kim, J. *et al.* Spatiotemporal Evolution of the Primary Glioblastoma Genome. *Cancer Cell* (2015). doi:10.1016/j.ccell.2015.07.013

172. Rutter, E. M., Banks, H. T. & Flores, K. B. Estimating intratumoral heterogeneity from spatiotemporal data. *Journal of Mathematical Biology* (2018).  
doi:10.1007/s00285-018-1238-6
173. Goldberg, K. B., Blumenthal, G. M., McKee, A. E. & Pazdur, R. The FDA Oncology Center of Excellence and precision medicine. *Exp. Biol. Med.* (2018).  
doi:10.1177/1535370217740861
174. fda & cder. FDA's label for Pembrolizumab. *Warn. Precautions* (2017).
175. First Tissue-Agnostic Drug Approval Issued. *Cancer Discov.* (2017).  
doi:10.1158/2159-8290.CD-NB2017-078
176. Filley, A. C., Henriquez, M. & Dey, M. Recurrent glioma clinical trial, CheckMate-143: the game is not over yet. *Oncotarget* (2017). doi:10.18632/oncotarget.21586
177. Sampson, J. H. *et al.* Preliminary safety and activity of nivolumab and its combination with ipilimumab in recurrent glioblastoma (GBM): CHECKMATE-143. *J Clin Oncol (Meeting Abstr.* (2015).
178. Meng, X., Huang, Z., Teng, F., Xing, L. & Yu, J. Predictive biomarkers in PD-1/PD-L1 checkpoint blockade immunotherapy. *Cancer Treat. Rev.* (2015).  
doi:10.1016/j.ctrv.2015.11.001
179. Patel, S. P. & Kurzrock, R. PD-L1 Expression as a Predictive Biomarker in Cancer Immunotherapy. *Mol. Cancer Ther.* (2015). doi:10.1158/1535-7163.MCT-14-0983
180. Patnaik, A. *et al.* Phase i study of pembrolizumab (MK-3475; Anti-PD-1 monoclonal antibody) in patients with advanced solid tumors. *Clin. Cancer Res.* (2015). doi:10.1158/1078-0432.CCR-14-2607
181. Mun, E. J., Babiker, H. M., Weinberg, U., Kirson, E. D. & Von Hoff, D. D. Tumor-treating fields: A fourth modality in cancer treatment. *Clinical Cancer Research* (2018). doi:10.1158/1078-0432.CCR-17-1117
182. Mehta, M., Wen, P., Nishikawa, R., Reardon, D. & Peters, K. Critical review of the

- addition of tumor treating fields (TTFields) to the existing standard of care for newly diagnosed glioblastoma patients. *Critical Reviews in Oncology/Hematology* (2017). doi:10.1016/j.critrevonc.2017.01.005
183. Kirson, E. D. *et al.* Chemotherapeutic treatment efficacy and sensitivity are increased by adjuvant alternating electric fields (TTFields). *BMC Med. Phys.* (2009). doi:10.1186/1756-6649-9-1
184. Hottinger, A. F., Pacheco, P. & Stupp, R. Tumor treating fields: A novel treatment modality and its use in brain tumors. *Neuro-Oncology* (2016). doi:10.1093/neuonc/nov182
185. Taillibert, S., Rhun, E. Le & Chamberlain, M. C. Tumor treating fields: A new standard treatment for glioblastoma? *Current Opinion in Neurology* (2015). doi:10.1097/WCO.0000000000000250
186. Clark, P. A. *et al.* The effects of tumor treating fields and temozolomide in MGMT expressing and non-expressing patient-derived glioblastoma cells. *J. Clin. Neurosci.* (2017). doi:10.1016/j.jocn.2016.10.042
187. Malats, N. & Real, F. X. Epidemiology of Bladder Cancer. *Hematology/Oncology Clinics of North America* (2015). doi:10.1016/j.hoc.2014.10.001
188. Burger, M. *et al.* Epidemiology and risk factors of urothelial bladder cancer. *Eur. Urol.* (2013). doi:10.1016/j.eururo.2012.07.033
189. Kirkali, Z. *et al.* Bladder cancer: Epidemiology, staging and grading, and diagnosis. in *Urology* (2005). doi:10.1016/j.urology.2005.07.062
190. Colombel, M. *et al.* Epidemiology, Staging, Grading, and Risk Stratification of Bladder Cancer. *European Urology, Supplements* (2008). doi:10.1016/j.eursup.2008.08.002
191. Kaufman, D. S., Shipley, W. U. & Feldman, A. S. Bladder cancer. *Lancet* **374**, 239–249 (2009).

192. Kamat, A. M. *et al.* Bladder cancer. *The Lancet* (2016). doi:10.1016/S0140-6736(16)30512-8
193. Yafi, F. A., North, S. & Kassouf, W. First- and second-line therapy for metastatic urothelial carcinoma of the bladder. *Current Oncology* **18**, e25-34 (2011).
194. Agarwal, N. & Hussain, M. Management of bladder cancer: Current and emerging strategies. *Drugs* **69**, 1173–1187 (2009).
195. Volkmer, J.-P. *et al.* Three differentiation states risk-stratify bladder cancer into distinct subtypes. *Proc. Natl. Acad. Sci.* (2012). doi:10.1073/pnas.1120605109
196. Van Batavia, J. *et al.* Bladder cancers arise from distinct urothelial sub-populations. *Nat. Cell Biol.* (2014). doi:10.1038/ncb3038
197. Volkmer, J.-P. *et al.* Three differentiation states risk-stratify bladder cancer into distinct subtypes. *Proceedings of the National Academy of Sciences* **109**, 2078–2083 (2012).
198. Shin, K. *et al.* Cellular origin of bladder neoplasia and tissue dynamics of its progression to invasive carcinoma. *Nat. Cell Biol.* **16**, 469–78 (2014).
199. Lerner, S. P. *et al.* Bladder Cancer Molecular Taxonomy: Summary from a Consensus Meeting. *Bl. Cancer* (2016). doi:10.3233/BLC-150037
200. Paraskevopoulou, V., Papafotiou, G. & Klinakis, A. KRT14 marks bladder progenitors. *Cell Cycle* (2016). doi:10.1080/15384101.2016.1220722
201. Shin, K. *et al.* Cellular origin of bladder neoplasia and tissue dynamics of its progression to invasive carcinoma. *Nat. Cell Biol.* (2014). doi:10.1038/ncb2956
202. Damrauer, J. S. *et al.* Intrinsic subtypes of high-grade bladder cancer reflect the hallmarks of breast cancer biology. *Proc. Natl. Acad. Sci.* (2014). doi:10.1073/pnas.1318376111
203. Powles, T. *et al.* MPDL3280A (anti-PD-L1) treatment leads to clinical activity in metastatic bladder cancer. *Nature* (2014). doi:10.1038/nature13904

204. Inman, B. A., Longo, T. A., Ramalingam, S. & Harrison, M. R. Atezolizumab: A PD-L1-blocking antibody for bladder cancer. *Clin. Cancer Res.* (2017).  
doi:10.1158/1078-0432.CCR-16-1417
205. Inman, B. A., Longo, T. A., Ramalingam, S. & Harrison, M. R. Atezolizumab: a PD-L1 blocking antibody for bladder cancer. *Clin Cancer Res* (2016).  
doi:clincanres.1417.2016 [pii]\r1078-0432.CCR-16-1417 [pii]\r10.1158/1078-0432.CCR-16-1417
206. F. Hoffmann-La Roche Ltd. Roche provides update on phase III study of TECENTRIQ (atezolizumab) in people with previously treated advanced bladder cancer. *Media Release* (2017).
207. Massard, C. *et al.* Safety and efficacy of durvalumab (MEDI4736), an anti-programmed cell death ligand-1 immune checkpoint inhibitor, in patients with advanced urothelial bladder cancer. *J. Clin. Oncol.* (2016).  
doi:10.1200/JCO.2016.67.9761
208. Brower, V. Anti-PD-L1 inhibitor durvalumab in bladder cancer. *The Lancet. Oncology* (2016). doi:10.1016/S1470-2045(16)30242-X
209. Sharma, P. *et al.* Nivolumab in metastatic urothelial carcinoma after platinum therapy (CheckMate 275): a multicentre, single-arm, phase 2 trial. *Lancet Oncol.* (2017). doi:10.1016/S1470-2045(17)30065-7
210. Sharma, P. *et al.* Nivolumab monotherapy in recurrent metastatic urothelial carcinoma (CheckMate 032): a multicentre, open-label, two-stage, multi-arm, phase 1/2 trial. *Lancet Oncol.* (2016). doi:10.1016/S1470-2045(16)30496-X
211. Bellmunt, J. *et al.* KEYNOTE-045: Randomized phase 3 trial of pembrolizumab (MK-3475) versus paclitaxel, docetaxel, or vinflunine for previously treated metastatic urothelial cancer. *ASCO Meet. Abstr.* (2015).
212. Farina, M. S., Lundgren, K. T. & Bellmunt, J. Immunotherapy in Urothelial Cancer:

- Recent Results and Future Perspectives. *Drugs* (2017). doi:10.1007/s40265-017-0748-7
213. Balar, A. V. *et al.* Pembrolizumab as first-line therapy in cisplatin-ineligible advanced urothelial cancer: Results from the total KEYNOTE-052 study population. *J. Clin. Oncol.* (2017). doi:10.1200/JCO.2017.35.6\_suppl.284
214. Buckner, J. C. Factors Influencing Survival in High-Grade Gliomas. in *Seminars in Oncology* (2003). doi:10.1053/j.seminoncol.2003.11.031
215. Weller, M. *et al.* Molecular predictors of progression-free and overall survival in patients with newly diagnosed glioblastoma: A prospective translational study of the German Glioma Network. *J. Clin. Oncol.* (2009). doi:10.1200/JCO.2009.23.0805
216. Allen Institute for Brain Science. Ivy Glioblastoma Atlas Project. (2015). Available at: <http://glioblastoma.alleninstitute.org/>.
217. Theocharidis, A., van Dongen, S., Enright, A. J. & Freeman, T. C. Network visualization and analysis of gene expression data using BioLayout Express(3D). *Nat. Protoc.* (2009). doi:10.1038/nprot.2009.177
218. Freeman, T. C. *et al.* Construction, visualisation, and clustering of transcription networks from microarray expression data. *PLoS Comput. Biol.* (2007). doi:10.1371/journal.pcbi.0030206
219. Lê, S., Josse, J. & Husson, F. FactoMineR : An R Package for Multivariate Analysis. *J. Stat. Softw.* (2008). doi:10.18637/jss.v025.i01
220. Subramanian, A. *et al.* Gene set enrichment analysis: A knowledge-based approach for interpreting genome-wide expression profiles. *Proc. Natl. Acad. Sci.* (2005). doi:10.1073/pnas.0506580102
221. Mootha, V. K. *et al.* PGC-1 $\alpha$ -responsive genes involved in oxidative phosphorylation are coordinately downregulated in human diabetes. *Nat. Genet.*

- (2003). doi:10.1038/ng1180
222. Ashburner, M. *et al.* Gene ontology: Tool for the unification of biology. *Nature Genetics* (2000). doi:10.1038/75556
223. The Gene Ontology Consortium. Expansion of the Gene Ontology knowledgebase and resources. *Nucleic Acids Res.* (2017). doi:10.1093/nar/gkw1108
224. Merico, D., Isserlin, R., Stueker, O., Emili, A. & Bader, G. D. Enrichment map: A network-based method for gene-set enrichment visualization and interpretation. *PLoS One* (2010). doi:10.1371/journal.pone.0013984
225. Morrissy, A. S. *et al.* Spatial heterogeneity in medulloblastoma. *Nat. Genet.* (2017). doi:10.1038/ng.3838
226. Wang, Q. *et al.* Tumor Evolution of Glioma-Intrinsic Gene Expression Subtypes Associates with Immunological Changes in the Microenvironment. *Cancer Cell* **32**, 42–56.e6 (2017).
227. Pedregosa, F. *et al.* Scikit-learn: Machine Learning in Python. *J. Mach. Learn. Res.* (2012). doi:10.1007/s13398-014-0173-7.2
228. Liberzon, A. *et al.* The Molecular Signatures Database Hallmark Gene Set Collection. *Cell Syst.* (2015). doi:10.1016/j.cels.2015.12.004
229. Colman, H. *et al.* A multigene predictor of outcome in glioblastoma. *Neuro. Oncol.* (2010). doi:10.1093/neuonc/nop007
230. Phillips, H. S. *et al.* Molecular subclasses of high-grade glioma predict prognosis, delineate a pattern of disease progression, and resemble stages in neurogenesis. *Cancer Cell* (2006). doi:10.1016/j.ccr.2006.02.019
231. Caleb Rutledge, W. *et al.* Tumor-infiltrating lymphocytes in glioblastoma are associated with specific genomic alterations and related to transcriptional class. *Clin. Cancer Res.* (2013). doi:10.1158/1078-0432.CCR-13-0551
232. Doucette, T. *et al.* Immune Heterogeneity of Glioblastoma Subtypes: Extrapolation

- from the Cancer Genome Atlas. *Cancer Immunol. Res.* (2013). doi:10.1158/2326-6066.CIR-13-0028
233. Preusser, M., Lim, M., Hafler, D. A., Reardon, D. A. & Sampson, J. H. Prospects of immune checkpoint modulators in the treatment of glioblastoma. *Nature Reviews Neurology* (2015). doi:10.1038/nrneurol.2015.139
234. Pardoll, D. M. The blockade of immune checkpoints in cancer immunotherapy. *Nature Reviews Cancer* (2012). doi:10.1038/nrc3239
235. van Elsas, A., Hurwitz, a a & Allison, J. P. Combination immunotherapy of B16 melanoma using anti-cytotoxic T lymphocyte-associated antigen 4 (CTLA-4) and granulocyte/macrophage colony-stimulating factor (GM-CSF)-producing vaccines induces rejection of subcutaneous and metastatic tumors accompanied . *J. Exp. Med.* (1999). doi:10.1084/jem.190.3.355
236. Li, B. *et al.* Anti-programmed death-1 synergizes with granulocyte macrophage colony-stimulating factor-secreting tumor cell immunotherapy providing therapeutic benefit to mice with established tumors. *Clin. Cancer Res.* (2009). doi:10.1158/1078-0432.CCR-08-1825
237. Minajeva, A. *et al.* Impact of Blood Vessel Quantity and Vascular Expression of CD133 and ICAM-1 on Survival of Glioblastoma Patients. *Neurosci. J.* **2017**, 5629563 (2017).
238. Homma, T. *et al.* Correlation among pathology, genotype, and patient outcomes in glioblastoma. *J. Neuropathol. Exp. Neurol.* (2006). doi:10.1097/01.jnen.0000235118.75182.94
239. Toth, G. B. *et al.* Current and potential imaging applications of ferumoxytol for magnetic resonance imaging. *Kidney International* (2017). doi:10.1016/j.kint.2016.12.037
240. Martinez-Garcia, M. *et al.* SEOM clinical guidelines for diagnosis and treatment of



- glioblastoma (2017). *Clin. Transl. Oncol.* **20**, 22–28 (2018).
241. Annibaldi, D. *et al.* Myc inhibition is effective against glioma and reveals a role for Myc in proficient mitosis. *Nat. Commun.* (2014). doi:10.1038/ncomms5632
242. Whitfield, J. R., Beaulieu, M.-E. & Soucek, L. Strategies to Inhibit Myc and Their Clinical Applicability. *Front. Cell Dev. Biol.* (2017). doi:10.3389/fcell.2017.00010
243. Marziali, G. *et al.* Metabolic/Proteomic Signature Defines Two Glioblastoma Subtypes with Different Clinical Outcome. *Sci. Rep.* (2016). doi:10.1038/srep21557
244. Yang, X., Lay, F., Han, H. & Jones, P. A. Targeting DNA methylation for epigenetic therapy. *Trends in Pharmacological Sciences* (2010). doi:10.1016/j.tips.2010.08.001
245. Lai, R. K. *et al.* Genome-wide methylation analyses in glioblastoma multiforme. *PLoS One* (2014). doi:10.1371/journal.pone.0089376
246. Jeong, J.-W. *et al.* Multi-modal imaging of tumor cellularity and Tryptophan metabolism in human Gliomas. *Cancer Imaging* (2015). doi:10.1186/s40644-015-0045-1
247. Data, M. Cancer Statistics, 2016. **66**, 7–30 (2016).
248. Fernández, M. I. *et al.* Prognostic Implications of Lymphangiogenesis in Muscle-Invasive Transitional Cell Carcinoma of the Bladder. *Eur. Urol.* **53**, 571–580 (2008).
249. Chung, J. H. *et al.* Brain and Skin Metastasis From Urothelial Carcinoma of the Bladder. 66–68 (2013).
250. Stein, J. P. & Skinner, D. G. Radical cystectomy for invasive bladder cancer: Long-term results of a standard procedure. *World J. Urol.* **24**, 296–304 (2006).
251. Sherif, A. *et al.* Neoadjuvant Cisplatinum Based Combination Chemotherapy in Patients with Invasive Bladder Cancer: A Combined Analysis of Two Nordic

- Studies. *Eur. Urol.* **45**, 297–303 (2004).
252. Shah, J. B., McConkey, D. J. & Dinney, C. P. N. New strategies in muscle-invasive bladder cancer: on the road to personalized medicine. *Clin. Cancer Res.* **17**, 2608–2612 (2011).
253. Mumenthaler, S. M. *et al.* The Impact of Microenvironmental Heterogeneity on the Evolution of Drug Resistance in Cancer Cells. *Cancer Inform.* **14**, 19–31 (2015).
254. Bouhout, S., Rousseau, A., Chabaud, S., Morissette, A. & Bolduc, S. Potential of Different Tissue Engineering Strategies in the Bladder Reconstruction. (2013). doi:10.5772/55838
255. Watson, S. S. *et al.* Microenvironment-Mediated Mechanisms of Resistance to HER2 Inhibitors Differ between HER2+ Breast Cancer Subtypes. *Cell Syst.* **6**, 329–342.e6 (2018).
256. Lin, C.-H., Lee, J. K. & LaBarge, M. A. Fabrication and Use of MicroEnvironment microArrays (MEArrays). *J. Vis. Exp.* (2012). doi:10.3791/4152
257. Wilson, T. R. *et al.* Widespread potential for growth-factor-driven resistance to anticancer kinase inhibitors. *Nature* **487**, 505–509 (2012).
258. Banerji, S. *et al.* LYVE-1, a new homologue of the CD44 glycoprotein, is a lymph-specific receptor for hyaluronan. *J. Cell Biol.* **144**, 789–801 (1999).
259. Jackson, D. G., Prevo, R., Clasper, S. & Banerji, S. LYVE-1, the lymphatic system and tumor lymphangiogenesis. *Trends in Immunology* (2001). doi:10.1016/S1471-4906(01)01936-6
260. Jackson, D. G. The lymphatics revisited: new perspectives from the hyaluronan receptor LYVE-1. *Trends Cardiovasc. Med.* **13**, 1–7 (2003).
261. Jackson, D. G. Biology of the lymphatic marker LYVE-1 and applications in research into lymphatic trafficking and lymphangiogenesis. *APMIS* (2004). doi:10.1111/j.1600-0463.2004.apm11207-0811.x

262. Ramani, P., Dungwa, J. V. & May, M. T. LYVE-1 upregulation and lymphatic invasion correlate with adverse prognostic factors and lymph node metastasis in neuroblastoma. *Virchows Arch.* (2012). doi:10.1007/s00428-011-1190-y
263. Ozmen, F. *et al.* Relationship between LYVE-1, VEGFR-3 and CD44 gene expressions and lymphatic metastasis in gastric cancer. *World J. Gastroenterol.* **17**, 3220–3228 (2011).
264. Ma, Y. *et al.* Intratumoral Lymphatics and Lymphatic Vessel Invasion Detected by D2-40 Are Essential for Lymph Node Metastasis in Bladder Transitional Cell Carcinoma. *Anat. Rec.* (2010). doi:10.1002/ar.21217
265. Barretina, J. *et al.* The Cancer Cell Line Encyclopedia enables predictive modelling of anticancer drug sensitivity. *Nature* (2012). doi:10.1038/nature11003
266. Lindgren, D. *et al.* Combined gene expression and genomic profiling define two intrinsic molecular subtypes of urothelial carcinoma and gene signatures for molecular grading and outcome. *Cancer Res.* (2010). doi:10.1158/0008-5472.CAN-09-4213
267. Earl, J. *et al.* The UBC-40 Urothelial Bladder Cancer cell line index: A genomic resource for functional studies. *BMC Genomics* (2015). doi:10.1186/s12864-015-1450-3
268. Jinesh G., G., Chunduru, S. & Kamat, a. M. Smac mimetic enables the anticancer action of BCG-stimulated neutrophils through TNF- but not through TRAIL and FasL. *J. Leukoc. Biol.* **92**, 233–244 (2012).
269. Schoppmann, S. F. *et al.* Lymphangiogenesis and lymphovascular invasion diminishes prognosis in esophageal cancer. *Surg. (United States)* **153**, 526–534 (2013).
270. Saban, M. R. *et al.* Neuropilin-VEGF signaling pathway acts as a key modulator of vascular, lymphatic, and inflammatory cell responses of the bladder to intravesical

- BCG treatment. *Am. J. Physiol. Renal Physiol.* (2010).  
doi:10.1152/ajprenal.00352.2010
271. Wang, S. J. & Bourguignon, L. Y. W. Role of hyaluronan-mediated CD44 signaling in head and neck squamous cell carcinoma progression and chemoresistance. *American Journal of Pathology* (2011). doi:10.1016/j.ajpath.2010.11.077
272. Perez, A. *et al.* CD44 interacts with EGFR and promotes head and neck squamous cell carcinoma initiation and progression. *Oral Oncol.* (2013).  
doi:10.1016/j.oraloncology.2012.11.009
273. Ocaña, A. *et al.* Neuregulin expression in solid tumors: Prognostic value and predictive role to anti-HER3 therapies. *Oncotarget* (2016).  
doi:10.18632/oncotarget.8648
274. Hobbs, S. S. *et al.* Neuregulin isoforms exhibit distinct patterns of ErbB family receptor activation. *Oncogene* (2002). doi:10.1038/sj.onc.1205960
275. Meyer, D. *et al.* Isoform-specific expression and function of neuregulin. *Development* (1997).
276. Talmage, D. a. Mechanisms of neuregulin action. *Novartis Found. Symp.* (2008).  
doi:10.1002/9780470751251.ch6
277. Gagnon-Bartsch, J. A., Jacob, L. & Speed, T. P. Removing Unwanted Variation from High Dimensional Data with Negative Controls. *Tech. Reports from Dep. Stat. Univ. California, Berkeley* (2013).
278. Gijbels, I. & Prosdocimi, I. Loess. *Wiley Interdiscip. Rev. Comput. Stat.* (2010).  
doi:10.1002/wics.104
279. Bland, J. M. & Altman, D. G. Tukey Multiple Comparison test. *Br. Med. J. J. Clin. Nurs.* (1995).
280. Shun, Z., Silverberg, A., Chang, C. K. & Ouyang, P. Dunnett's many-to-one test and least square means. *J. Biopharm. Stat.* (2003). doi:10.1081/BIP-120017723

